

DESIGN AND MANUFACTURING OF A TACTICAL UNMANNED AIR VEHICLE

**A THESIS SUBMITTED TO
THE GRADUATE SCHOOL OF NATURAL AND APPLIED SCIENCES
OF
MIDDLE EAST TECHNICAL UNIVERSITY**

BY

ENGİN ŞENELT

**IN PARTIAL FULFILLMENT OF THE REQUIREMENTS
FOR
THE DEGREE OF MASTER OF SCIENCE
IN
AEROSPACE ENGINEERING**

SEPTEMBER 2010

Approval of the thesis:

DESIGN AND MANUFACTURING OF A TACTICAL UNMANNED AIR VEHICLE

submitted by **ENGİN ŞENELT** in partial fulfilment of the requirements for the degree
of **Master of Science in Aerospace Engineering Department, Middle East Technical
University** by,

Prof. Dr. Canan Özgen
Dean, Graduate School of **Natural and Applied Sciences**

Prof. Dr. Ozan Tekinalp
Head of Department, **Aerospace Engineering**

Prof. Dr. Nafiz Alemdaroğlu
Supervisor, **Aerospace Engineering Dept., METU**

Examining Committee Members:

Prof. Dr. Serkan Özgen
Aerospace Engineering Dept., METU

Prof. Dr. Nafiz Alemdaroğlu
Aerospace Engineering Dept., METU

Prof. Dr. Yusuf Özyörük
Aerospace Engineering Dept., METU

Prof. Dr. Levent Parnas
Mechanical Engineering Dept., METU

Assoc. Prof. Dr. Altan Kayran
Aerospace Engineering Dept., METU

Date: 13.09.2010

I hereby declare that all information in this document has been obtained and presented in accordance with academic rules and ethical conduct. I also declare that, as required by these rules and conduct, I have fully cited and referenced all material and results that are not original to this work.

Name, Last Name : Engin ŞENELT

Signature :

ABSTRACT

DESIGN AND MANUFACTURING OF A TACTICAL UNMANNED AIR VEHICLE

Şenelt, Engin

M.Sc., Department of Aerospace Engineering

Supervisor: Prof. Dr. Nafiz Alemdaroğlu

September 2010, 119 pages

The aim of this study is to describe the conceptual design, performance analysis to validate the design and manufacturing steps of Middle East Technical University Tactical Unmanned Air Vehicle (METU TUAV). The system requirements are adopted from a market study and assumed as is. Utilizing competitor search and conceptual design methodology, the rough parameters of the aircraft are defined and a performance analysis is conducted to validate the requirements. After the design team is content that the design is meeting the requirements, material and production techniques are evaluated.

The male and female molds of the aircraft are manufactured with glass fibre fabric and special mold resin. Using the female molds; with glass, carbon and aramid fibre materials and epoxy matrix; utilizing wet-layup and vacuum bagging techniques the METU TUAV is manufactured. Wing, tail and fuselage skins are manufactured first and the reinforcing structures are integrated and cured inside the skins. Then the skins are assembled and the separate components are obtained. The rear landing gear and tail booms are also manufactured from carbon fibre composites. The individual parts are assembled together in special alignment jigs and the METU TUAV is completed.

Keywords: Tactical UAV, composite mold manufacturing, composite manufacturing.

Öz

TAKTİK BİR İNSANSIZ HAVA ARACININ TASARIMI VE İMALATI

Şenelt, Engin

Yüksek Lisans, Havacılık ve Uzay Mühendisliği Bölümü

Tez Yöneticisi: Prof. Dr. Nafiz Alemdaroğlu

Eylül 2010, 119 sayfa

Bu çalışmanın amacı Orta Doğu Teknik Üniversitesi Taktik İnsansız Hava Aracı'nın (ODTÜ TİHA) konsept tasarımı, konsept tasarımın performans analiziyle doğrulanması ve üretim adımlarını anlatmaktadır. Sistem gereksinimleri piyasa araştırması sonucu kararlaştırılıp olduğu gibi kabul edilmiştir. Rakip değerlendirmesi ve konsept tasarım metodolojisi ile kaba parametreler tanımlanmış ve bu parametrelerin doğrulanması için performans analizi gerçekleştirilmiştir. Tasarım takımı tasarımın gereksinimleri karşıladığından emin olduktan sonra malzeme ve üretim teknikleri değerlendirilmiştir.

Uçağın erkek ve dişi kalıpları cam fiber kumaş ve özel kalıp reçinesi ile üretilmiştir. ODTÜ TİHA dişi kalıplar kullanılarak, cam, karbon ve aramid fiber malzeme ve epoksi reçine ile, ıslak yatırma ve vakum torbalama tekniğiyle üretilmiştir. Kanat, kuyruk ve gövde kabukları öncelikli olarak üretilmiş ve güçlendirici yapılar daha sonra kabukların içine entegre edilip kürlenmiştir. Daha sonra kabuklar birleştirilmiş ve ayrı komponentler elde edilmiştir. Arka iniş takımı ve kuyruk boruları da karbon fiber kompozit malzemeden üretilmiştir. Tüm komponentler hizalama kalıplarında birleştirilerek ODTÜ TİHA'nın üretimi tamamlanmıştır.

Anahtar Kelimeler: Taktik İHA, kompozit kalıp üretimi, kompozit üretimi.

ACKNOWLEDGMENTS

I would like to express my wholehearted thanks to my supervisor Prof. Dr. Nafiz ALEMDAROĞLU for initiating METU TUAV Project and providing his invaluable expertise and support. Without his confidence and trust in me, completion of this thesis would not be possible.

I would also like to thank Assoc. Prof. Dr. Altan KAYRAN for his valuable comments and steering. I would also like to present my gratitude to the former METU TUAV members for bringing the project to a successful stage where, while taking over, I could hardly find a step left out.

I would like to thank Murat CEYLAN, Erdinç BALABAN and Ali İŞCANOĞLU for teaching me the secret art of manufacturing.

I would like to thank and give my greatest appreciation to TÜBİTAK - BİDEB for supporting me during my studies. I would also like to thank TÜBİTAK for supporting the METU TUAV project.

I would like to acknowledge the support and motivation of those who never gave up with me, my family, my friends and all my beloved ones.

Finally I would like to thank my grandpa for being an inspiration for me.

TABLE OF CONTENTS

ABSTRACT.....	iv
ÖZ.....	v
ACKNOWLEDGMENTS.....	vi
TABLE OF CONTENTS	vii
LIST OF TABLES.....	xi
LIST OF FIGURES.....	xii
LIST OF SYMBOLS	xvi
CHAPTERS	
1. INTRODUCTION.....	1
1.1. Unmanned Air Vehicles (UAV's).....	1
1.2. Metu tactical unmanned air vehicle (METU TUAV)	2
1.3. Competitor study	2
1.4. Design and manufacturing phases	4
2. CONCEPTUAL DESIGN	6
2.1. Requirements.....	6
2.2. Initial Weight Estimation.....	8
2.2.1. Payload Weight Estimation	8
2.2.2. Empty Weight Fraction Estimation.....	8
2.2.3. Fuel Weight Fraction Estimation	9
2.3. Critical Performance Parameters	12
2.3.1. Maximum Lift Coefficient.....	12
2.3.2. Wing Loading.....	13
2.3.3. Power to Weight Ratio	15
2.4. Configuration Layout.....	17
2.4.1. Engine	17
2.4.2. Tractor/Pusher choice	17
2.4.3. Fuselage Sizing.....	18
	vii

2.4.4.	Wing Configuration	18
2.4.5.	Fuel Tank Size and Position	19
2.4.6.	Center of Gravity Estimate	19
2.4.7.	Horizontal and Vertical Tail Sizing	21
2.4.8.	Propeller Sizing.....	22
2.4.9.	Landing Gear Placement.....	23
2.4.10.	Wing Placement	23
2.4.11.	Better Weight Estimation.....	23
3.	PERFORMANCE ANALYSIS.....	26
3.1.	Wing Loading.....	26
3.2.	Power Loading.....	26
3.3.	Power Required and Power Available Curves	27
3.4.	Rate of Climb and Climb Velocity	30
3.5.	Time to Climb	32
3.6.	Best Angle and Rate of Climb	33
3.7.	Range.....	33
3.8.	Endurance	34
3.9.	Maximum Load Factor.....	34
3.10.	V-N Diagram	36
3.11.	Landing Distance	37
3.12.	Take-off Distance.....	38
4.	MATERIAL SELECTION	39
5.	MANUFACTURING.....	43
5.1.	Wings.....	43
5.1.1.	Mold Manufacturing	43
5.1.1.1.	Male Mold Manufacturing.....	43
5.1.1.2.	Female Mold Manufacturing	44
5.1.2.	Wing Manufacturing.....	46
5.1.2.1.	Skin Manufacturing.....	46
5.1.2.2.	Spar Manufacturing	47
5.1.2.3.	Rib Manufacturing and Wing Assembly.....	50
5.2.	Fuselage.....	52
5.2.1.	Mold Manufacturing	54

5.2.1.1.	Male Mold Manufacturing	54
5.2.1.2.	Female Mold Manufacturing	55
5.2.2.	Fuselage Manufacturing	60
5.2.2.1.	Skin Manufacturing	60
5.2.2.2.	Bulkheads and Assembly.....	63
5.3.	Vertical and Horizontal Tails.....	66
5.3.1.	Mold Manufacturing	67
5.3.1.1.	Male Molds	67
5.3.1.2.	Female Molds.....	68
5.3.2.	Tail Manufacturing	68
5.3.2.1.	Skins	68
5.3.2.2.	Spars.....	72
5.3.2.3.	Assembly	76
5.4.	Landing Gear	77
5.4.1.	Main Landing Gear	78
5.4.1.1.	Male Mold.....	78
5.4.1.2.	Skin	78
5.4.1.3.	Wheels and Brake System.....	79
5.4.2.	Nose Landing Gear	80
5.4.2.1.	Metal Production	81
5.4.2.2.	Wheels	81
5.4.2.3.	Steering System.....	81
5.5.	Detail Production and Assembly	83
5.5.1.	Wing	83
5.5.1.1.	Control Surfaces.....	83
5.5.1.2.	Servo Doors and Covers	84
5.5.1.3.	Cable Channels.....	88
5.5.1.4.	Torque Box.....	90
5.5.1.5.	Tail Boom Connections	93
5.5.2.	Fuselage.....	96
5.5.2.1.	Access Door Covers	96
5.5.2.2.	Section Walls.....	97
5.5.2.3.	Parachute Box and Cover.....	98

5.5.2.4. Torque Box Connections	100
5.5.2.5. Engine Mount.....	101
5.5.2.6. Surface Finish and Final Layout.....	103
5.5.3. Tail	104
5.5.3.1. Tail Assembly.....	104
5.5.3.2. Control Surfaces.....	107
5.5.3.3. Servo Doors and Covers	108
5.5.3.4. Cable Channels.....	109
6. DISCUSSION, CONCLUSION AND FUTURE WORK	111
6.1. DISCUSSION	111
6.2. CONCLUSION AND FUTURE WORK.....	116
REFERENCES.....	118

LIST OF TABLES

TABLES

Table 1: Competitor study	3
Table 2: Requirements of METU UAV	6
Table 3: Verification of Weight Estimations	25
Table 4: Materials used in Tactical UAV	41

LIST OF FIGURES

FIGURES

Figure 1: Flow Chart of Conceptual Design Steps.....	7
Figure 2: Mission Profile.....	9
Figure 3: NACA 63-412 airfoil section.....	13
Figure 4: Drag variation graph.....	27
Figure 5: Lift to drag ratios graph.....	28
Figure 6: Power required and available graph	30
Figure 7: Variation of best rate of climb velocity with altitude graph	31
Figure 8: Rate of climb variation with altitude graph	31
Figure 9: Time to climb altitude graph	32
Figure 10: Hodograph for climb performance	33
Figure 11: Load factors graph.....	35
Figure 12: Turn rates graph.....	35
Figure 13: V-N diagram.....	37
Figure 14: Properties of metal and organic/inorganic fibre materials (AIPMA, 2009) ..	40
Figure 15: Male mold (a), male mold positioned for female mold production (b).....	44
Figure 16: Frame of the male mold (a), root support (b), epoxy resin smeared over the male mold (c), glass fibre fabric laid (d), wooden skeleton on the back side (e), final view of the female molds (f)	45
Figure 17: Polyester coating (a), glass fibre layer (b), Rohacell 31A layer (c), carbon strips and vacuum aids (d), vacuum bagging process (e), cured lower skin (f) ...	47
Figure 18: Main spar core positioned (a), rear spar core positioned (b), aluminium rear spar root positioned (c), spar root covered with carbon fibre (d), structure prepared for vacuum (e)	49
Figure 19: Rear spar cured and trimmed (a), hornbeam main spar root positioned (b), structure prepared for vacuum (c), both spars integrated on to lower skin (d).....	50

Figure 20: Ribs positioned (a), adhered (b) and fixed for hardening (c), final positions of ribs (d), adhesive applied to contact surfaces (e) and molds are clamped together (f)	52
Figure 21: Composite Mold Manufacturing (a), Composite Fuselage Manufacturing (b)	53
Figure 22: Male mold (a), Pool for female mold (b), Resin application over the male mold (c)	56
Figure 23: Smearing mold resin over the fibre-glass fabric (a), Back view of the female mold before the wooden skeleton is built (b), (c)	57
Figure 24: Wooden skeleton production and integration with the female mold (a), (b)	59
Figure 25: Final view of the female molds (a), (b).....	59
Figure 26: Double sided adhesive tape attached to the periphery of the mold (a), Polyester coating as the first layer on the mold (b), Laying fibre-glass and aramid fibre fabrics (c)	61
Figure 27: Positioning punctured foil to prevent adhesion (a), Positioning composite blanket to remove extra resin (b), Covering the mold with vacuum bag (c).....	62
Figure 28: Cured fuselage skin inside the mold (a), Trimmed fuselage skin (b).....	63
Figure 29: Laminated wood bulkheads (a), Bulkheads positioned in respective stations (b,c), Bulkheads adhered to their positions with glass fibre and epoxy resin (d,e,f)	65
Figure 30: The fuselage assembly with inner structure taken out of the molds (a), Cutting off the access doors (b), Reinforcement of the skin connection line (c)	66
Figure 31: Final view of the tail molds (a)	68
Figure 32: Placement of glass fibre layers (a), Rohacell 31A foam (b) and the carbon fibre strips (c) for the vertical tail, Placement of glass fibre layers and Rohacell 31A foam for the horizontal tail (d).....	70
Figure 33: Molds covered with punctured nylon foil (a) and composite blanket(b), additional composite blanket pieces placed to the vacuum port positions (c), vacuum bag placed (d)	71
Figure 34: Vacuum setup (a), Vertical tail (b) and horizontal tail (c) skin after curing ..	72

Figure 35: Core foam of horizontal tail main spar (a), main spar ready for curing (b), cured main spar (c), rear spar being prepared (d), cured and trimmed spars (e).....	74
Figure 36: Vertical tail spar core (a), U shaped carbon fibre sheet placement (b), Inner structure finalized for vertical and horizontal tails (c)	75
Figure 37: Two versions of the horizontal tail with different rear spars (a)	76
Figure 38: Adhesive is applied to surfaces of contact (a), Polyurethane foam is sprayed to hollow areas (b), Molds are clamped together (c).....	77
Figure 39: Main landing gear as being cured (a) and as removed from the mold (b)....	79
Figure 40: Main wheels with brake disks and callipers (a), with connections (b).....	80
Figure 41: Nose landing gear front (a) and side (b) view	82
Figure 42: Control surfaces cut out of the wings (a), Gaps are filled with wooden parts (b) and adhesives (c), attached hinges (d), final view of control surfaces	84
Figure 43: Servo doors cut out in two steps (a) and (b).....	85
Figure 44: Servo door frames formed over the male mold (a), Frames cut in desired shape (b).....	86
Figure 45: Servo door frame clamped in position (a), Servo door cover template (b), Servo door frame surface finish (c), Servo doors in final view (d).....	87
Figure 46: Sheet metal stuck over the wing to mold the servo door cover (a), Servo door cover curing over the wing (b), Servo door cover trimmed and positioned (c)	88
Figure 47: Holes through the ribs for cable channels (a), Cable channels laid through the wings (c)	89
Figure 48: Cable channels fixed to the base (a) and ribs (b), final layout of the cable channels (c).....	90
Figure 49: Wing spars correctly positioned (a), Carbon fibre fabric wrapped around the spars (b), Tips of the torque box reinforced (c), Torque box squeezed with clamps (d), Torque box separated from the spars (e,f), Torque box (g).....	92
Figure 50: Two ribs in boom position (a), Sandwich structure for boom connection (b), Sandwich structures places (c) and adhered (d)	94
Figure 51: Tail boom tube fixed to the wing (a), Tip of the tube cut out (b), Tip part manufactured separately (c).....	95

Figure 52: Access Door Covers (a,b,c)	97
Figure 53: Section Walls (a)	98
Figure 54: Parachute Box (a), Parachute compartment and cover (b)	100
Figure 55: Torque box positioned over the bulkhead (a), Torque box fixed to the bulkhead with wetted carbon fibre fabric (b)	101
Figure 56: Sheet metal pasted to the bottom of the fuselage (a), Final view of rear end of the fuselage (b)	102
Figure 57: Bulkheads and engine mount (a)	103
Figure 58: Final view of the Tactical UAV (a)	104
Figure 59: Tail assembly aligned with a jig (a), Connection surface is filled for complete match (b), Connection surface (c), Carbon fibre tube attached to the vertical tail (d), Tube attachment strengthened with glass fibre (e), Tube attachment surface finish (f)	106
Figure 60: Tail jigged for final assembly (a), tail assembly (b), tube-to-boom connection bolt attached(c)	107
Figure 61: Control surfaces attached to horizontal (a) and vertical (b) tails.....	108
Figure 62: Servo door cut and servo placed inside (a), Prototype servo door cover (b), Servo door cover mold (c), Further production of servo door covers (d) ...	109
Figure 63: Holes drilled to pass cable channels (a), Holes closed and covered (b).....	110

LIST OF SYMBOLS

ROMAN SYMBOLS

A	Weight Estimation Constant
AR	Aspect Ratio
b	Span
c	Chord
C	Weight Estimation Constant
C_{bhp}	Specific Fuel Consumption
C_{fe}	Skin Friction Constant
C_{Lmax}	Maximum Lift Coefficient
$C_{Lmax, 2d}$	Airfoil Maximum Lift Coefficient
$C_{Lmax, 3d}$	Plane Wing Max. Lift Coefficient
$C_{m_{a.c}}$	Moment Coefficient
d	Reference Length
D	Drag
E	Endurance
e	Form Factor
j	Ground Roll Parameter
K_{vs}	Weight Estimation Constant
L/D	Lift to Drag Ratio
l	Aircraft Length Fuselage Length
n	Load Factor
N	Reaction Time
P	Power
q	Dynamic Pressure
R	Range
R/C	Rate of Climb
Re	Reynolds Number
S	Area
S_g	Ground Roll Distance
T/W	Thrust to Weight Ratio
V	Velocity
W	Weight
w	Width
x	Distance of CG
Z	Altitude
ΔC_{Lmax}	High Lift Device Additional Lift

GREEK SYMBOLS

μ	Viscosity
μ_r	Friction Coefficient
λ	Taper Ratio
ρ_∞	Air Density
ψ	Turn Rate
η	Propeller Efficiency

SUBSCRIPTS

0	Reference
3k	3000ft Altitude
A	Available
a/c	Aircraft
cr	Cruise
e	Empty
f	Fuel / Fuselage
HT	Horizontal Tail
L	Landing
loiter	Loiter
p	Payload
R	Required
r	Root
RC	Rate of Climb Condition
ref	Reference
SL	Sea Level
stall	Stall Condition
t	Tip
TD	Touch Down
TO	Take Off
v	Vertical
VT	Vertical Tail
wet	Total Wetted Surface
i	Induced

CHAPTER 1

INTRODUCTION

1.1 UNMANNED AIR VEHICLES (UAV'S)

The concept of unmanned air vehicles has been in the minds of people long before the manned aircraft designs came true. Years before Wright Brothers achieved the first manned and powered air mission, there have been unmanned air vehicles flying back and forth. The missions were not as long and sophisticated back then but considering the few-seconds-long first flight of the Wright Brothers, it was no failure. In the modern age, the manned aircraft are the technology of yesterday whereas the unmanned fliers are moving forward with great leaps.

Since the dawn of UAV's, there have been various requirements and different classes of UAV's adopting different missions. In the current day, both Micro Air Vehicles (MAV) weighing few hundred grams and giant UAV's weighing several tonnes find themselves a place in UAV market. Extensive research is being conducted to utilize the MAV's indoors, replacing human in undesired conditions such as indoor fires and terror acts [1]. On the other hand, the higher end of UAV's both weight-wise and size-wise is also getting its own missions such as replacing reconnaissance and even bombardment aircrafts, as the consequences of getting a hit by the enemy air defence network to a manned aircraft are much severe [2].

As the variety is that large, classifying the UAV's is not an easy task. Different authorities make different classifications. For instance Global Security Organization classifies the UAV's in accordance with their capabilities and sizes as: Micro, Mini, Tactical, Medium Altitude Long Endurance (MALE) and High Altitude Long Endurance (HALE) [3]. On the other hand, roles can be used for categorizing the UAV's such that

the UAV's are divided into six functional groups being: Target and Decoy, Reconnaissance, Combat, Logistics, Research and Development, Civil and Commercial [4]. Much detailed academic classifications can be found by weight, endurance and range, maximum altitude, wing loading and engine types [5].





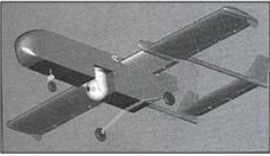

1.2 METU TACTICAL UNMANNED AIR VEHICLE (METU TUAV)

In the desire to design, manufacture and fly a completely authentic unmanned air vehicle, the design team has discussed and brainstormed the technology level, the global and local requirements, the capabilities possessed and those longed for with people working in different fields having a relation to aerospace engineering. As a result of these long lasting dialogues, the team decided to work on a Tactical Unmanned Air Vehicle (TUAV) with a set of preliminary capability requirements. Even though a lot of time and effort has been spent on deciding on the concept of a TUAV, this thesis will not prove the validity of the choice of working on a TUAV, yet the choice has not only technical basis, but also some political, military and subjective aspects that make it more feasible than its alternatives. The thesis rather focuses on the technical aspects of the design where the requirements are permanently set.

1.3 COMPETITOR STUDY

The missions that the METU TUAV will need to perform are pre-decided by classifying it as a Tactical UAV. In order to get a starting point for the design, UAV's with similar designs were evaluated and a competitor study was conducted by the design team. In stages where no theoretical data was present to help, primary estimations were performed using the data of these competitors. Six competitors were presented in **Table 1** whose performance parameters, design choices and geometries helped to initiate the design team's studies [6].

Table 1: Competitor study

Name	<i>Aerosky</i>	<i>Kestrel II</i>	<i>SHADOW 200-T</i>
Producer	Aeronautics Defence Systems Ltd, Israel	Chung-Shan Institute of Science and Technology	AAI Corp, ABD
Photo			
MTOW (kg)	70	120	118.2
Payload (kg)	18	25-30	28.2
Endurance (h)	5	5	4+
Range (km)	150-200	N/A	N/A
Wing Span (m)	4.5	5	3.89
Length (m)	3.05	4	3.1
Engine Power (hp)	18	20	26
Flight Altitude (m)	N/A	N/A	N/A
Maximum Altitude (m)	3000	2400	4500
Name	<i>Seeker II</i>	<i>UAV Experimentation System</i>	<i>Aerostar</i>
Producer	DENEL (PTY) LTD.	BAE SYSTEMS, Australia	Aeronautics Defence Systems Ltd, Israel
Photo			
MTOW (kg)	136	100	210
Payload (kg)	50	N/A	50
Endurance (h)	10	2	12
Range (km)	500	50+	200
Wing Span (m)	6.4	4.13	7.51
Length (m)	3.96	4.22	4.5
Engine Power (hp)	50	24.1	38
Flight Altitude (m)	5500	N/A	3000
Maximum Altitude (m)	N/A	N/A	6000

In selection of the competitors, those flying in the field successfully that have similar roles to the intended Tactical UAV are preferred. For instance, all the competitors are designed for reconnaissance missions and all are equipped with camera systems. A benchmark analysis has been performed with the competitors presented and some critical decisions were made before getting into detailed design phases, such as the boom tail structure or high wing design.

1.4 DESIGN AND MANUFACTURING PHASES

The design process is generally divided into three main parts where the first part, conceptual design, draws a flexible layout of the aircraft including the overall shape, size, weight and performance. With the flexible design made in conceptual design phase, the success of the design in meeting the requirements is questioned in performance analysis step and if the answer is positive, the next design phase is initiated, being the preliminary design phase. In the preliminary design phase, some structural, aerodynamic and control system analysis are done with possibly making wind tunnel testing. In this phase, major changes cannot be done on the aircraft, as that will change the estimates of conceptual design phase critically, so if major changes are required, the conceptual design phase is repeated with the insight obtained and the size, weight and performance estimates re-obtained before making preliminary design. Lastly, when the aircraft is finalized on the paper, the detail design phase is reached where the design is revised with a manufacturer's point of view. Selecting the materials, deciding on every single bolt to be used during manufacturing and designing the manufacturing tools.

After the design phases are all completed, the prototype manufacturing starts, where some serious manufacturability problems may come out. These problems are handled trying not to change the design significantly and a prototype is obtained at the end. Then some non-destructive structural tests are done on the aircraft to validate the analysis done on paper. The ground tests are done and finally the prototype gets airborne. After being able to realize the simple flight missions, the aircraft is forced to expand its flight envelope, going from easier tasks to the harder ones, and only when the aircraft is capable of performing everything it is supposed to perform, the design is called to be successful. After having a prototype that is meeting the requirements, the development phase begins. In the development phase, the aircraft is improved in terms of manufacturability, maintainability, cost, efficiency etc. reaching a balanced design.

The current design begins with the requirements and mainly focuses on the conceptual design. The preliminary design phase is rather overlooked and suspended until the first prototype is built. Some basic analyses have been done, yet the minor

modifications are left to be done after the prototype flies and real flight data is obtained. Furthermore, due to time limitations and the lack of on the job experience, some of the detailed design is done in coherence with the manufacturing process. Composite materials are not manufactured with very high precision due to the nature of the manufacturing technique; therefore the exact match of the parts during assembly requires tools and jigs to keep the parts in position while assembling. The tools and jigs needed for positioning and assembly are designed right before they are needed. The detailed design of the aircraft is changed slightly from time to time to ease manufacturing. The thesis overlooks the conceptual design and performance analysis, which verifies the conceptual design. Detailed design is not a part of this thesis and critical design choices are referenced in chapters describing the manufacturing of the METU TUAV. The design and manufacturing validation can either be through flight testing or computer aided analysis which includes structural analysis and stability analysis. Some structural analysis has been performed on the wing structure by members of the design team which is referenced in the related chapter [7], [8]. Additionally, stability analysis of the aircraft was performed by another member of the design team which is also referenced to validate the design choices [9]. Outside the scope of this thesis, there is some unfinished work being performed by other members of the METU TUAV team on structural analysis of the composite structures, which will be available in the near future.

CHAPTER 2

CONCEPTUAL DESIGN

2.1 REQUIREMENTS

Some basic requirements were figured out as mentioned before, so that the end product of the research and development would be valuable in both an academic and an economic point of view. The resulting requirements to have a useful Tactical Unmanned Air Vehicle are listed in **Table 2**. The payload weight is necessary for a standard camera system to be placed on the TUAV. The gross weight, endurance, range and flight level are approximated based on competitor study which are more or less critical for reconnaissance missions. The stall speed and cruise speed both should be low to ensure easy camera recording:

Table 2: Requirements of METU TUAV

Gross Weight	120 kg
Payload Weight	20 kg
Endurance	5 hrs
Range	600 km
Flight Ceiling	3000 m
Stall Speed	65 km/h
Cruise Speed	130 km/h
Maximum Speed	200 km/h

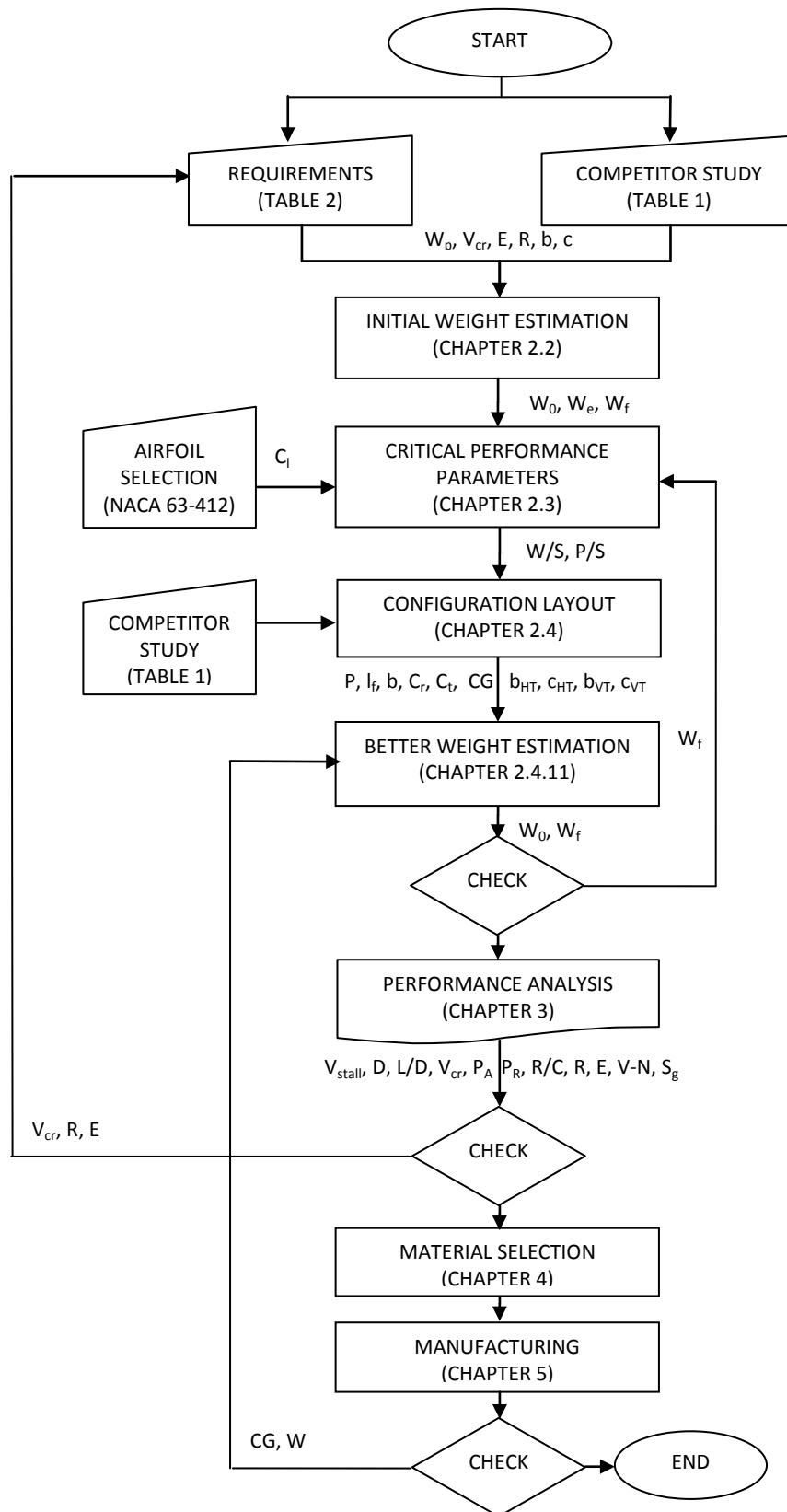


Figure 1: Flow Chart of Conceptual Design Steps

Rough sizing estimates that result from the competitor study are as follows:

$$\text{Span (b)} = 4\text{m}$$

$$\text{Chord (c)} = 0.5\text{m}$$

$$\text{Reference Area (S}_{\text{ref}}) = 2\text{m}^2$$

$$\text{Aspect Ratio (AR)} = 8$$

$$\text{Wet Area (S}_{\text{wet}}) / \text{Reference Area (S}_{\text{ref}}) = 4$$

2.2 INITIAL WEIGHT ESTIMATION

During the conceptual design, the steps of [10] have been followed. A flowchart of the design steps is given in **Figure 1**.

The gross weight of the METU TUAV is divided into three main weights as formulated in Eq(1).

$$W_0 = W_p + W_f + W_e \quad (1)$$

2.2.1 PAYLOAD WEIGHT ESTIMATION

Payload is determined as 20kg by referencing the competitor UAV's.

2.2.2 EMPTY WEIGHT FRACTION ESTIMATION

$$\frac{W_e}{W_0} = A W_0^c K_{vs} \quad (2)$$

Eq(2) acquired from page 16 of [10] is used empirically to calculate the empty weight to total weight ratio where the constants vary according to the materials used and the manufacturing methods employed. The following options are considered, that

are listed in the same reference, where the constants are for calculation in Imperial units:

1. Home-built Composite ($A=0.99$, $C=-0.09$, $K_{vs}=1.0$)
2. Home-built Metal-Wood ($A=1.19$, $C=-0.09$, $K_{vs}=1.0$)
3. Powered Sailplane ($A=0.91$, $C=-0.05$, $K_{vs}=1.0$)

2.2.3 FUEL WEIGHT FRACTION ESTIMATION

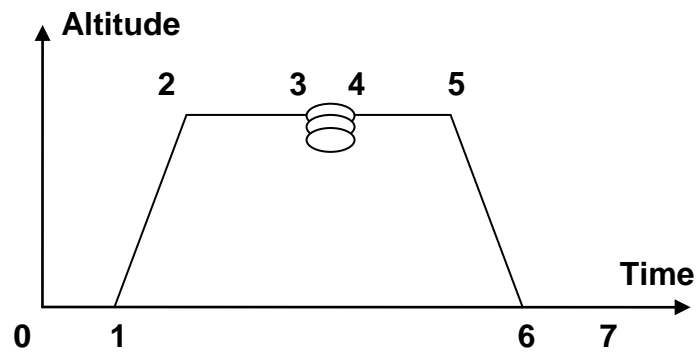


Figure 2: Mission Profile

For a sample mission where the mission radius is 150km and the loiter duration is 3h, the altitude variation with time is plotted in **Figure 2**. As the aircraft is planned to be capable of flying 5 hours for an endurance mission and fly up to 600km in a cruise mission, this combination well represents a balanced mixture. The warm up, taxi and ground roll is performed between stations 0 and 1; climb is performed between stations 1 and 2; cruise at a velocity sustaining maximum range is performed both between stations 2 - 3 and 4 – 5; cruise at a velocity sustaining maximum endurance is performed between stations 3 and 4; descend is performed between stations 5 and 6; finally the aircraft taxis and finalizes the mission between stations 6 and 7.

$$\frac{W_7}{W_0} = \left(\frac{W_7}{W_6} \cdot \frac{W_6}{W_5} \cdot \frac{W_5}{W_4} \cdot \frac{W_4}{W_3} \cdot \frac{W_3}{W_2} \cdot \frac{W_2}{W_1} \cdot \frac{W_1}{W_0} \right) = W_{75} \cdot W_{54} \cdot W_{43} \cdot W_{32} \cdot W_{21} \cdot W_{10} \quad (3)$$

For the Eq(3), which relates the overall weight ratio to mission leg weight ratios, the following fractional weight estimations are made; where W_{75} , W_{21} and W_{10} are assumed empirically referencing to [10]:

1. $W_{10}=0.97$ (warm up and take off)
2. $W_{21}=0.985$ (climb)
3. $W_{75}=0.995$ (landing)
4. 2-3 is a cruise flight where:

$V=130\text{km/h}$; Range=150km;

$L/D=14$ (for a wetted aspect ratio of 2, L/D_{\max} is read on Fig 3.6 in [10] empirically)

$C_{bhp} = 375\text{g/hp}$ (fuel consumption data is acquired from the engine specification graphs for the cruise velocity range)

Propeller Efficiency (η_p)=0.8 (referring to page 23 in [10], a high efficiency is used as the propeller blade is designed specifically for the METU TUAV to optimize the characteristics for the mentioned cruise velocities.)

$$C_{cr} = C_{bhp} \cdot \frac{V}{\eta_p} \quad (4)$$

$$W_{23} = e^{\frac{R \cdot C_{cr}}{V \cdot (L/D)}} \quad (5)$$

Utilizing Eq(4) and Eq(5), which are acquired from [10] that empirically defines the cruise weight ratio, with imperial units the desired parameter is calculated.

$$W_{32}=1/W_{23} \text{ so } W_{32}=0.982$$

5. $W_{54} = W_{32} = 0.982$ (Noting that the missions 4-5 and 2-3 are identical.)

6. 3-4 is a loiter flight where:

Endurance=3h;

$V_{loiter}=100\text{km/h}$ (assumed roughly as $(0.75).V_{cr}$ based on competitor study)

Propeller Efficiency (η_p)=0.7 (referring to page 23 in [10], a lower efficiency compared to cruise is used)

$(C_{bhp})= 375\text{g/hp}$ (same as the cruise SFC)

$L/D_{loiter}=(0.866).(L/D)=12.124$ (referring to page 27 in [10])

$$C_{loiter} = C_{bhp} \cdot \frac{V}{\eta_p} \quad (6)$$

$$W_{34} = e^{\frac{E \cdot C_{loiter}}{L/D}} \quad (7)$$

Utilizing Eq(6) and Eq(7), with imperial units the desired parameter is calculated.

$W_{43} = 1/W_{34}$ so $W_{43}=0.953$

Combining all weight fractions in Eq(3), one can obtain $W_{70}=0.872$ which yields the fuel fraction as $W_f/W_0=1-W_{70}=0.128$

Considering the reserve fuel and that there will be trapped fuel in the fuel depots and the fuel hoses, 20% safety factor is added to this amount. The resulting fuel fraction is: $W_{f0}=0.154$

Considering that there are three alternatives for the empty weight estimation as presented in the previous section, one should evaluate all three and decide on the manufacturing method and material. The following calculations are made combining Eq(1) and Eq(2) using the fuel fraction and payload weight.

1. Home-built Composite ($A=0.99$, $C=-0.09$, $K_{vs}=1.0$)

Solving Eq(2) for W_0 with the above given A and C yields: $W_0=191.97\text{lb}$

That is $W_0=87.26\text{kg}$

2. Home-built Metal-Wood ($A=1.19$, $C=-0.09$, $K_{vs}=1.0$)

Solving Eq(2) for W_0 with the above given A and C yields: $W_0=319.34\text{lb}$

That is $W_0=145.15\text{kg}$

3. Powered Sailplane ($A=0.91$, $C=-0.05$, $K_{vs}=1.0$)

Solving Eq(2) for W_0 with the above given A and C yields: $W_0=276.69\text{lb}$

That is $W_0=125.77\text{kg}$

Evaluating these values, one can state that a home-built metal-wood structure or a powered sailplane will be too heavy for the requirements. Furthermore, aiming for a low-weight design has its advantages in the future steps of the design giving more flexibility. So the initial weight estimate is 87.26 kg.

2.3 CRITICAL PERFORMANCE PARAMETERS

2.3.1 MAXIMUM LIFT COEFFICIENT

NACA 63-412 airfoil is selected after evaluating several choices. The candidates are selected among the airfoils of similar aircraft and the choice was made considering the following properties of NACA 63-412:

1. High maximum lift coefficient, Cl_{max}
2. Acceptable drag coefficient, $C_{D,0}$
3. Favourable stall characteristics
4. Favourable moment coefficient, $Cm_{a.c.}$

For the aforementioned airfoil section, the following parameters are known, which are evaluated by the design team and validated in [7] through CFD analysis:

$$Re=3.0 \times 10^6$$

$$C_{l_{max,2d}}=1.6$$

$$C_{l_{max,3d}}=(0.9) \times C_{l_{max,2d}}=1.44$$

$$\Delta C_{l_{max}}=0.9$$

$$C_{L,max} \text{ with } 45^\circ \text{ flap deflection}=2.34$$

The airfoil section whose properties are given above is represented in **Figure 3**.

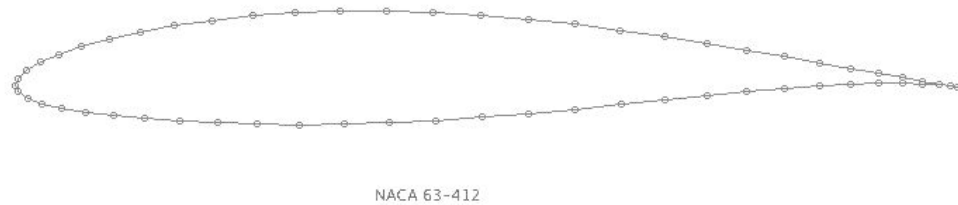


Figure 3: NACA 63-412 airfoil section

2.3.2 WING LOADING

1. Wing Loading is firstly limited by Stall Speed where:

Stall Velocity (V_{stall}) = 65km/h as given in **Table 2**.

Air density (ρ_∞) = 1.225 kg/m³

$$W/S_{\text{stall}} = 0.5 \frac{\rho_{\infty} \cdot V_{\text{stall}}^2 \cdot C_{L\text{max}}}{g} \quad (8)$$

Eq(8) which is a form of lift equation gives a wing Loading at stall of 47.63 kg/m²

2. Wing Loading during Cruise (10,000ft, 130km/h)

To maximize cruise distance, parasite drag is equal to induced drag which are equated in Eq(9) parametrically.

$$q \cdot S \cdot C_{D,0} = q \cdot S \frac{C_L^2}{\pi e \cdot AR} \quad (9)$$

$$C_{D,0} = \frac{S_{\text{wet}}}{S} \cdot C_{fe}$$

where

C_{fe} is a function of Reynolds number so that should be evaluated first:

$$d = 0.5 \text{m}$$

$$\mu = 1.73 \times 10^{-5} \text{ N.s/m}^2 \text{ for air at sea level,}$$

$$Re = 1.28 \times 10^6$$

$$\text{So: } C_{fe} = 0.008 \text{ as read from Fig 2, page 6-2 [11] and } C_{D,0} = 0.032$$

$$AR = 8 \text{ and } e \text{ can be approximated to } 0.95 \text{ as described in page 81 of [12].}$$

$$\text{At } 10,000 \text{ft } \rho_{\infty} = 0.904 \text{ kg/m}^3$$

$$W/S_{\text{cr}} = \left[\frac{1}{2} \cdot (\rho_{\infty}) V_{\text{cr}}^2 \right] \cdot \frac{\sqrt{C_{D0} \cdot \pi \cdot AR \cdot e}}{g} \quad (10)$$

$$\text{Eq(10) which is a combination of Eq(8) and Eq(9) yields } W/S_{\text{cr}} = 52.52 \text{ kg/m}^2$$

3. Wing Loading during Loiter (10,000ft, 100km/h)

Repeating the procedure in step 2, the following is obtained:

To maximize endurance by minimizing the total drag, the aircraft flies at an angle of attack resulting in a parasite drag that is equal to 1/3 of the induced drag, which is given parametrically in Eq(11), therefore:

$$W/S_{\text{loiter}} = \left[\frac{1}{2} \cdot (\rho_{\infty}) \cdot V_{\text{loiter}}^2 \right] \cdot \frac{\sqrt{3C_{D0} \pi AR \cdot e}}{g} \quad (11)$$

Eq(11) yields $W/S_{\text{loiter}} = 53.82 \text{ kg/m}^2$

4. Final Wing Loading and Reference Area:

Among the three wing loadings, the least one was selected for reference area calculation as that would be the smallest area that is supposed to be built in order to survive all of the cases.

Wing Loading = 47.63 kg/m^2

$S_{\text{ref}} = W_0 / (W/S)$ yielding $S_{\text{ref}} = 1.832 \text{ m}^2$

2.3.3 POWER TO WEIGHT RATIO

1. According to V_{max} Requirement:

At maximum weight, maximum speed and cruise ceiling the power required is as follows: For $V_{\text{max}} = 240 \text{ km/h}$ and $W/S = 47.63 \text{ kg/m}^2 = 467.25 \text{ N/m}^2$

$$\frac{T}{W} = \frac{1}{2} \cdot \rho_{\infty} \cdot V_{\text{max}}^2 \cdot \frac{C_{D0}}{W/S} + \frac{2K}{\rho_{\infty} \cdot V_{\text{max}}^2} \cdot W/S \quad (12)$$

Eq(12) formulating the thrust to weight ratio yields $T/W = 0.147$

$$\frac{P}{W} = \frac{T}{W} \cdot \frac{V_{\text{max}}}{550 \frac{\text{ft} \cdot \text{lb}}{\text{sec} \cdot \text{hp}} \cdot \eta_{\text{pcruise}}} \quad (13)$$

Eq(13) formulating power to weight ratio where $\eta_p = 0.8$ and V_{max} is in ft/sec yields $P/W = 0.0730 \text{ hp/lb}$

Resulting in a power required value of: $P_R=14.03$ hp at cruise ceiling,

Correcting this value with respect to the sea level, $P_R=19.03$ hp

2. According to Vmax Requirement at Sea Level:

The power ratio of sea level requirement and 10000ft requirement are related with the ratio of the air densities; that results in:

$P/W=0.0959$ and $P_R=18.42$ hp

3. According to Service Ceiling (20,000ft):

At 20,000ft where $\rho_\infty=0.653$ kg/m³, Eq(14) defines the rate of climb

$$V_{RCmax} = \sqrt{\frac{2}{\rho_\infty}} \cdot \sqrt{\frac{K}{3C_{D,0}}} \cdot \frac{W_0}{S_{ref}} \quad (14)$$

that is $V_{RCmax}=30.394$ m/s. Knowing that the service ceiling is defined as the level where $RC_{max}=100$ ft/min, the corresponding power to weight ratio is formulated in Eq(15).

$$\frac{P}{W} = \frac{1}{\eta_{pcruise}} \cdot \left[RC_{max} + V_{RCmax} \left(\sqrt{K \cdot \frac{C_{D0}}{3}} + \sqrt{3 \cdot K \cdot C_{D0}} \right) \right] \quad (15)$$

Eq(15) yields $P/W=3.951$ m/s which corresponds to:

$P_{ceiling}=344.76$ (N.s)=4.52 hp With power matching to sea level, $P_R=8.49$ hp

4. Final Power Requirement:

The highest power requirement is for reaching the maximum velocity, that is: $P_R=19.03$ hp

2.4 CONFIGURATION LAYOUT

2.4.1 ENGINE

To fulfil the power required with a safety factor of 10%, Limbach L275 two-stroke, two-cylinder and piston-prop engine was selected which provides 21 BHP at 7000rpm at sea level and has 8 kg dry weight.

2.4.2 TRACTOR/PUSHER CHOICE

Both the configurations have their specific advantages and disadvantages; however, one specific benefit of pusher aircraft forced the decision. As the UAV will be used for tactical means, specifically for carrying camera systems, the nose section of the aircraft is rather left available for the payload. As the required power is not so high to make two engines on each wing feasible, the pusher design is adopted. The only critical problem with the pusher design is possible cooling problems of the engine that is blocked by the fuselage.

Furthermore, the pusher configuration has a drawback of affecting the centre of gravity adversely. In current case where there is no cockpit at the front of the aircraft, this might be a worse problem. In order to balance the adverse moment, the tail should have a large moment arm. To handle this without coming up with a huge aircraft, a boom tail is preferred. By this manner, a longer tail can be built without adding a lot of extra weight to the aircraft.

2.4.3 FUSELAGE SIZING

$$l_f = a \cdot W_{0i}^c \quad (16)$$

Fuselage length is empirically related to the gross weight by Eq(16) given in Table 6.3 in [10] where for a home-built composite aircraft:

$$a=1.28; C=0.23 \quad \text{that gives} \quad l_{a/c}=3.575\text{m}$$

However, the empirical formula above is valid for aircraft with conventional tail. In our case, as the aircraft tail has a boom for connection, the tail is not considered in the fuselage length. Taking the value above as the total length of the aircraft, a factor of 0.55 is used for fuselage to total length fraction, keeping the fuselage slightly longer than the half length of the aircraft as is common along the competitor aircraft. Then the fuselage length becomes: $l_f=1.966\text{m}$

The height and width of the fuselage are also initially guessed. Considering the competitor aircraft and taking into account the practicality of placing the payload, fuel and electronics to the fuselage section, a square fuselage section of 0.3m wide and 0.3m high is adopted. Not to confuse with stability parameters, letter h is reserved and w is used instead. Thus $w_f=0.3\text{m}$

2.4.4 WING CONFIGURATION

The aspect ratio previously found is relatively high to eliminate tip effects, but still a slight taper will help increase the aerodynamic efficiency of the wing. Therefore a mild taper of 0.45 is selected. For the sake of easy manufacturing, a zero quarter chord sweep angle is used. The design choices mentioned are formulated below:

$$b = \sqrt{AR \times S_{ref}} \quad \text{that is} \quad b=3.828$$

$$C_r = \frac{S_{ref}^2}{(1+\lambda) \times b} \quad C_r=0.605 \text{ m} \quad \text{and} \quad C_t=0.272 \text{ m}$$

$$\bar{c} = \frac{2}{3} C_r \left(\frac{1+\lambda+\lambda^2}{1+\lambda} \right) \quad \bar{c} = 0.460\text{m}$$

$$\bar{y} = \frac{b}{6} \left(\frac{1+2\lambda}{1+\lambda} \right) \quad \bar{y} = 0.836 \text{ m}$$

The choice between high, mid and low wing configurations is made in favour of high wing configuration. The advantages of high wing design in aerodynamic efficiency and stability were the reasons behind the choice. A mid-wing design would divide the precious space in the fuselage making it harder and less efficient to arrange the payload configuration within the fuselage. On the other hand, a lower wing has the major benefit of being able to place the landing gear on the wings easily however, having a pusher configuration with boom tail, the load of the tail will be carried by the wings and adding the landing loads to the wings as well would require very rigid and heavy wings, making the design less and less feasible.

2.4.5 FUEL TANK SIZE AND POSITION

Considering the fuel fraction and total weight, the fuel weight can be calculated:

$$W_f = W_{f0} * W_0 \quad \text{that is} \quad W_f = 13.438 \text{ kg}$$

$\rho_{\text{gasoline}} = 737 \text{ kg/m}^3$ and considering the 2% oil additive to 2-stroke engines:

$$V_f = 18.598 \text{ liters}$$

Considering the wings with a high aspect ratio, there is significant number of beam and rib structure within the wings. Also considering the thickness of the wings being relatively small, placing the fuel tanks inside the wings will be unfeasible. Therefore, a separate fuel tank is placed inside the fuselage.

2.4.6 CENTER OF GRAVITY ESTIMATE

A detailed weight build-up is required for the centre of gravity estimation. So each structure was evaluated separately. The most realistic way of weight estimation at this stage is through statistical methods where the weight is related to the wetted surface of the structure. The empirical constants for those relations are listed in

Table 15.2 in [10] where the centre of gravity of the structure is also approximated.

1. Fuselage:

As defined before, the fuselage has a square cross-section, thus

$$S_{wet,f} = (4 * w_f * l_f + 2 * w_f * w_f) = 2.539m^2$$

$$W_f = (1.4) * S_{wet,f} = 16.565kg \quad \text{where} \quad x_f = l_f / 2 = 0.983m$$

2. Wing:

$$W_w = (2.5) * S_{ref} = 22.409kg \quad \text{where} \quad x_w = 40\%MAC \text{ of the wing commonly}$$

3. Engine:

$$W_e = 8kg \quad \text{where} \quad x_e = 0.95 \text{ of } l_f \quad \text{due to the engine location.}$$

4. Payload:

$$W_p = 20kg \quad \text{where} \quad x_p = 0.10 \text{ of } l_f \text{ (as the camera system will be at the front of the aircraft)}$$

$$\bar{x} = \frac{W_e x_e + W_p x_p + W_f x_f}{W_e + W_p + W_f} \quad (17)$$

Using Eq(17) adding up the CG contributions of components, $\bar{x} = 0.789m$ and as $X_{wing} = \bar{x} + (0.40 - 0.25)\bar{c}$; that is $X_{wing} = 0.858m$

In order not to change the centre of gravity of the aircraft as the fuel is drained, the fuel tank should be placed at the centre of gravity of the whole aircraft as much as possible. As the fuel tank will be a separate bladder within the fuselage, it can be placed exactly at the centre of gravity; thus, it doesn't affect the centre of gravity. Now the weights of the wing are included as well for a second guess of the centre of gravity.

$$\bar{x} = \frac{W_e x_e + W_p x_p + W_f x_f + W_w x_w}{W_e + W_p + W_f + W_w} \quad (18)$$

Than using Eq(18) which is the total CG of the aircraft, the initial guess for \bar{x} and iterating the wing position several times, the centre of gravity ends up at $\bar{x} = 0.823m$. A more detailed C.G. analysis has been performed by another member of the design team in along with stability analysis [9].

2.4.7 HORIZONTAL AND VERTICAL TAIL SIZING

1. Horizontal Tail:

$$V_{HT} = \frac{l_{HT} \cdot S_{HT}}{\bar{c} \cdot S_{ref}} \quad (19)$$

Eq(19) formulating the volume ratio is known as 0.5 for homebuilt composite aircraft [10].

The tail is placed to $x_{tail}=3m$ which is an initial guess for one of the major dimensions of the aircraft. The guess was made in accordance with competitor study and the resulting stability character was found competitive in detailed stability analysis of this [9].

With the given tail position, the moment arm is $l_{HT}=x_{HT}-x_{CG}=2.177m$

As a result using Eq(19) $S_{HT}=0.194m^2$

$$b_{HT} = \sqrt{AR_{HT} \times S_{HT}} \quad (20)$$

Selecting a typical aspect ratio of $AR_{HT}=4$, using Eq(20) one gets:

$b_{HT} = 0.881m$, and choosing a simple rectangular plan form, $c_{HT}=0.220m$

NACA 0009 which is a typical symmetric airfoil is selected for the horizontal tail as it carries significantly lower loads when compared to the wing and manufacturability becomes more critical at that stage.

2. Vertical Tail:

$$V_{VT} = \frac{l_{VT} \cdot S_{VT}}{b \cdot S} = 0.04 \quad (21)$$

Eq(21) formulating the volume ratio is given in [10] as 0.04 for homebuilt composite aircraft.

The tail is placed again to $x_{tail}=3m$ so the moment arm becomes

$$l_{HT}=x_{HT}-x_{CG}=2.177m$$

Additionally dividing by 2 to get S value for a single vertical tail
 $S_{VT}=0.0644m^2$

A typical AR for the vertical tail is 1.2 so $h_{VT} = 0.278m$ using Eq(22)

$$h_{VT} = \sqrt{AR_{VT} \times S_{VT}} \quad (22)$$

A taper ratio of 0.6 is chosen for the vertical tail so:

$$c_r=0.290m \quad \text{and} \quad c_t=0.174m$$

Vertical location of the mean aerodynamic chord is: $z_{VT}=0.127m$

Mean aerodynamic chord is: $c_{VT}=0.237m$

The same symmetric airfoil as in the horizontal tail, which is NACA0009 is used for the vertical tail.

2.4.8 PROPELLER SIZING

For two bladed propellers, the propeller diameter is calculated by the following empirical formula:

$$D = (2.2) \times P^{0.25} = 47.095in = 1.196m$$

It should be checked if the tip speed creates any compressibility problems:

$V_{tip} = \pi \cdot n \cdot D = 438m/s$ where $n=7200rpm$, which is well above the speed of sound at the sea level. Therefore the diameter is limited with tip speed constraint and can no longer be optimized with the empirical formula given.

In a more detailed calculation, the total velocity of the blade tip performing a helical motion is equal to the speed of sound for the limiting value of the blade diameter that is free from compressibility effects. The speed of sound mentioned above should be the speed of sound at the service ceiling so that the blade tips never face compressibility effect throughout the aircrafts flight envelope.

Thus: $\sqrt{V_{tip}^2 + V_{max}^2} = c$ where c is the speed of sound at 20,000ft, that is $c=316\text{m/s}$ so $V_{tip}=308.9\text{m/s}$ and the corresponding diameter is $D=0.819\text{m}$. Giving a safety factor of 10%, our limiting value for propeller diameter is $D=0.737\text{m}$.

2.4.9 LANDING GEAR PLACEMENT

The engine is at the back of the aircraft; therefore the tail dragger configuration is not suitable for the aircraft. Furthermore, the bicycle configuration is not stable enough for the ground roll and requires additional wing tip wheels for the sake of stability. Therefore the choice is to adopt the tricycle configuration.

2.4.10 WING PLACEMENT

$$\frac{x_{acwb}}{\bar{c}} = \frac{x_h}{\bar{c}} - V_{HT} \frac{a_t}{a} \quad (23)$$

where in Eq(23) defining static margin $K_n = \frac{x_n - \bar{x}}{\bar{c}} = 0.1$ and $a_t = a$ one gets, $X_n = 0.869\text{m}$ and $x_{acwb} = 0.639\text{m}$

2.4.11 BETTER WEIGHT ESTIMATION

A structure based weight estimation was used for major parts of the aircraft for calculation of the centre of gravity. The same procedure based on the Table 15.2 in [10] is followed for all the structures and components of the aircraft to come up with a better weight estimation.

1. Fuselage:

$$W_{\text{fuselage}} = (1.4) * S_{\text{wet, fuselage}} = 16.57\text{kg}$$

2. Wing:

$$W_{\text{wing}} = (2.5) \cdot S_{\text{ref}} = 22.41 \text{ kg}$$

3. Engine:

$$W_{\text{engine, installed}} = (1.4) W_{\text{engine}} = 11.40 \text{ kg}$$

4. Payload:

$$W_{\text{payload}} = 20.00 \text{ kg}$$

5. Horizontal Tail:

$$W_{\text{HT}} = (2.0) \cdot S_{\text{HT}} = 1.90 \text{ kg}$$

6. Vertical Tail:

$$W_{\text{VT}} = (2.0) \cdot S_{\text{VT}} = 0.63 \text{ kg} \quad \text{each adding up to} \quad W_{\text{VT}} = (2.0) \cdot S_{\text{VT}} = 1.26 \text{ kg}$$

7. Tail Boom:

$$W_{\text{Boom}} = 1.20 \text{ kg}$$

8. Landing Gear

$$W_{\text{LG}} = (0.057) W_0 = 4.97 \text{ kg}$$

9. Remaining Weight:

$$W_{\text{remaining}} = (0.1) W_0 = 8.73 \text{ kg}$$

10. Fuel Weight:

$$W_{\text{fuel}} = (0.154) W_0 = 13.44 \text{ kg}$$

The total weight sums up to:

$$W_0 = 101.88 \text{ kg}$$

As some of the calculations depend on the gross weight, the new gross weight should be used and the weight calculation should be iterated to find a better weight estimation. The total weight of fuselage, wings, engine, payload, tails and tail boom are independent of gross weight W_{constant} . The rest is a function of gross weight as follows $W_{\text{rest}} = (0.057 + 0.1 + 0.154) W_0$

Then: $W_0 = 74.732\text{kg} + (0.311) \cdot W_0$ solving the equation gives $W_0 = 108.46\text{kg}$

In these circumstances, the size of the fuel tank now becomes:

$W_f = (0.154)W_0 = 16.704\text{kg}$ and $V_f = 23.117$ litres

The better weight estimation is verified by weighing the aircraft at the end of manufacturing process. Table 3 represents the verification of the estimations made. When the percentage of errors is evaluated, the estimations can be found appropriate especially for the wings, which is a rather complicated part to estimate. The total error being around 6% can prove the estimation procedure's effectiveness for tactical size UAV's.

Table 3: Verification of Weight Estimations

Component	Weight Estimation	Weight Measurement	Percent Error in Estimation
Fuselage	16,57	14,14	17,19%
Left Wing	11,20	10,86	3,13%
Right Wing	11,20	10,97	2,10%
Engine	11,40	9,31	22,45%
Tail	3,16	2,93	7,85%
Tail Boom	1,20	2,03	40,89%
Landing Gear	4,97	5,96	16,61%
Total Empty Weight	59,70	56,20	6,23%

CHAPTER 3

PERFORMANCE ANALYSIS

Performance analysis has been conducted to verify that the requirements are met and the next phase of design and manufacturing can be initiated.

3.1 WING LOADING

Wing loading is calculated using the previously found total weight and reference area calculations as follows:

$$W/S = \frac{W_0}{S_{ref}} \quad \text{with } W_0=101.87\text{kg and } S_{ref}=1.832\text{m}^2$$

$W/S = 55.61 \text{ kg/m}^2$ where aimed value was slightly lower ($W/S=47,63 \text{ kg/m}^2$).

$$V_{stall} = \sqrt{\frac{W/S \cdot g}{0.5 \rho_{\infty} \cdot C_{Lmax}}} \quad \text{with } C_{Lmax}=2.34$$

$V_{stall}=19.51\text{m/s} = 70.23\text{km/h}$ where the aimed value was $V_{stall}=65\text{km/h}$.

3.2 POWER LOADING

Using final weight estimation and real engine power value:

$$\frac{P}{W_0} = 0.194 \frac{\text{hp}}{\text{kg}} \text{ which is relatively higher than the aimed value of } 0.161 \frac{\text{hp}}{\text{kg}}.$$

3.3 POWER REQUIRED AND POWER AVAILABLE CURVES

$$D = D_0 + D_i$$

$$D_0 = \frac{1}{2} \cdot \rho_{\infty} \cdot V_{\infty}^2 \cdot S_{\text{ref}} \cdot C_{D0} \quad (24)$$

$$D_i = \frac{2 \cdot K \cdot S_{\text{ref}}}{\rho_{\infty} \cdot V_{\infty}^2} W^2 / S^2 \quad (25)$$

Figure 4 is drawn using basic drag equations Eq(24) and Eq(25) with $C_{D0}=0.032$, $K=0.04$, which were calculated during conceptual design phase while calculating wing loading. The graph represents the lowest drag value at around 30m/s which corresponds to the loiter velocity assumed before as 100km/h=28m/s

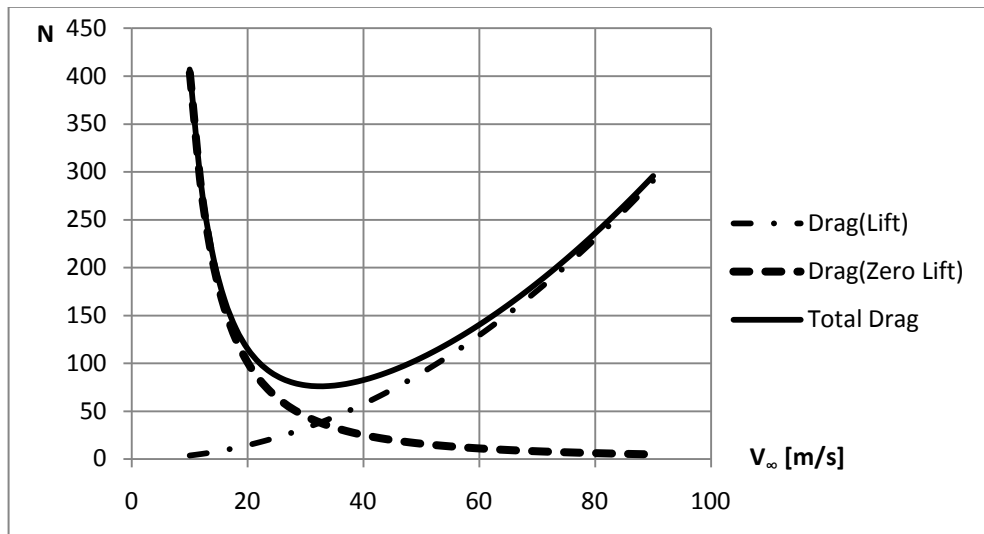


Figure 4: Drag variation graph

Fuel weight is not a major part of the total weight therefore the fuel spent during takeoff and climb is neglected and W_{cr} is replaced with W_0 in Eq(26), Eq(27) and Eq(28) which are straightforward formulation of lift to drag ratios. The neglecting

also provides a small safety factor to the calculations. The resulting variations are graphed in **Figure 5**.

$$\frac{CL}{CD} = \frac{\frac{2 \cdot W_0 \cdot g}{\rho_{\infty} \cdot S_{\infty} \cdot V_{\infty}^2}}{C_{D0} + K \left(\frac{2 \cdot W_0 \cdot g}{\rho_{\infty} \cdot S_{ref} \cdot V_{\infty}^2} \right)^2} \quad (26)$$

$$\frac{CL^{3/2}}{CD} = \frac{\left(\frac{2 \cdot W_0 \cdot g}{\rho_{\infty} \cdot S_{\infty} \cdot V_{\infty}^2} \right)^{3/2}}{C_{D0} + K \left(\frac{2 \cdot W_0 \cdot g}{\rho_{\infty} \cdot S_{ref} \cdot V_{\infty}^2} \right)^2} \quad (27)$$

$$\frac{CL^{1/2}}{CD} = \frac{\left(\frac{2 \cdot W_0 \cdot g}{\rho_{\infty} \cdot S_{\infty} \cdot V_{\infty}^2} \right)^{1/2}}{C_{D0} + K \left(\frac{2 \cdot W_0 \cdot g}{\rho_{\infty} \cdot S_{ref} \cdot V_{\infty}^2} \right)^2} \quad (28)$$

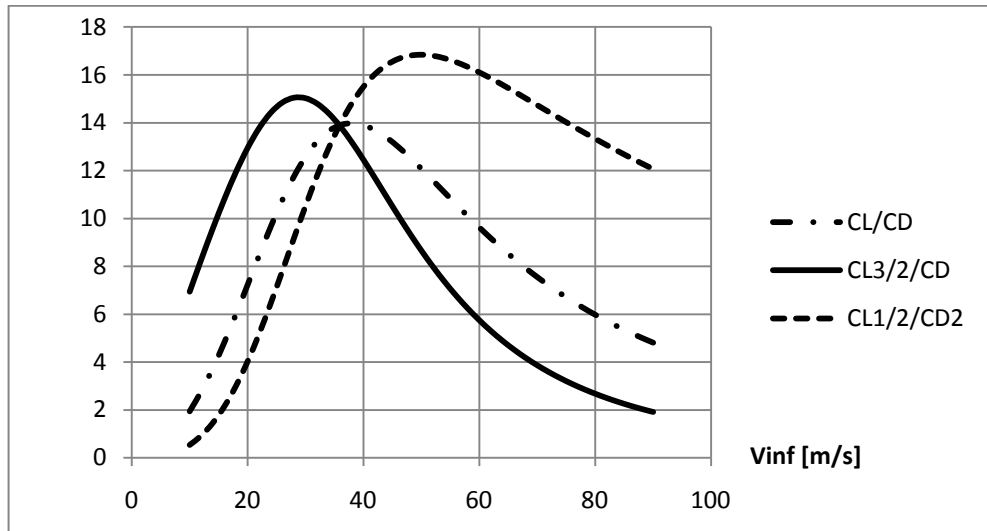


Figure 5: Lift to drag ratios graph

The Lift to Drag Ratios represents different flight conditions. For example:

- When the aircraft flies at its $(C_L/C_D)_{\max}$ velocity, it travels to its maximum range, thus this velocity is used for cruise missions. In **Figure 5** the lowest C_L/C_D ratio is at around 40m/s with $C_L/C_D=14$. The exact value of the cruise velocity is given in Eq(29).
- When the aircraft flies at its $(C_L^{3/2}/C_D)_{\max}$ velocity, it travels for its maximum endurance, thus this velocity is used for loiter missions. In **Figure 5** the lowest $C_L/C_D^{3/2}$ is at around 30m/s as is also concluded in **Figure 4**. The lowest $C_L/C_D^{3/2}$ value is around 15.
- The $(C_L^{1/2}/C_D)_{\max}$ value is also used for certain calculations such as required power as a function of velocity, giving a characteristic of the aircraft. In **Figure 5** the lowest $C_L/C_D^{1/2}$ is at around 50m/s with $C_L/C_D^{1/2}=17$.

$$V(L/D_{\max}) = \sqrt{\frac{2}{\rho_{\infty}} \sqrt{\frac{K}{C_{D0}}} \frac{W_0}{S_{\text{ref}}}} g = 37.90\text{m/s} = 136.45\text{km/h} \quad (29)$$

Power Required:

Power required and power available varies as in Eq(30) and Eq(31), which are calculated in cruise altitude.

$$P_R = \frac{W_0 \cdot g}{[C_L^{1/2}/C_D]} \sqrt{\frac{2 \cdot W_0 \cdot g}{\rho_{\infty} \cdot S_{\infty} \cdot V_{\infty}^2}} \quad (30)$$

$$P_{A,3k} = P \cdot \frac{\rho_{\infty,3k}}{\rho_{\infty}} = 15.497\text{hp} \quad (31)$$

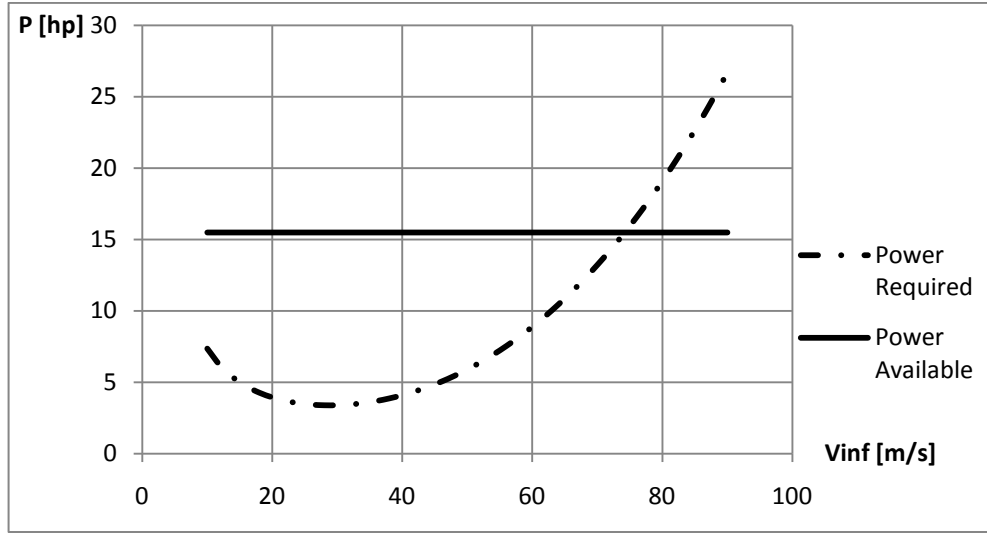


Figure 6: Power required and available graph

The intersection point, where power available and power required curves drawn in **Figure 6** coincide, is the maximum velocity point of the aircraft at 3000m altitude after which the power of the engine is not sufficient to sustain the velocity of the aircraft. This maximum velocity at cruise altitude can be read from **Figure 6** which is calculated precisely as Maximum Velocity at 3000m is: $V_{\max 3k} = 74.2 \text{ m/s} = 267 \text{ km/h}$ which is quite above the requirement of 200km/h given in **Table 2**.

3.4 RATE OF CLIMB AND CLIMB VELOCITY

The following formula is a rough general formula for density variation with altitude:

$$\rho_{\infty, Z} = (6.10) \cdot 10^{-19} \cdot Z^4 - (7.10) \cdot 10^{-14} \cdot Z^3 + (4.10) \cdot 10^{-9} \cdot Z^2 - 10^{-4} \cdot Z + 1.225$$

Best rate of climb rate is given in Eq(32) which is plotted in **Figure 7**. Additionally rate of climb variation with altitude is given in Eq(33) and plotted in **Figure 8**.

$$V_{R/C(\text{altitude})} = \sqrt{\frac{2}{\rho_{\infty}} \cdot \sqrt{\frac{K}{3 \cdot C_{D0}}} \cdot \frac{W_0}{S_{\text{ref}}} \cdot g} \quad (32)$$

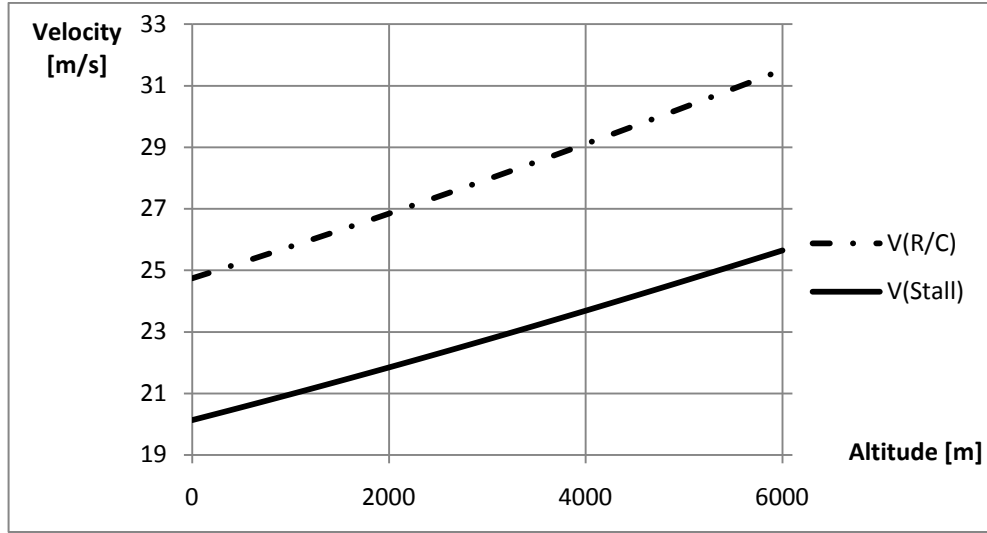


Figure 7: Variation of best rate of climb velocity with altitude graph

$$R/C_{(altitude)} = \frac{\eta_p \cdot P_{inf,altitude}}{W_0 \cdot g} - \left(\sqrt{\frac{2}{\rho_{inf,altitude}} \cdot \sqrt{\frac{K}{3 \cdot C_{D0}} \cdot \frac{W_0}{S_{ref}} \cdot g}} \right) \cdot \frac{1.155}{L/D_{max}} \quad (33)$$

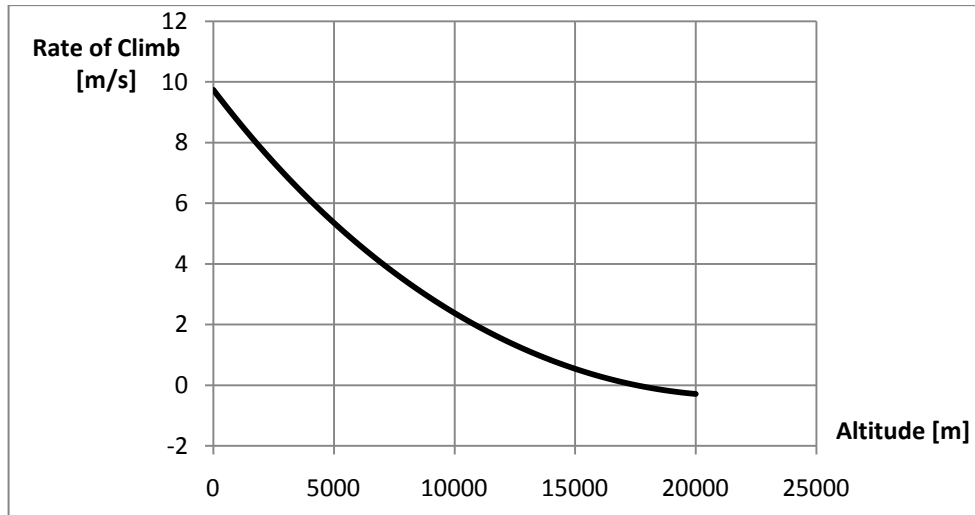


Figure 8: Rate of climb variation with altitude graph

Figure 7 represents the best rate of climb velocity which increases with altitude and is higher than the stall velocity at all altitudes. Absolute Ceiling is where Rate of Climb is zero and the service ceiling is where Rate of Climb is 100ft/min; that is 0.508m/s. When the graph in **Figure 8** is considered, the rate of climb is as high as 10m/s at sea level and decreases to 0.5m/s at 15000m which is the service ceiling and decreases to a vertical level at 17500m which is the absolute ceiling of the aircraft. Which are not quite realistic considering the non-linear drop of performance of the reciprocating engine at those altitudes but still as these altitudes are very well above the intended flight altitudes of the aircraft there is a large safety margin for these values.

3.5 TIME TO CLIMB

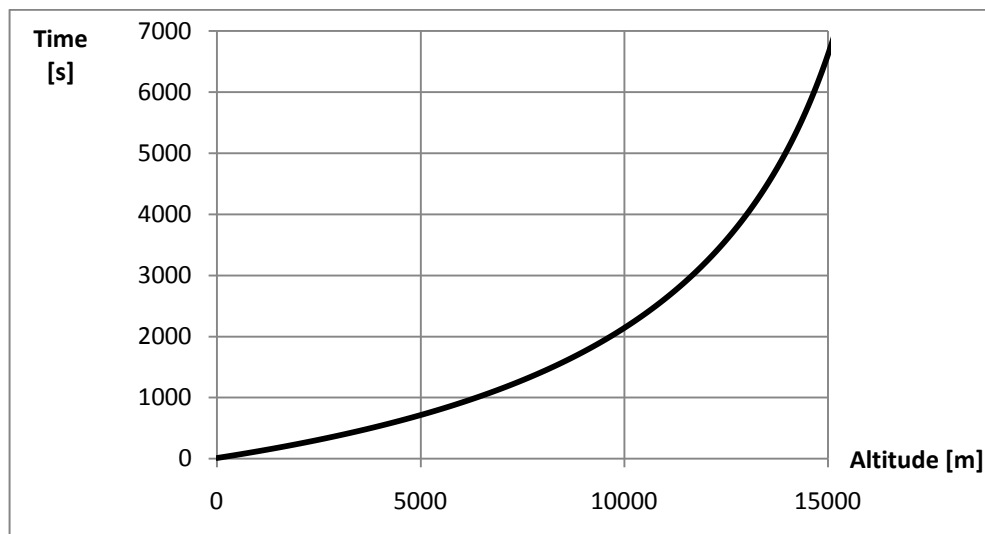


Figure 9: Time to climb altitude graph

By evaluating the **Figure 9**, which is drawn by integrating the rate of climb over time, the following key times to climb are calculated: $t_{3000}=6.1$ minutes and $t_{15000}=107.1$ minutes where 6 minutes to climb the cruise altitude is sufficient for operation.

3.6 BEST ANGLE AND RATE OF CLIMB

Vertical velocity is calculated by: $V_v = \left(\frac{P \cdot \eta_p}{W_0 \cdot g \cdot V_\infty} - \frac{D}{W_0 \cdot g} \right) \cdot V_\infty$, where D is the total drag at the velocity V_∞ calculated previously.

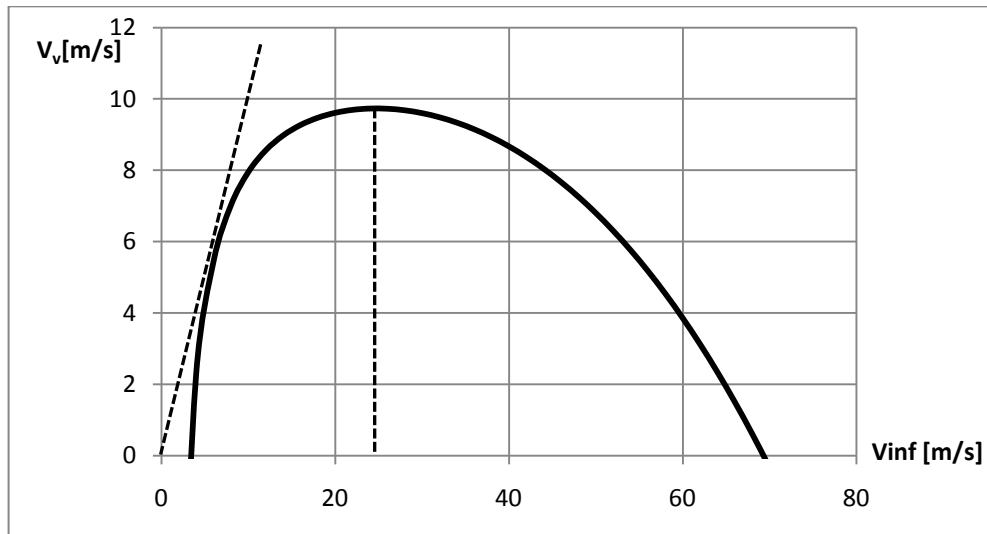


Figure 10: Hodograph for climb performance

The best angle of climb is around 6m/s in the graph in **Figure 10**, however, taking into consideration that this velocity is way below the stall velocity (20.130m/s), the aircraft should climb at its stall velocity for best climb angle. The fastest climb is at around 25m/s which is the top point on **Figure 10**, supporting the previous findings.

3.7 RANGE

Range of the aircraft can be calculated using Eq(34) given in [10].

$$R = \frac{\eta_p}{C} \cdot (L/D)_{\max} \cdot \ln \frac{W_0}{W_0 - W_f} = 1367.378 \text{ km} \quad (34)$$

where $C_{bhp} = 0.375 \text{ kg/hp-h} = 1.370 \times 10^{-6} \text{ [1/m]}$

Which is significantly higher than the requirement of 600km.

3.8 ENDURANCE

Endurance can be calculated using Eq(35) given in [10]

$$E = \frac{\eta_p}{C} \cdot \sqrt{2 \cdot \rho_{\infty} \cdot S_{\text{ref}}} \cdot \left(\frac{C_L^{3/2}}{C_D} \right)_{\max} \cdot ((W_0 - W_f)^{-1/2} - (W_0)^{-1/2}) \quad (35)$$

At Sea Level: $E = 43414 \text{ s} = 12.060 \text{ hrs}$

At Cruise Altitude: $E = 37294 \text{ s} = 10.360 \text{ hrs}$

The engine has a fixed pitch propeller so its efficiency at endurance speed is lower (taken as 0.7). The endurance value is also way higher than the requirement of 5 hours.

3.9 MAXIMUM LOAD FACTOR

Load factors can be calculated using Eq(36) and are drawn in **Figure 11**. With turn rates in Eq(38), **Figure 12** was drawn.

$$n_{\max} = \sqrt{\frac{1}{2} \rho_{\infty} V_{\infty}^2 \left[\left(\frac{P}{V_{\infty} W_0 g} \right) - \frac{1}{2} \rho_{\infty} V_{\infty}^2 \frac{C_{D0}}{S_{\text{ref}} g} \right]} \quad (36)$$

$$n_{\max \text{ Stall, SL}} = \frac{1}{2} \rho_{\text{inf}} V_{\text{inf}}^2 \frac{C_{L \max}}{S_{\text{ref}} g} \quad (37)$$

$$\psi = \frac{g \sqrt{n^2 - 1}}{V_{\infty}} \quad (38)$$

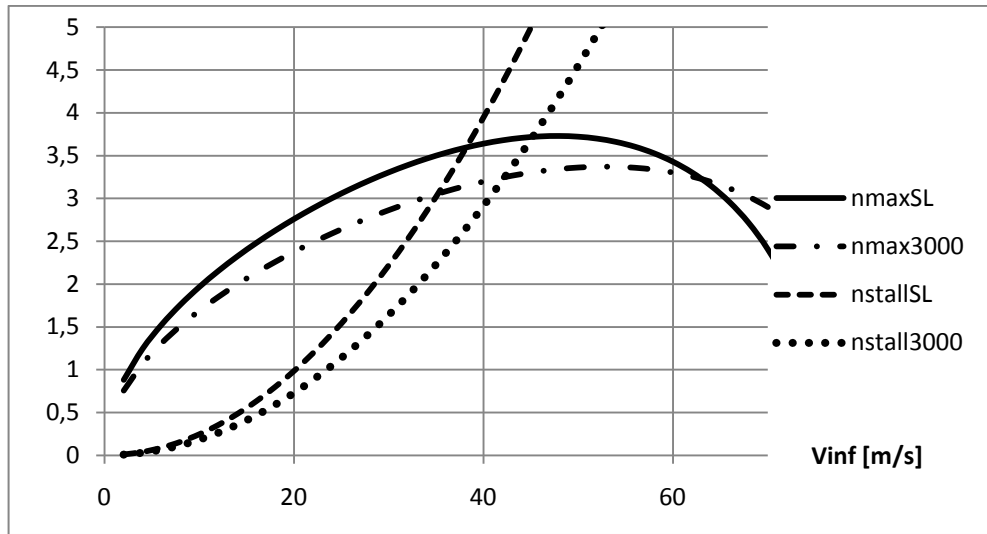


Figure 11: Load factors graph

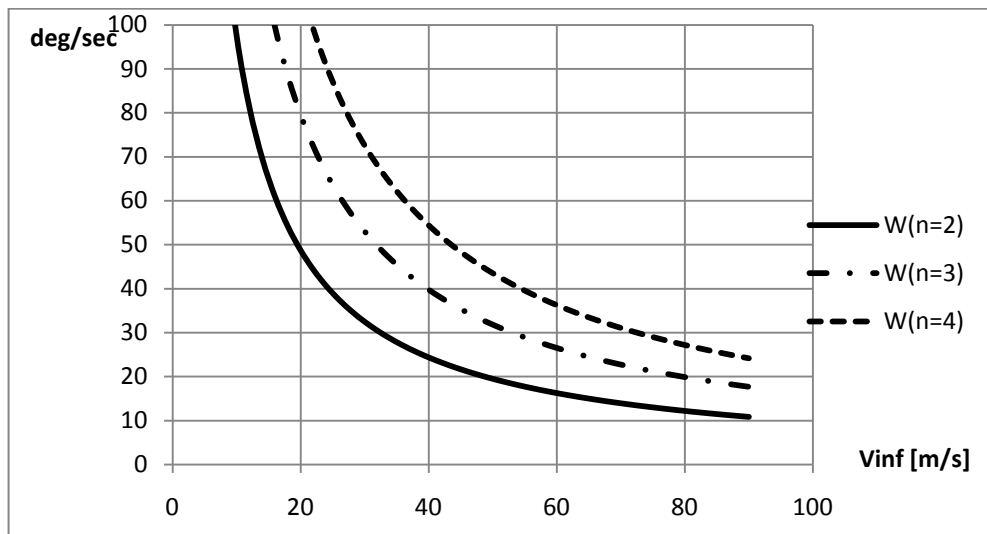


Figure 12: Turn rates graph

Figure 11 represents that the aircraft can reach load factors up to 3.8 at sea level and up to 3.4 at cruise altitude. The stall lines represent the flight envelope which justifies the straight flight stall velocities of around 20m/s at sea level and around 23m/s at

cruise altitude. **Figure 12** represents that for instance at cruise velocity of around 40m/s, staying below the load factor limit of 3.8, the aircraft can make manoeuvres with turn at rates up to 50 degrees per second.

3.10 V-N DIAGRAM

The load factors are limited to certain standard values which yield the flight envelope of the aircraft. Below are the standard and calculated limitations which yield the flight envelope in **Figure 13**.

$$n_{\text{maxpositive}} = 3.8 \quad (\text{read from Figure 11})$$

$$n_{\text{maxnegative}} = (-0.4).n_{\text{maxpositive}} = -1.52$$

$$V_{\text{Dive}} = 1.25 V_{\text{max10k}} = 92.75 \text{m/s}$$

$$V_{\text{Never Exceed}} = 0.9 V_{\text{Dive}} = 83.475 \text{m/s}$$

$$C_{L\text{max}} = 1.44 \quad (\text{as the flaps are not used during flight})$$

$$C_{L\text{maxnegative}} = -1.0$$

Stall speeds under positive and negative maximum load factors are given in Eq(39) and Eq(40) which are basic forms of lift equation.

$$V_{\text{Stall,(n)}} = \sqrt{\frac{n_{\text{maxpositive}}}{\frac{1}{2}\rho_{\infty} \frac{C_{L\text{max}}}{S_{\text{ref}}} \frac{W_0}{g}}} \quad (39)$$

$$V_{\text{Stall,(-n)}} = \sqrt{\frac{n_{\text{maxnegative}}}{\frac{1}{2}\rho_{\text{inf}} \frac{C_{L\text{max}}}{S_{\text{ref}}} \frac{W_0}{g}}} \quad (40)$$

Eq(39) yields $V_{\text{Stall,(n)}} = 50.022 \text{m/s}$ and Eq(40) yields $V_{\text{Stall,(-n)}} = 37.964 \text{m/s}$

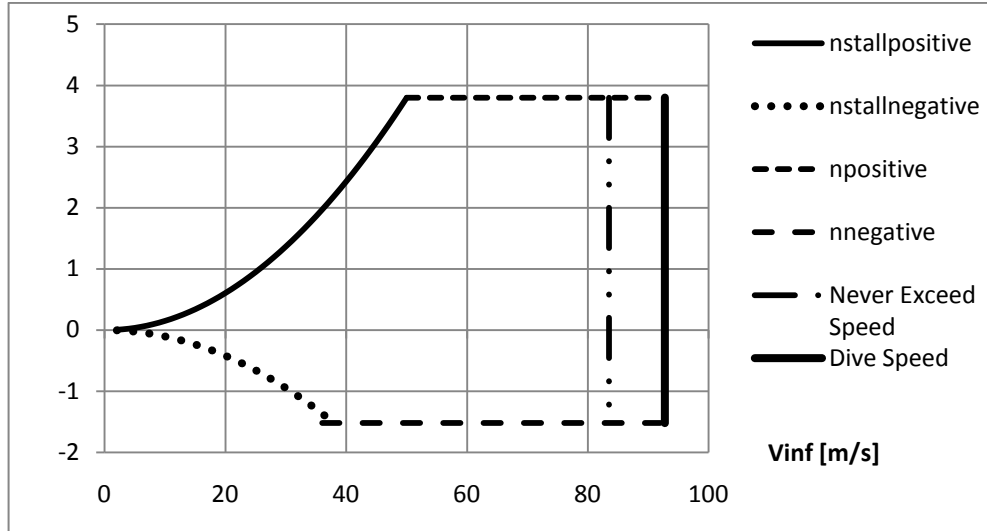


Figure 13: V-N diagram

Figure 13 describes the load factors and velocity combinations at which the aircraft can fly at cruise altitude. For instance with 2g load, the aircraft stalls below the velocity of 36m/s and likewise can manoeuvre with -1g only at speeds above 32m/s.

3.11 LANDING DISTANCE

The parameter in landing distance, $j=1.15$ for commercial airplanes and 1.1 for military airplanes. The configuration is similar to a commercial airplane so $j=1.15$

Reaction time (N)=3s as a pilot standard

Friction coefficient (μ_r)=0.4 that is for both dry concrete and hard turf.

Without flap deflection $CL_{max}=1.44$, so as the wing angle is not known, it is assumed that $CL=1.00$ during ground roll. Then L/W at $0.7 V_{TD}=0.25$

The parameters are used in Eq(41) for evaluation of the landing distance.

$$S_{g,L} = j \cdot N \cdot \sqrt{\frac{2}{\rho_{\infty}} \frac{W_0}{S_{ref}} \frac{1}{C_{Lmax}}} + \frac{j^2 \frac{W_0 \cdot g}{S_{ref}}}{g \cdot \rho_{\infty} \cdot C_{Lmax} \cdot \mu_r \cdot \left(1 - \frac{L}{W_{0.7V_{TD}}}\right)} = 160.50m \quad (41)$$

The landing distance is relatively low for a tactical size aircraft. The value is low due to the fairly low stall velocity which is the result of relatively high lift coefficient. The low landing distance gives the aircraft more value as it will be operable in small air fields making it more functional. Additionally, during operational necessities, the aircraft is capable of making very short emergency landings.

3.12 TAKE-OFF DISTANCE

Similar to landing distance calculation, the same parameters are used in evaluation of Eq(42).

$$S_{g,TO} = \frac{1.21 \frac{W_0 \cdot g}{S_{ref}}}{\frac{P \cdot \eta_p}{g \cdot \rho_{\infty} \cdot C_{Lmax} \cdot \frac{0.77 \times V_{Stall}}{W_0 \cdot g}}} = 37.583m \quad (42)$$

The take-off distance is even lower than the landing distance. The key reason for the significantly low take-off distance is the advantageous reciprocating engine which gives fairly high excess power for the aircraft weight and configuration. The relatively low stall velocity due to high lift coefficient is also reducing the take-off distance.

CHAPTER 4

MATERIAL SELECTION

Most important design choices in manufacturing of Tactical UAV are the material and production technique. Even if the aircraft does not have the mission to act as a protective shield and keep the pilots and crew away from the external dangers, due to the fact that the aircraft is unmanned, it can perform way beyond human limitations. Additionally, opposite to goals of the last century for the manned aircraft of creating more powerful and much bigger aircraft which can carry the most payload, the current trend is to manufacture the smallest and lightest unmanned aircraft possible for the aimed missions. Considering the *de facto* requirements, the current aircraft should be much lighter and should withstand much higher loads. It is why the aerospace industry is one of the leading industries requiring and developing lighter and much stronger materials. The composite material technology is the most promising development that enabled mankind to ask for lighter and stronger materials. The advantages of composite materials against traditional metals can be easily distinguished from **Figure 14** which represents their strength to weight ratio in vertical axis [13]. The organic/inorganic fibres have specific strength and specific stiffness much higher compared to metals such as steel and aluminium. Even if these values are reduced when the fibres are placed inside resin matrices, the advantages are still significant.

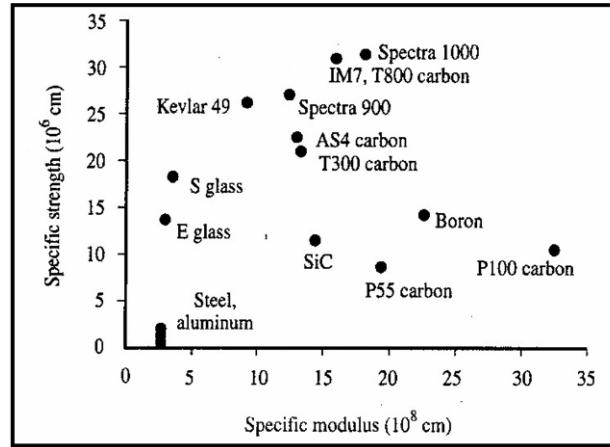


Figure 14: Properties of metal and organic/inorganic fibre materials [13]

Apart from the quantitative advantages of composite materials, they can be machined, formed and repaired much easily; making them even better materials for prototype manufacturing where mold expenses cannot be divided among the mass produced end products and is a significant expenditure item. Additionally, as the prototypes will be used harshly in test flights, reparability is also crucial where repair of metal is not only complicated, but also adds a lot of weight to combine the repaired parts and left-over parts of the aircraft. In contrast, in a composite aircraft, the crashed area can be cut off, sanded, covered with additional composite layers and left for curing for a couple of hours before taking the next mission with no significant weight addition. Due to the numerous advantages of composite materials in unmanned air vehicle manufacturing and specifically in prototype manufacturing, Tactical UAV was manufactured mainly with carbon fibre, aramid fibre (kevlar fibre) and glass fibre woven fabrics with epoxy resin as matrix material. A summary of the composite materials used in Tactical UAV can be found in **Table 4**.

Table 4: Materials used in Tactical UAV

Assembly	Sub-Assembly	Fibre Material	Matrix Material	Additional Materials
Wing	Mold	300gr Glass	Mold Resin	Laminated Wood
	Skin	300gr Glass, 300gr Carbon	Araldite LY 5052 Epoxy	Rohacell 31A
	Spars	300gr Carbon	Araldite LY 5052 Epoxy	Polystyrene Foam, Hornbeam Wood, Aluminium 7075-T6
	Ribs	300gr Carbon	Araldite LY 5052 Epoxy	Polystyrene Foam, Laminated Wood
Fuselage	Mold	300gr Glass	Mold Resin	Laminated Wood
	Skin	300gr Glass, 300gr Carbon 60gr Aramid	Araldite LY 5052 Epoxy	
	Bulkheads			Laminated Wood
	Torque Box	300gr Carbon, 300gr Glass	Araldite LY 5052 Epoxy	
	Parachute Box	300gr Glass	Araldite LY 5052 Epoxy	
Tail	Mold	300gr Glass	Mold Resin	Laminated Wood
	Skin	300gr Glass, 300gr Carbon	Araldite LY 5052 Epoxy	Rohacell 31A
	Spars	300gr Carbon	Araldite LY 5052 Epoxy	Polystyrene Foam
	Booms	Manufactured Externally from a Specially Woven Carbon Fabric		
Landing Gear	Mold			Laminated Wood
	Main	300gr Carbon	Araldite LY 5052 Epoxy	
	Nose			Aluminium 7075-T6

Another critical design choice was the production technique. There are various techniques to administer matrix material into woven fibres. These can be titled as using woven fibres previously impregnated with resin (pre-preg), employing Resin Transfer Molding (RTM) technique and wet lay-up techniques. Pre-preg is the most professional of the three but due to the high costs and difficulties in procurement, transfer and storage, it was not adopted. RTM on the other hand, is beneficial for complicated and highly variable geometries where wet lay-up technique cannot assure homogeneous resin distribution. The RTM entails higher resin consumption and requires additional equipment and expendables. Due to the simplicity of the geometries and the additional costs RTM would introduce, Tactical UAV was mainly produced with wet lay-up technique.

The curing of matrix material can be achieved in different environmental conditions. Two critical parameters that affect the strength of the end product are the temperature and pressure of the curing environment. When the curing is achieved under vacuum, the excessive matrix material not needed to keep the woven fabric together is extracted out of the system both increasing strength due to higher homogeneity and decreasing weight. Additionally, the air trapped inside the system is extracted out of the system preventing air bubble formation during curing which both reduce strength and generate load concentration points resulting in formation of crack mechanisms [14].

Depending on the matrix material used, curing at slightly higher temperatures than atmospheric conditions both decreases viscosity resulting in a more homogenous matrix with the help of vacuum, and results in better cured matrix resulting in a stronger structure. Tactical UAV was mostly manufactured under vacuum and in a temperature-controlled oven [15].

CHAPTER 5

MANUFACTURING

5.1 WINGS

The wing structure of the Tactical UAV is one of the most critical parts that require utmost effort in design and workmanship. Wing design and manufacturing including male and female mold preparation, skin manufacturing, spar and rib integration and wing assembly of Tactical UAV were described in detail by a group including the author of this thesis, so a repetition has not been found necessary [7], [16]. Instead, the wing manufacturing is summarized for the sake of completeness and further detailed within the scope of this thesis. The production of the wings was performed in several steps that can be titled as male and female mold manufacturing, skin manufacturing, spar and rib integration, and finally wing assembly.

5.1.1 MOLD MANUFACTURING

5.1.1.1 MALE MOLD MANUFACTURING

The three-dimensional wing geometry was drawn and produced out of polystyrene foam using a foam cutting machine in two parts span-wise. The remaining parts of the foams were kept unharmed to be used as base material during production. The two parts of each wing were adhered together and covered with glass fibre and epoxy resin to strengthen the male molds one side at a time. The surfaces of the molds were finished using filling material and abrasive paper. When the desired

surface finish was obtained, the male molds were painted and made ready for female mold preparation. The final surface finish of male mold can be seen in **Figure 15(a)** and the male mold positioned over the remaining foam and fixed over the table ready for female mold production can be seen in **Figure 15(b)**.

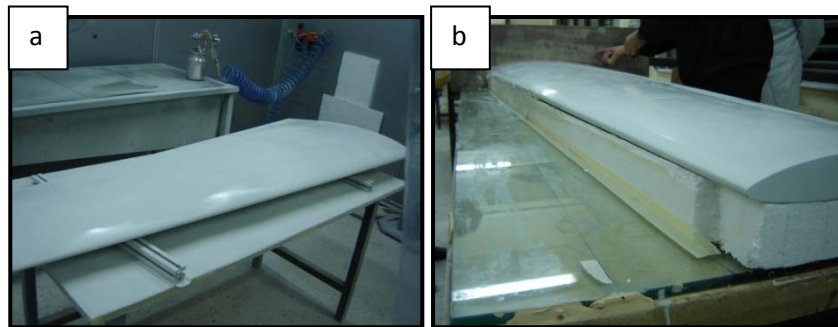


Figure 15: Male mold (a), male mold positioned for female mold production (b)

5.1.1.2 FEMALE MOLD MANUFACTURING

After the male mold was manufactured and positioned correctly, it was framed by a wooden structure to enable production of female mold, as in **Figure 16(a)**. The frame acted as an additional mold surface to give shape to the female mold such that two parts of the female mold faced each other and enabled correct match. The root of the mold was blocked by another wooden plate to create another reference surface in female mold as in **Figure 16(b)**. When the structure was finished, epoxy resin was smeared over the male mold surface and generated the surface of the female mold as in **Figure 16(c)**. After the epoxy resin was hardened yet not completely cured, the surface was covered with several layers of largely woven glass fibre fabric as in **Figure 16(d)**. When sufficient mold thickness was obtained so that the mold would not be distorted during operation, the surface which was actually the back surface of the

mold was strengthened using a wooden skeleton as in **Figure 16(e)**. After the half mold was cured, the structure was turned upside down over the table and after removing the foam support, the same steps were repeated for the second half of the female mold. The final view of the female molds after cleaning and painting can be seen in **Figure 16(f)**.

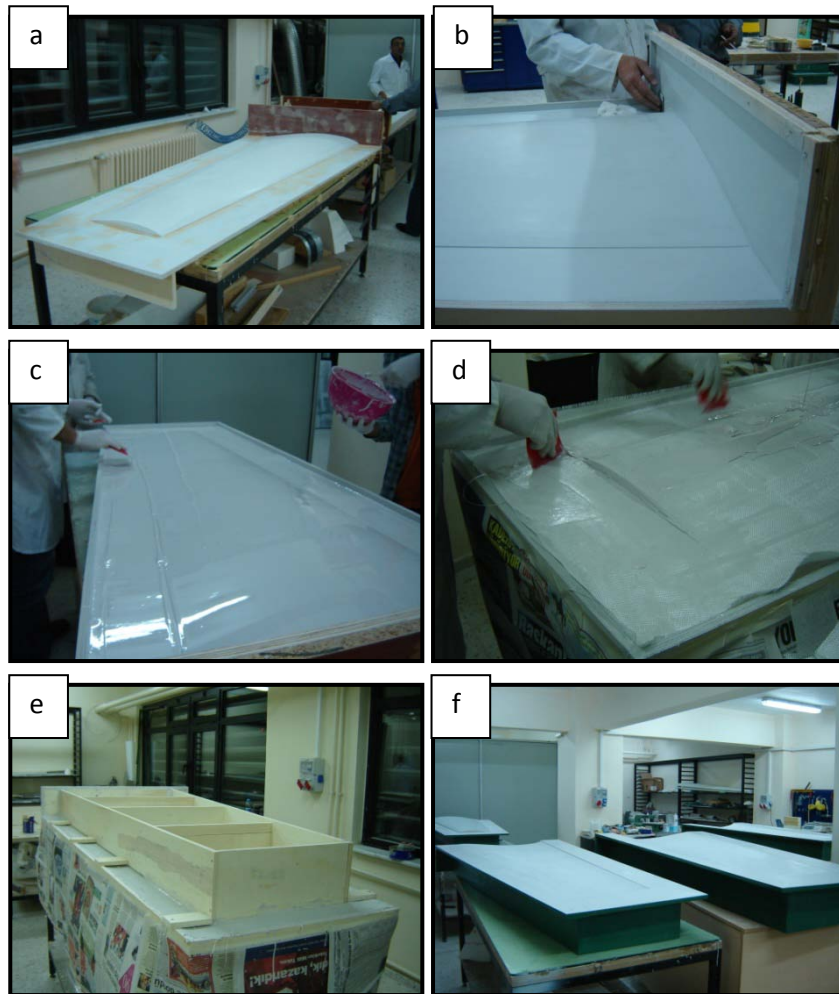


Figure 16: Frame of the male mold (a), root support (b), epoxy resin smeared over the male mold (c), glass fibre fabric laid (d), wooden skeleton on the back side (e), final view of the female molds (f)

5.1.2 WING MANUFACTURING

The loads wing structure are supposed to carry are mainly axial loads as the bending forces acting on the wing create tensile and compressive forces on the lower and upper surfaces of the wing respectively. Second most important type of loads are torsional loads which are carried by torque boxes created inside the wing structure with the help of ribs positioned in right angles to the spars. In overall design, the skin was manufactured out of glass fibre fabric as it was reinforced with inner structures and by itself, the skin did not need to carry significant forces. To prevent skin buckling, skin was thickened using Rohacell 31A foam between glass fibre layers. The reinforcement structures were mainly produced out of carbon fibre fabric as they carried the majority of axial forces due to both bending and torsion. In order to prevent buckling of reinforcing structures, they were thickened by using core materials such as foam cores in spars and both foam and wooden core structures in ribs.

5.1.2.1 SKIN MANUFACTURING

Initially polyester coating was applied as in **Figure 17(a)** for better surface quality. After letting the polyester coating harden for a short time, two layers of glass fibre fabric were laid and wetted with epoxy resin as in **Figure 17(b)**. As the third layer, 2mm thick Rohacell 31A foam was placed and the part of the Rohacell 31A foam where the spar root block would be positioned was cut out and replaced with thin strips of glass fibre fabric as in **Figure 17(c)** to prevent delamination under high loads. Carbon strips were placed along the lines where the spars would be placed to act as the lower surface of the spar structure and create additional strength against tensile loads generated during upward bending of the wings in flight. The composite skin structure was covered with punctured nylon foil and composite blanket as in **Figure 17(d)**. Vacuum ports were positioned, the mold was covered with airtight vacuum bag and the system was pressurized as in **Figure 17(e)**. The wings were cured under

vacuum and in a temperature controlled oven set to 45°C overnight and the resulting lower wing was as in **Figure 17(f)**.

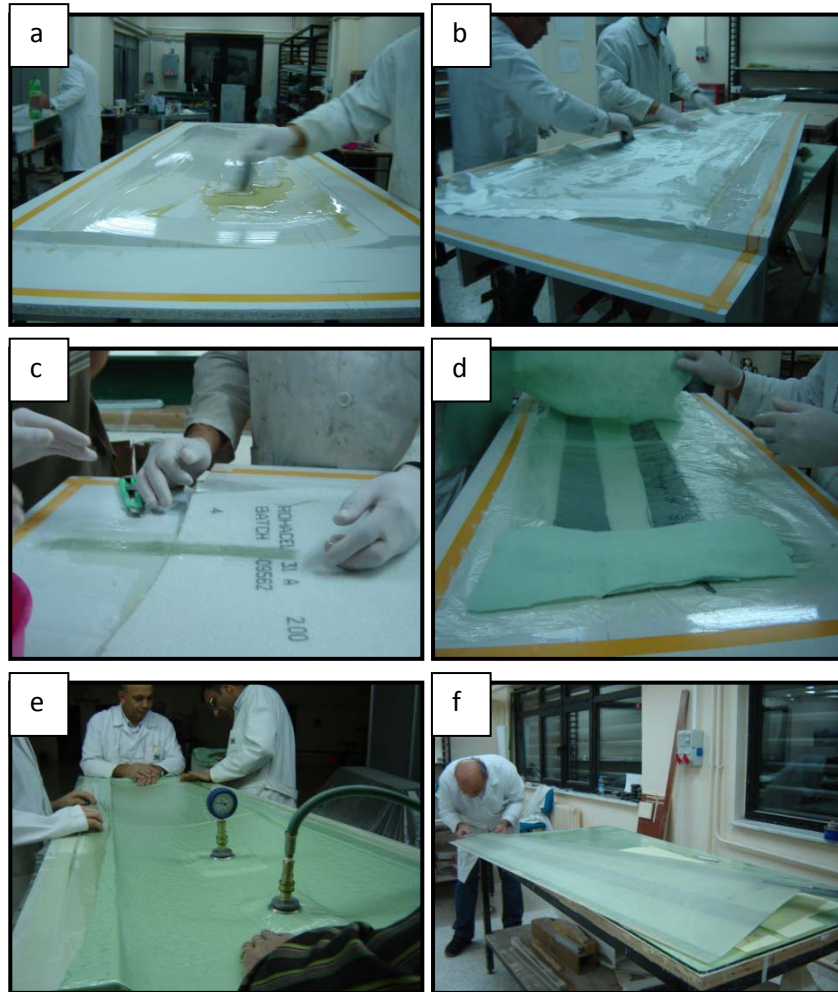


Figure 17: Polyester coating (a), glass fibre layer (b), Rohacell 31A layer (c), carbon strips and vacuum aids (d), vacuum bagging process (e), cured lower skin (f)

5.1.2.2 SPAR MANUFACTURING

The spars are the main load carrying structures of the wing. Rather than manufacturing them separately and adhering them on the wing skins, that would both increase weight due to adhesives and decrease strength losing the advantage of curing the structure once at its position; composite structures of the spars were formed in their positions and cured together with the wings. Thus the spar cores were reinforced with carbon fibre fabric at their sides and were positioned and fixed in position as in **Figure 18(a)** and **Figure 18(b)**. The spars were cured one by one to prevent shifting of the cores. The aluminium block that was supporting the root of the rear spar was placed in position and fixed as in **Figure 18(c)**. The rear spar was covered with five layers of carbon fibre fabric wetted with epoxy resin forming a “U” shape as in **Figure 18(d)** and prepared for curing under vacuum as in **Figure 18(e)**. The main spar which was not being cured that can be seen on the left in **Figure 18(e)** was also stacked with foams and blankets to prevent sharp edges from puncturing the vacuum bag.

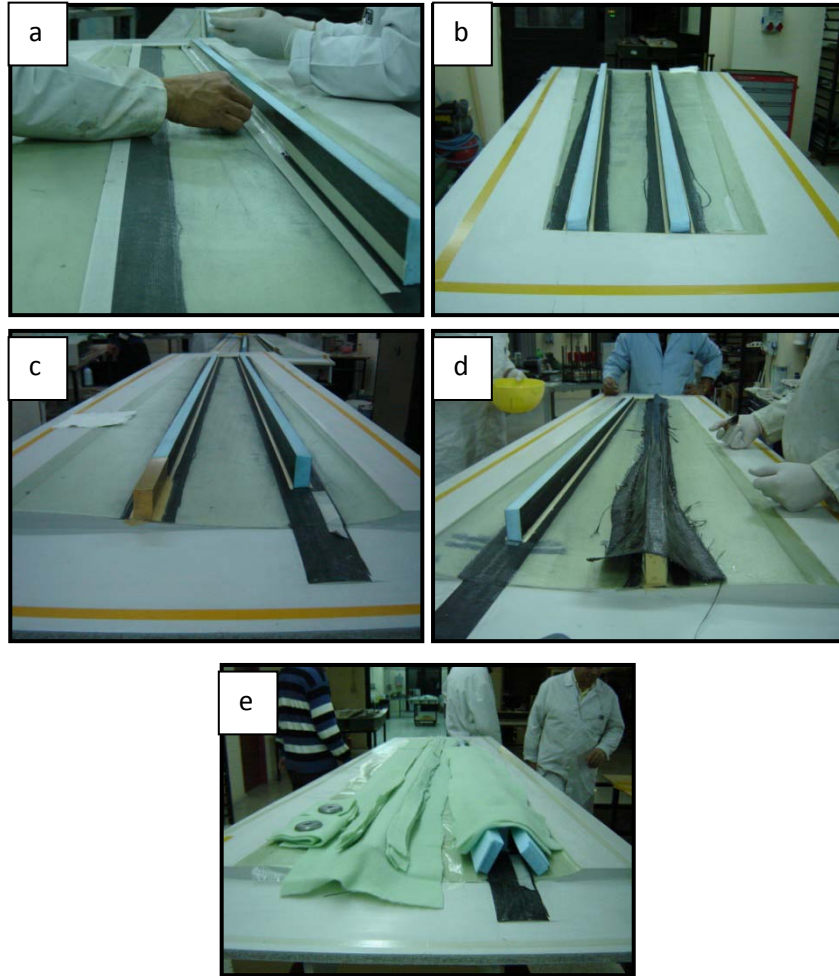


Figure 18: Main spar core positioned (a), rear spar core positioned (b), aluminium rear spar root positioned (c), spar root covered with carbon fibre (d), structure prepared for vacuum (e)

After curing of the rear spar, the vacuum aids were removed and the fringes were trimmed as in **Figure 19(a)**. The main spar root was backed up with a hornbeam block that was aligned and fixed as in **Figure 19(b)**. Five layers of carbon fibre fabric wetted with epoxy were placed over the spar core as done with the rear spar and prepared for curing as in **Figure 19(c)**. The final view of the lower skin after both spars were cured can be seen in **Figure 19(d)** where the skin is being removed from the mold by inserting wedges at the edges.

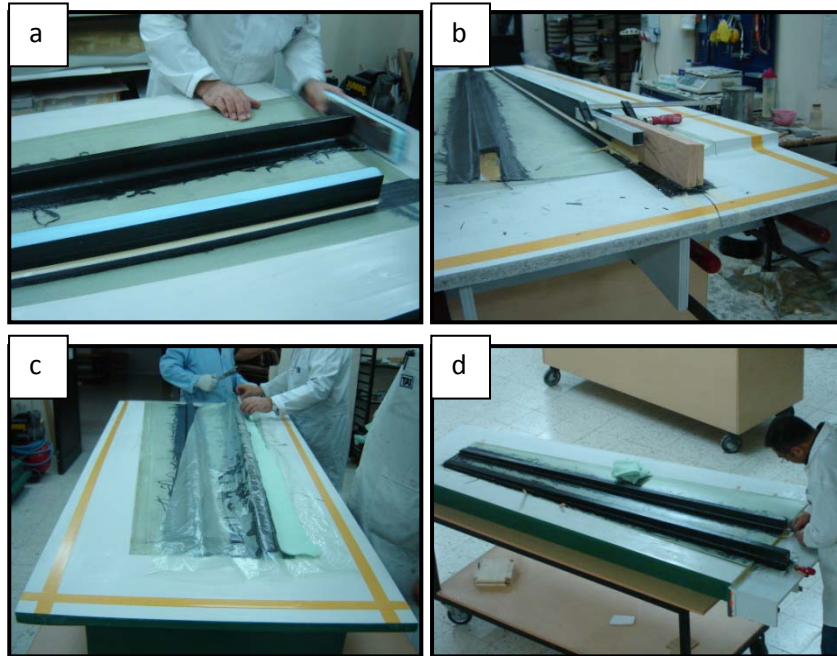


Figure 19: Rear spar cured and trimmed (a), hornbeam main spar root positioned (b), structure prepared for vacuum (c), both spars integrated on to lower skin (d)

5.1.2.3 RIB MANUFACTURING AND WING ASSEMBLY

The ribs parts were prepared in several laminates to sustain the desired thickness and strength. Firstly, a thin wooden laminate was covered with carbon fibre fabric on both sides getting a sandwich structure. The rib geometries were cut out of this laminate two per geometry. The same geometry was cut out of 2cm thick foam and the wooden laminates were adhered to the sides of the foam. The resulting rib was composed of four carbon fibre fabric layers, two wooden laminates and a foam core arranged in the order described above. As the inner spaces of the wings were separated by the spars, each rib was composed of three parts that were divided by

the two spars. The ribs were cut precisely to let perfect match with the upper skin with a tolerance for the adhesives.

The rib parts were positioned and adhered to the lower skin and the spars as in **Figure 20(a)**. The adhesion was strengthened by placing glass fibre fabric wetted with epoxy resin to the edges of the connection surfaces as in **Figure 20(b)**. The ribs were pressed against the skin by clamping wooden pieces to the edges of the mold as in **Figure 20(c)** so that the ribs would not get loose or move while the adhesive was hardening. The ribs were placed at pre-defined distances from each other where the tail boom position was further reinforced by placing two ribs close to each other. The final layout of the ribs can be seen in **Figure 20(d)**. Later on the surfaces which would face the upper skin, that are the spar and rib upper surfaces and the edges of the skin, were covered with adhesive mixed with chopped wood as in **Figure 20(e)**. The use of chopped wood further strengthens the adhesion creating another composite structure where the chopped wood acts as discontinuous fibres and the adhesive acts as the matrix material. The skins positioned inside the molds were brought together and aligned with the alignment bolts and pressed against each other using clamps as in **Figure 20(f)**. After the adhesive was hardened, the assembled wings were obtained.

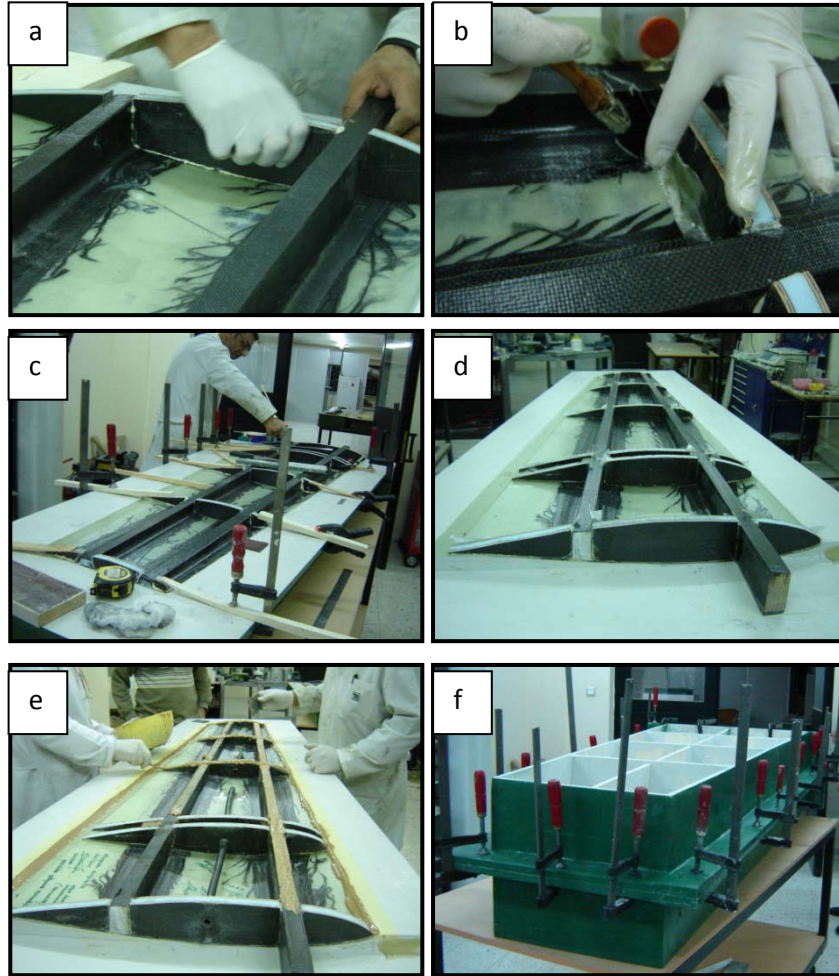


Figure 20: Ribs positioned (a), adhered (b) and fixed for hardening (c), final positions of ribs (d), adhesive applied to contact surfaces (e) and molds are clamped together (f)

5.2 FUSELAGE

After completion of conceptual and detail design, some performance analysis were conducted and in the light of required structural strength and allowable weight, some material and manufacturing choices were made. After making those decisions, which are discussed in detail under the title “Material Selection and Production

Techniques”, male mold production, female mold production, fuselage skin production using the female molds, integral part production and assembly, fuselage assembly, detail manufacturing and surface finish were performed in the given order. During fuselage production, mainly composite materials were used. Scarcely, laminated wood was used for internal parts such as bulkheads which still can be grouped under composite material title. **Figure 21** represents two phases of fuselage manufacturing. In **Figure 21(a)**, female mold was manufactured and wooden structure around the mold was being built for additional rigidity and usage practicality. Yet the figure is not the completed mold structure. On the contrary, **Figure 21(b)** represents the process where the right and left fuselage skins are combined with the help of the inner bulkheads. With the detail structures and surface finish, the fuselage production will be finalized [17].

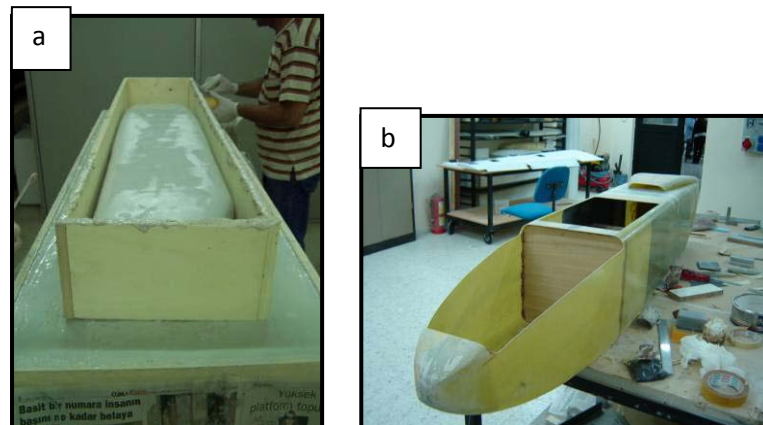


Figure 21: Composite Mold Manufacturing (a), Composite Fuselage Manufacturing (b)

Composite Fuselage Manufacturing is performed in two phases that are mold manufacturing and fuselage manufacturing.

5.2.1 MOLD MANUFACTURING

5.2.1.1 MALE MOLD MANUFACTURING

Male mold manufacturing was initialized when the detail design phase was finished; the exact aircraft geometry was obtained and drawn with a CAD program. From the three dimensional drawing, at predefined stations, two dimensional cross section geometries were extracted. The stations were positioned more closely at the regions where the cross section changed significantly. Utilizing a foam cutting machine, white foam was cut in desired two dimensional geometries generating fuselage slices. These slices generated all through the fuselage were adhered together with polyurethane foam and by checking the dimensions and angles frequently, a three dimensional copy of the fuselage was produced from white foam. The surface was straightened with the help of abrasive paper stuck to a long wooden bar, by which, the geometrical errors caused by slope approximation resulting from using finite number of slices were corrected and a continuous surface was obtained. Later on the surface finish was further improved by using finer abrasive paper.

The surface of the foam male mold was covered with composite material composed of glass fibre fabric and resin specially used for mold manufacturing. [6] To prevent the male mold from straining or breaking during female mold manufacturing, covering of the male mold with the aforementioned composite material was repeated with several laminates. The dimensions of the male mold were reduced during sanding process and with the addition of composite layers; the reduced dimensions were increased towards the original values.

Finally, some operations were conducted to increase surface quality. The roughnesses and holes naturally occurring due to the woven fabric were filled with steel putty which was applied with spatula and sanded repeatedly to get desired surface finish. Sanding was performed starting from dry sanding with coarse abrasive paper and continuing with fine abrasive paper and wet sanding. When sanding was satisfactory, the male mold was painted with undercoating paint and the manufacturing of male mold was finalized. The surface quality of male mold affects

the surface quality of female mold directly, and consequently affects the skin surface quality. If the surface roughnesses are eliminated earlier in the manufacturing process, it gets easier to obtain a more precise product with less effort and material. Thus, an extra effort has been expended to get the best surface finish possible on the male mold. **Figure 22(a)** corresponds to the male mold.

5.2.1.2 FEMALE MOLD MANUFACTURING

From manufacturing point of view, the key design criteria for female mold are; how many parts the mold will be, from which cross-sections the mold will be divided and how the production will be performed. For practicality of production of both the mold and the parts afterwards, the female fuselage mold of the Tactical UAV are produced in two parts lying symmetrical with respect to the vertical plane (pitch plane). In this configuration, the two symmetrical molds can be used separately for fuselage skin production using vacuum bagging technique. The internal parts are positioned while the skins are still inside the molds so that they do not stretch the fuselage and the two skin structures are combined with high accuracy again with the help of the molds.

As the first step of female mold production, a thin wooden laminate with a rectangular outer profile was cut to fit around the male mold at its vertical symmetry axis. This wooden frame acts as a surface for both of the molds to face each other perfectly during fuselage production steps. As can be seen from the **Figure 22 (b)**, a rectangular frame with roughly 5cm thickness was fastened around the laminate to create a pool around the male mold constraining the composite fabrics and resin from the outside. The surfaces of both the male model and the wooden structure that was built around the male mold were further sanded to increase the surface quality of the female mold to be produced with this setup. The surface of the mold was covered with a release agent and as seen on the **Figure 22 (c)**, several layers of mold resin were smeared and glass fibre fabrics wetted with resin were laid over the mold. For the layers closer to the surface, a finely woven glass fibre fabric was used to reduce surface pores when the fabric absorbs the mold resin and cures.

Furthermore, the air captured inside the fabric creates air bubbles with fewer radiuses, decreasing the extra effort, cost and loss in structural integrity to get rid of these air bubbles while improving the surface quality. Yet, the processes to improve the surface quality is never as feasible as creating an already smooth surface cost-wise, weight-wise and strength-wise. Thus, at all the steps of production, to decrease man-power and increase overall surface quality, finely woven fabrics were used at the layers closer to the surfaces.

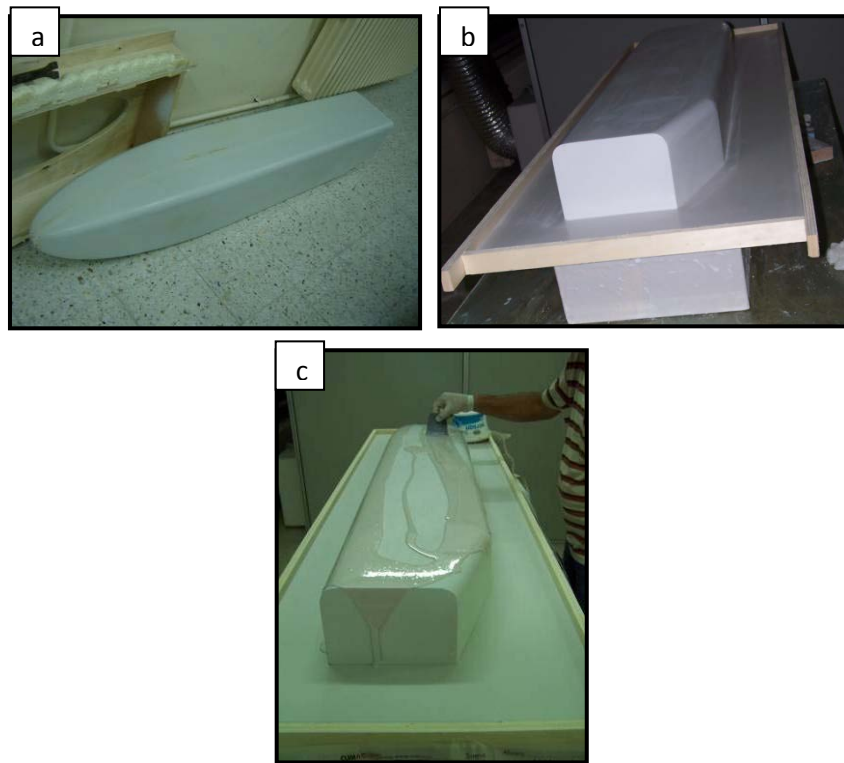


Figure 22: Male mold (a), Pool for female mold (b), Resin application over the male mold (c)

Fabric layers were laid one over another wetting the fabric in between with mold resin till the mold reached 2cm of thickness. Mold resin was smeared over the fabric

layers as can be seen on **Figure 23(a)**. The mold with desired thickness can be seen on **Figure 23(b)** and **Figure 23(c)**.

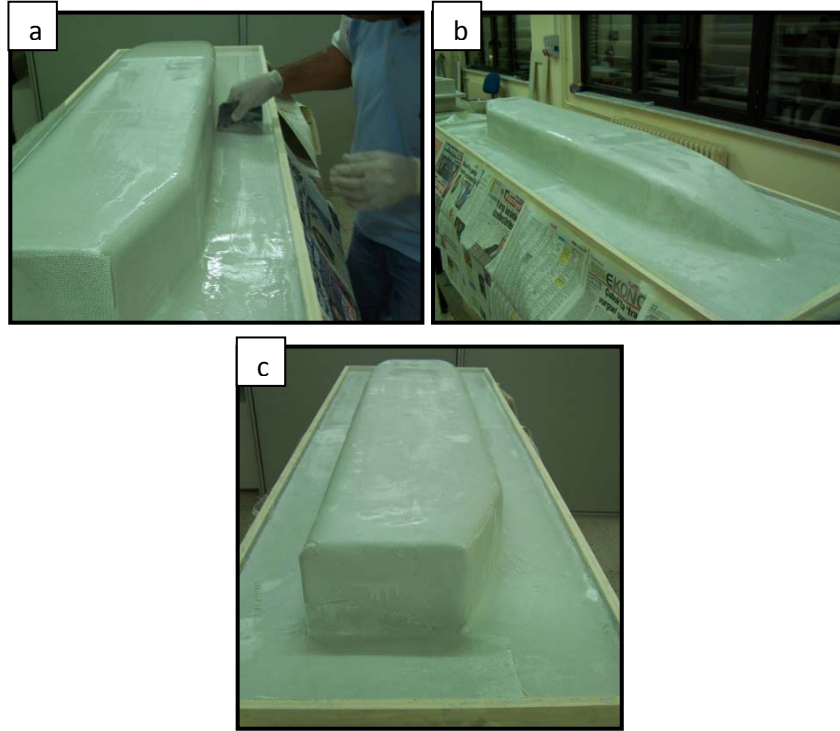


Figure 23: Smearing mold resin over the fibre-glass fabric (a), Back view of the female mold before the wooden skeleton is built (b), (c)

When the mold reached the desired thickness, the back side of the mold was backed up with a wooden skeleton against stretching, warping and breaking as can be seen on **Figure 24 (a)** and **Figure 24 (b)**. The female mold was turned upside down and placed over the skeleton, which acted as a base for the mold. The male mold was kept inside the female mold for further use on the production of the second half of the mold. The wooden structure acting as a pool and constraining the mold was removed from the mold and the mold surfaces were cleaned from particles and

chemicals. Another wooden frame was fixed around the present female mold to act as a pool for the second female mold. Another layer of release agent was applied to the mold surfaces and the exact same procedures for the first female mold were repeated. After backing up the second female mold with a wooden skeleton, two symmetric female molds with the male mold stuck inside were obtained. The adhesiveness of the molds were weakened with the use of release agent, thus with the help of this weakness, the molds were stretched out and separated by slightly forcing them away. Compressed air was blown inside the mold from the separated surfaces further weakening the bond and the female molds were separated. Similar procedures were applied to separate the male mold from the female mold it was stuck inside and all three molds were separated with some extra effort. Female mold surfaces were cleaned from release agent and residues of the paint of male mold with wet abrasive paper and cleaning chemicals. The air bubbles close to the surface were opened up with needles and the holes were filled with mold resin. When the newly filled resins were cured, the surface was re-sanded with wetted abrasive paper and when a smooth surface was obtained, the molds became ready for fuselage skin production. The molds were painted for both protection against environmental effects and aesthetical reasons, and reached the final stage that can be seen on **Figure 25 (a)** and **Figure 25 (b)**.

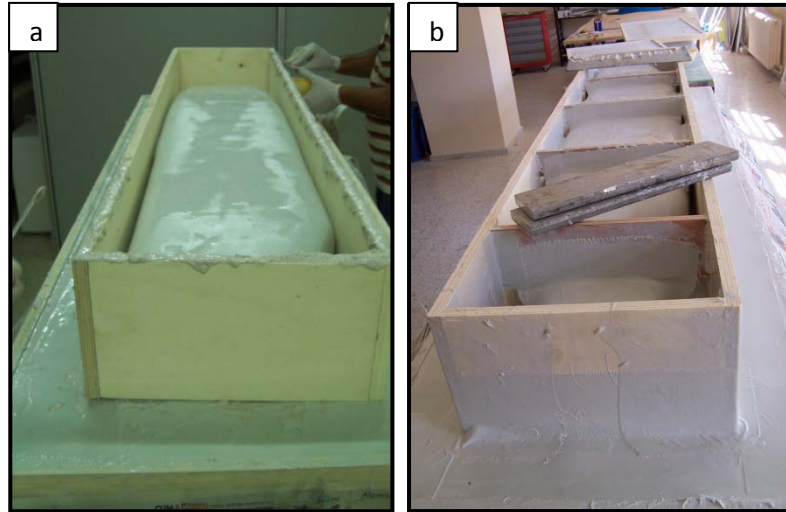


Figure 24: Wooden skeleton production and integration with the female mold (a), (b)

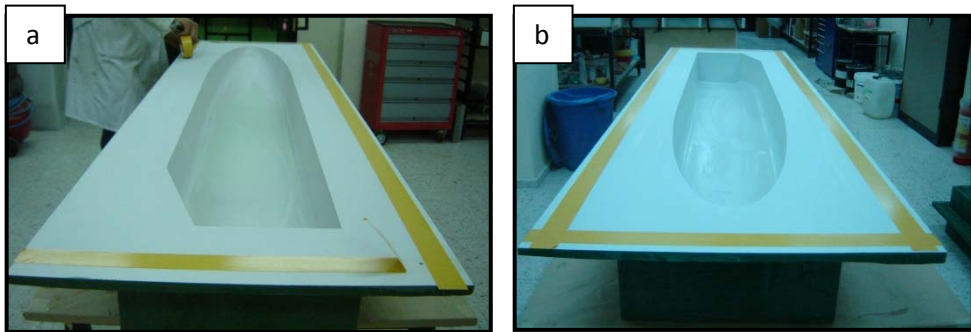


Figure 25: Final view of the female molds (a), (b)

5.2.2 FUSELAGE MANUFACTURING

5.2.2.1 SKIN MANUFACTURING

In fuselage design, unlike the wing design, shear forces act a more important role than axial forces and a better fuselage stands against those shear forces. Loads are concentrated on the areas where wings, landing gear and engine are connected to the fuselage and the rest of the fuselage requires an average strength to withstand aerodynamic forces and carry internal structures such as payloads and fuel tank. Another special requirement for the fuselage is to keep its integrity even after hitting an obstacle so that both the inner structure is kept intact and the fuselage can be repaired easily on the field without spending too much effort or technology. When these requirements are evaluated, aramid fibre is used as the main element of the structure. Glass fibre is used as a filler to increase thickness, to provide strength in axial directions and with its machinability, to help create a smoother surface. Additionally carbon fibre reinforcement is used in the mid section where the concentrated loads are present due to the wing and the landing gear connections. The aramid fibre, as widely used in body armours, has very high energy absorption capability that helps the fuselage keep its integrity even after hard landings or collisions; and as the inner structure is intact, only replacing or repairing the aramid skin makes the prototype ready for the next mission.

As the first step in fuselage skin production, double sided adhesive tape was attached to the periphery of the mold as can be seen on **Figure 26 (a)** to be used during the vacuum process to fix the vacuum bag to the mold and release agent was applied to the mold surface to ease the separation of the skin from the mold. To increase surface quality, as can be seen on **Figure 26 (b)**, the mold was coated with a film of polyester which has a lower viscosity and a shorter cure time when compared to the standard resin used during skin production. After the polyester film was cured, one layer of glass fibre fabric and one layer of aramid fibre fabric were laid smearing resin in between until the desired skin thickness was reached, as can be seen on **Figure 26 (c)**.

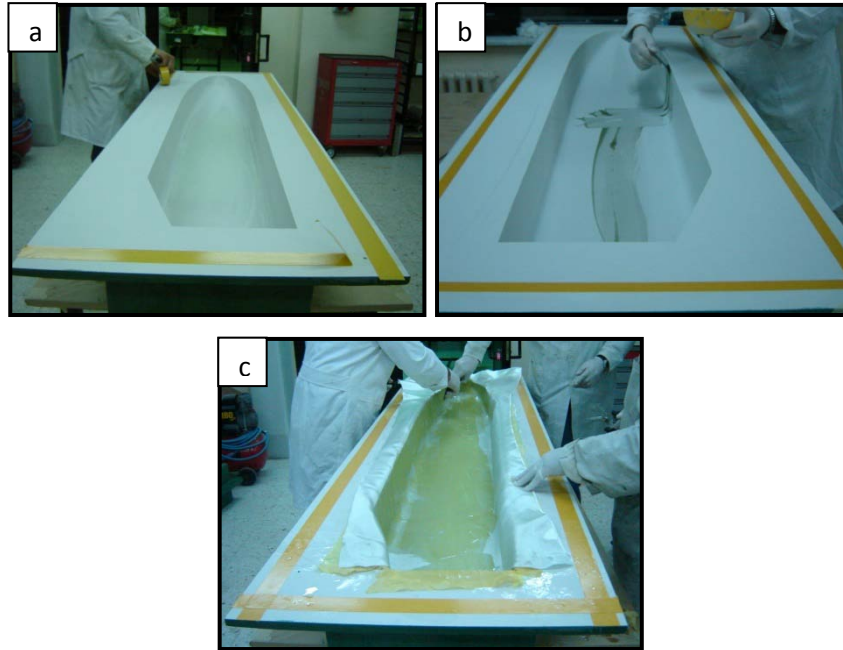


Figure 26: Double sided adhesive tape attached to the periphery of the mold (a), Polyester coating as the first layer on the mold (b), Laying fibre-glass and aramid fibre fabrics (c)

For the mid-section, where the concentrated loads are present, two carbon fibre layers were placed and wetted with resin, which can be seen on **Figure 27 (a)**.

When the layout of the skin was completed, preparations for vacuum process started. Over the last fabric layer, a punctured nylon foil that can be seen on **Figure 27 (a)** was placed to prevent adhesion of composite blanket to the composite layers. Over the puncture foil, a layer of disposable blanket used in composite manufacturing was placed to remove excessive resin from the skin. Extra layers of composite blanket were placed around the spots where the vacuum ports were to be placed, as can be seen on **Figure 27 (b)**. The base parts of the vacuum ports were placed over the extra layers of composite blanket and the mold was covered with vacuum bag as can be seen on **Figure 27 (c)**. In order to prevent the vacuum bag from stretching and breaking, the bag was cut larger than the mold and placed loosely over the mold. Then the bag was affixed to the mold using the double-sided adhesive

tape attached to the mold at the beginning of the skin production procedure. Due to the looseness of the vacuum bag, the edge of the bag was longer than the circumference of the mold and to ensure sealing, the edge was folded over itself where the bag was loose at the edge and affixed to the mold and to itself using adhesive tape. When the whole periphery of the mold was covered, the vacuum bag was punctured with a utility knife at the vacuum port positions and the ports were attached to the port bases tightly. The mold was vacuumed taking extra care on the tightness of the bag, moving the bag by hand when necessary to prevent overstretching. The vacuum was checked to have at least $0.8atm$ of negative pressure and until the desired vacuum was obtained, the edges were reinforced with extra adhesive tape and play dough where the leaks were present. The molds were placed inside a temperature controlled oven and kept at $45^{\circ}C$ and under vacuum overnight for curing.

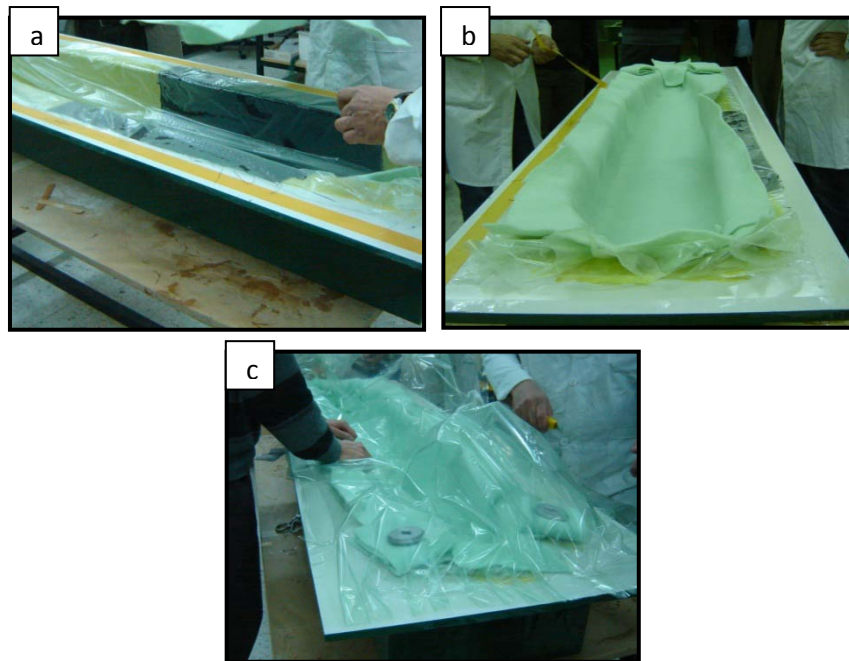


Figure 27: Positioning punctured foil to prevent adhesion (a), Positioning composite blanket to remove extra resin (b), Covering the mold with vacuum bag (c)

When the curing process was over the next morning, the mold was taken out of the oven, the vacuum equipments were removed and the punctured foil was stripped off with the help of a spatula. The fuselage skin was forced out of the mold using a spatula and pressurized air and with the help of weak adhesiveness provided by the release agent, the fuselage skin was separated from the mold.

The exact same procedure was followed for the other half skin and the production of two half skins were completed. **Figure 28 (a)** displays the fuselage skin cured and taken out of the oven yet still inside the mold. **Figure 28 (b)** displays the other half skin trimmed and made ready for assembly. As can be clearly seen on the **Figure 28 (a)** and **Figure 28 (b)**, the inner layers at the mid-section are composed of carbon fibre fabric.

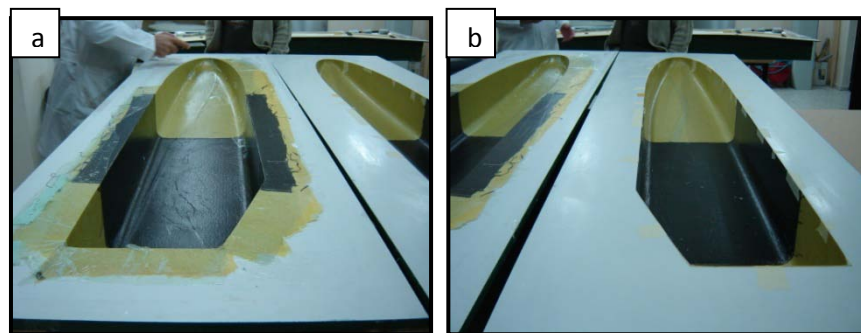


Figure 28: Cured fuselage skin inside the mold (a), Trimmed fuselage skin (b)

5.2.2.2 BULKHEADS AND ASSEMBLY

After the production of fuselage skin, the inner structure of the fuselage was prepared. Three bulkheads were cut out of laminated wood and were placed at three load centres along the fuselage as can be seen on the **Figure 29 (a)** . The outer dimensions of the bulkheads were determined by the geometry of the stations they were to be placed at and the interior parts of two of the bulkheads were removed to reduce weight, creating frame structures with skin thicknesses of around 5cm. The laminated wood bulkhead seen at the front in **Figure 29 (a)** is the bulkhead carrying the engine. The bulkheads were positioned at desired locations and adhered there as can be seen on **Figure 29 (b)** and **Figure 29 (c)**. The most forward bulkhead that is at the back on **Figure 29 (b)** was prepared to cover approximately the lower half of the fuselage cross section and the interior part was removed leaving a frame with around 5cm thickness. The bulkhead was positioned at the wing main spar position leaving enough space for the main spar box which would enclose the main spars. The second bulkhead that can be seen in **Figure 29 (c)** was prepared to fit in the main landing gear station and the interior part was removed to reduce weight and allow connection through the fuselage leaving a frame with around 5cm thickness. The bulkheads were fixed to the fuselage strongly by using glass fibre fabric wetted with epoxy resin as can be seen on **Figure 29 (d)**, **Figure 29 (e)** and **Figure 29 (f)**. The half bulkhead at the back on **Figure 29 (b)** will carry the loads of the main wing spar and the bulkhead on **Figure 29 (c)** will carry the loads of the main landing gear and the rear wing spar. Lastly, the full laminated wood bulkhead which will carry the loads of the engine was adhered to the rear surface of the fuselage skin. This bulkhead will transfer both the weight and the thrust of the engine to the fuselage preventing concentrated loads.

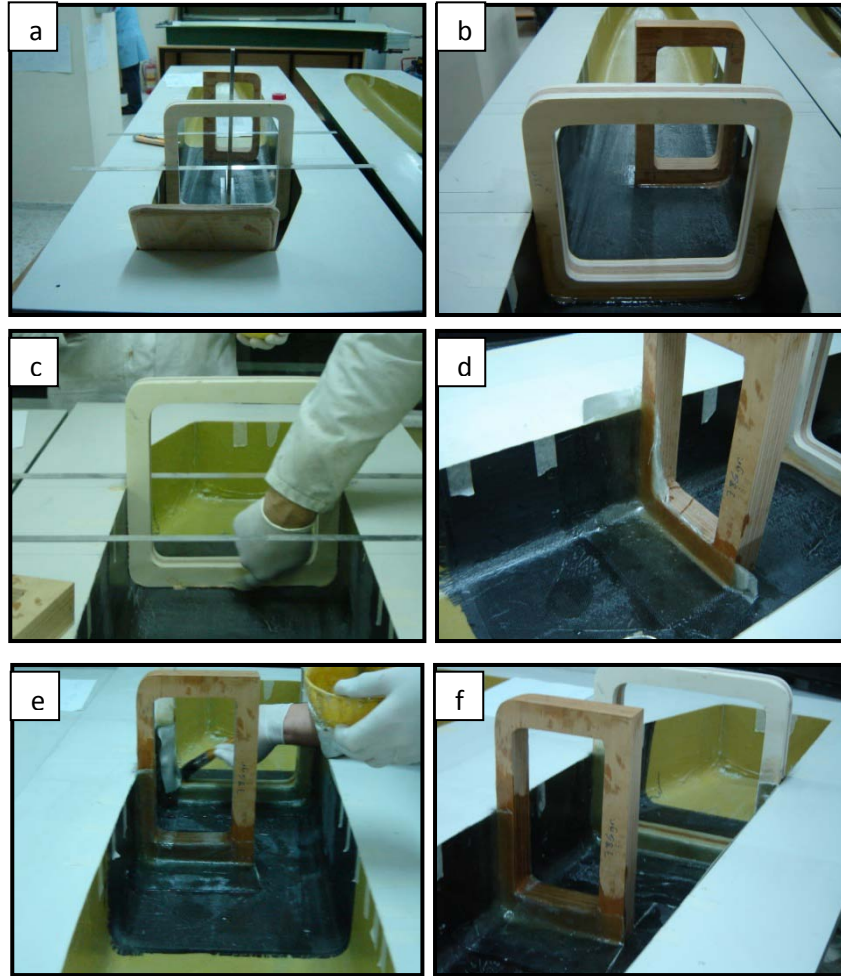


Figure 29: Laminated wood bulkheads (a), Bulkheads positioned in respective stations (b,c), Bulkheads adhered to their positions with glass fibre and epoxy resin (d,e,f)

After the three bulkheads were fixed to one side of the skin while the skin was still inside the female mold, the surfaces which will confront the other skin were covered with adhesives; the two female molds were positioned face to face and clamped together to prevent shifting or warping of the fuselage. The skin assembled with the inner structure was taken out of the female molds with the help of spatulas and pressurized air and the assembly taken out of the molds as can be seen in **Figure 30 (a)**. In order both to access the inside of the fuselage during manufacturing and to

use the fuselage as cargo and accessory bays, access doors were cut through the fuselage skin as can be seen on **Figure 30 (b)**. Through the access doors, the skin connection line was reinforced from the inside using glass fibre fabric wetted with epoxy resin as can be seen on **Figure 30 (c)**.



Figure 30: The fuselage assembly with inner structure taken out of the molds (a), Cutting off the access doors (b), Reinforcement of the skin connection line (c)

5.3 VERTICAL AND HORIZONTAL TAILS

Tail configuration of the Tactical UAV was determined as two vertical winglets at the sides connected with a horizontal tail at the top altogether connected to the wings

from the bottom of the winglets with two booms. This configuration is beneficial keeping in mind the tractor layout as there is a turbulent area right behind the propeller, where placing the horizontal tail above the vertical tails keeps the control surfaces away from turbulence. The geometries of both vertical and horizontal tail are simple especially because of the selected airfoil. Even if the areas of tail surfaces are significantly lower than the wing areas, the centre of gravity of the tail assembly is farther away from the connection point making the bending effect of additional weight important. Thus, to reduce the required strength of the tail booms, whose carbon fibre composite production can only be done with professional tools and machines, tail weight was reduced by manufacturing the tail from composite materials as well.

5.3.1 MOLD MANUFACTURING

5.3.1.1 MALE MOLDS

Male mold manufacturing was performed very similar to the wing and fuselage male mold manufacturing processes. As the vertical and horizontal tails are both simple geometries, numerous slices cut in frequent cross sections were not necessary. Rather than that, the cross sections of the two ends of the geometries, that is hub and tip geometries for the vertical tails and two tip geometries for the horizontal tail are used to cut the male molds at once. Using a foam cutting machine, the male molds were produced from white foam in one piece each. The surfaces of the male molds were straightened and smoothened by abrasive paper and were strengthened with several layers of glass fibre fabric wetted with mold resin.

Surface finish of the male molds was done the same way as of the wings and fuselage; the surface pores and roughness were filled with steel putty and sanded both dry and wet with different sizes of abrasive paper to get a smoother surface finish. Finally, the mold was painted for further smoothness.

5.3.1.2 FEMALE MOLDS

Female molds were designed to be as two symmetrical half molds dividing the vertical and horizontal tail airfoils into two through their respective chord lines. The production of the female molds was identical to the process of female fuselage mold production described previously. When the process was finished, the outcomes were four separate molds two for the horizontal tail and two for the vertical tails. The final views of the female molds are as can be seen in **Figure 31(a)**.

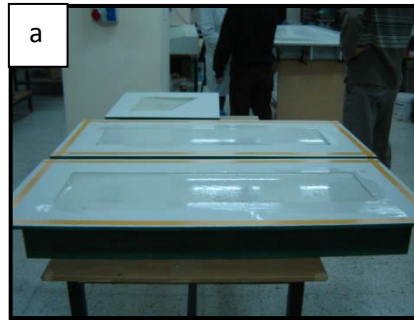


Figure 31: Final view of the tail molds (a)

5.3.2 TAIL MANUFACTURING

5.3.2.1 SKINS

The vertical and horizontal tails withstand similar loads to the wing structure where only the magnitudes of the forces are significantly lower especially for the vertical tails. Skin elements of the tail were selected from light weight and moderately strong materials. The overall skin was manufactured with glass fibre fabric and epoxy resin where a layer of Rohacell 31A foam was used to increase the skin thickness indirectly

increasing the bending strength and puncture resistance of the skin. To carry bending loads of both the vertical and horizontal tails, spars were utilized and during skin production, the areas where the main spars to be placed were reinforced with narrow sheets of carbon fibre fabric.

The horizontal tail and one of the vertical tail skins with their both sides were produced together at once and the other vertical tail was manufactured separately with a completely same procedure as the first vertical tail skin. During the production, firstly double sided duct tape was adhered to the mold contour and the surface of the mold was coated with release agent. A layer of polyester resin was applied for increased surface quality. Following the polyester layer, one layer of glass fibre fabric was placed and wetted with epoxy resin. A sheet of 2mm thick Rohacell 31A foam was placed and a second layer of glass fibre fabrics was laid symmetrically and wetted. To reinforce the spar areas, narrow carbon sheets were placed as the most inner layer. **Figure 32(a)** shows the placement of glass fibre layers for the vertical tail, the **Figure 32(b)** displays the placement of the 2mm Rohacell 31A foam and **Figure 32(c)** displays the skin structure before curing where the carbon fibre layers are also placed. The same steps are displayed in **Figure 32(d)** for the horizontal tail.

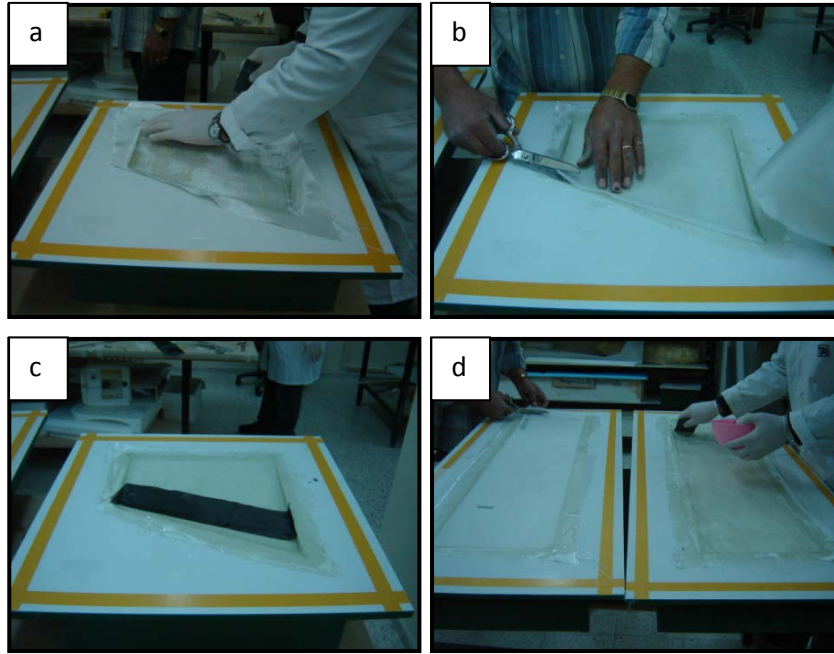


Figure 32: Placement of glass fibre layers (a), Rohacell 31A foam (b) and the carbon fibre strips (c) for the vertical tail, Placement of glass fibre layers and Rohacell 31A foam for the horizontal tail (d)

When the structure of the skin for the tail elements were completely placed, the surface of the composite layers were covered with punctured nylon foil as in **Figure 33(a)** and composite blankets were placed over the nylon as in **Figure 33(b)**. Additional blanket pieces were placed to the positions where the vacuum ports were planned to be placed as in **Figure 33(c)** and after placing the base parts of the vacuum ports, the molds were covered with vacuum bags. The bags were tightly adhered to the double sided duct tapes as in **Figure 33(d)**.

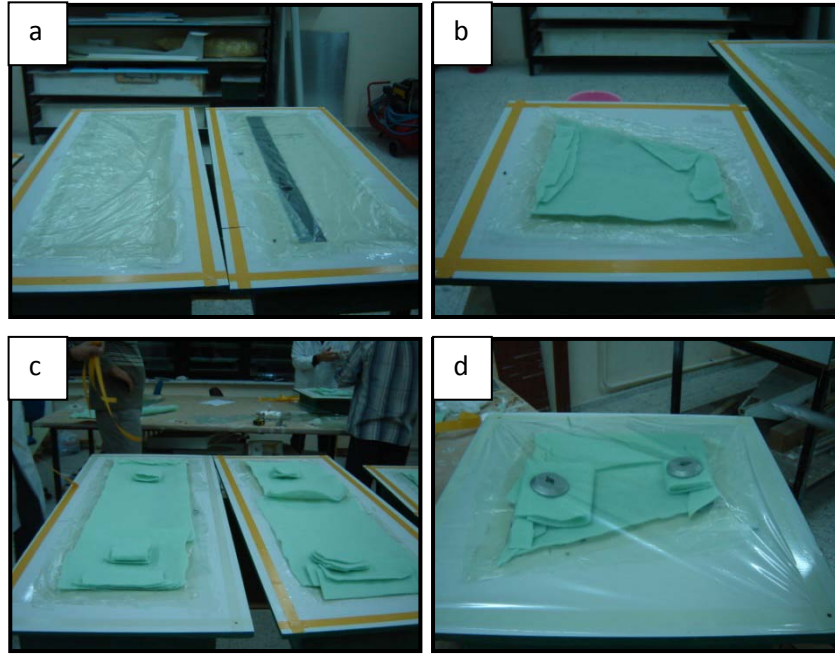


Figure 33: Molds covered with punctured nylon foil (a) and composite blanket(b), additional composite blanket pieces placed to the vacuum port positions (c), vacuum bag placed (d)

The parts to be cured are relatively small, the circumference of the molds are short and the molds are shallow making the vacuum tightness of the elements significantly high. Keeping this in mind and considering the limited time and tools, the vacuum ports for four elements to be cured were connected to each other and vacuumed with a single pump. The gage pressure at the farthest place from the pump was measured and was assured to be more than $0.8atm$. All the molds were placed inside the curing oven and left at $45^{\circ}C$ overnight. The vacuum setup of the molds inside the oven can be seen in **Figure 34(a)**. The vacuum apparatus and materials were removed next morning and the cured vertical and horizontal tail skins before being removed from the molds looked like **Figure 34(b)** and **Figure 34(c)**. The positions of the carbon fibre strips can easily be seen from **Figure 34(b)** and **Figure 34(c)**.

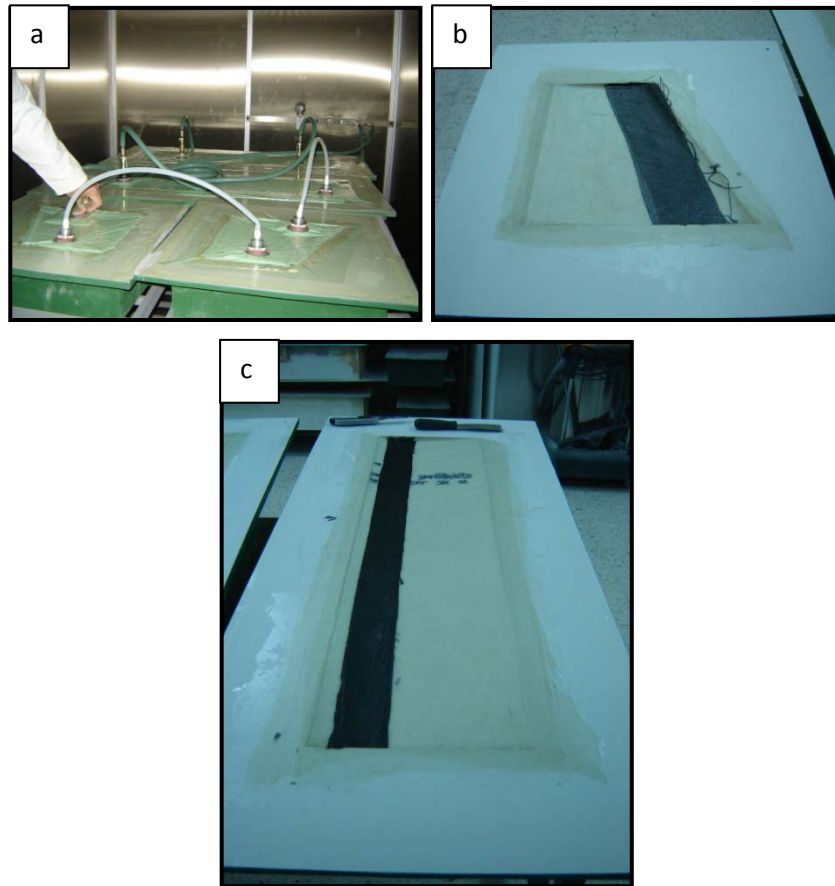


Figure 34: Vacuum setup (a), Vertical tail (b) and horizontal tail (c) skin after curing

5.3.2.2 SPARS

The horizontal tail is reinforced with two spars which are prepared and cured separately. Similar to the wind structure, there is a thicker main spar which carries the majority of the bending forces and a thinner rear spar carries the rest. The bottom side of the main spar is already present within the lower skin in the form of a narrow carbon fibre laminate. The core of the spar is composed of a foam bar which keeps the carbon shell structure in position and prevents buckling of the sheets. The main spar core is fixed in position as can be seen in **Figure 35(a)** and carbon fibre fabric sheets are placed around the core generating a “U” shape with some extensions parallel to the skin surface for better adhesion. The preparations for

curing can be seen on **Figure 35(b)** where the main spar is positioned. The part is cured in heated oven under pressure and the cured skin with the main spar can be seen in **Figure 35(c)**.

The rear spar for the horizontal tail, considering the lower loads it will carry, was designed with a thinner core profile and a weaker composite structure produced in atmospheric conditions. The core profile was affixed to the skin in desired position and carbon fibre strips were adhered to both sides of the core foam making “L” shapes whose bases were on the lower surface of the skin and the posts were adhered to the sides of the core foam as can be seen in **Figure 35(d)**. After curing the rear spar in atmospheric conditions, the fringes were trimmed and two “L” shaped beams were obtained as can be seen in **Figure 35(e)**.

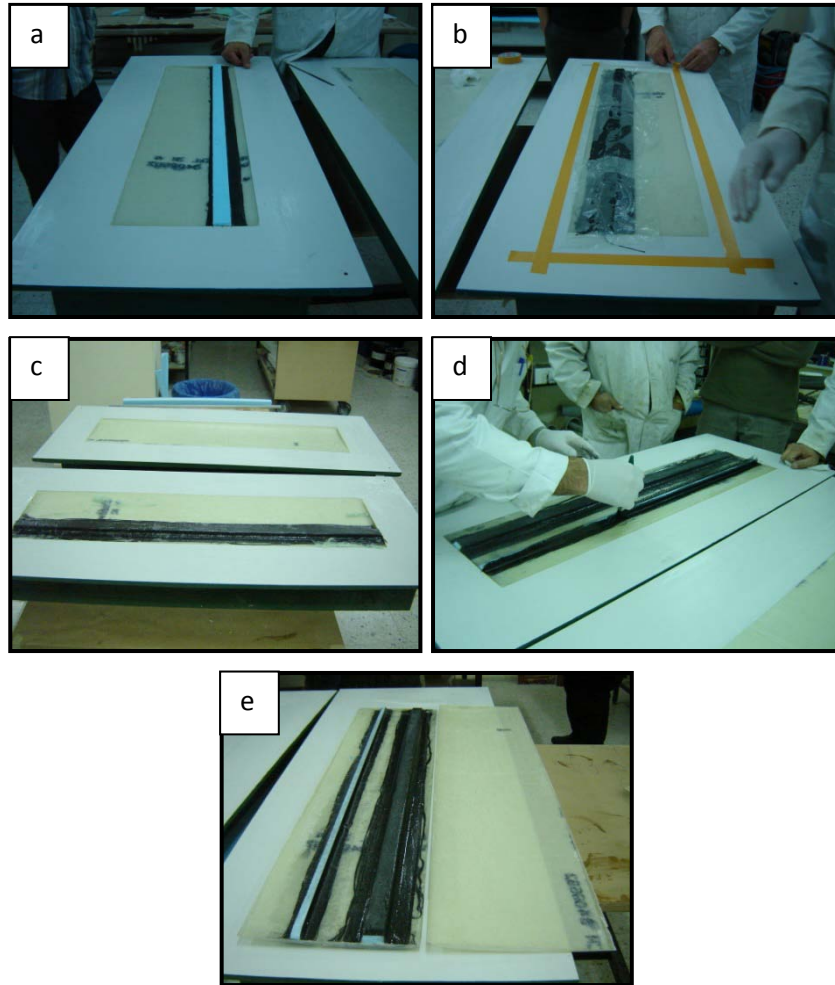


Figure 35: Core foam of horizontal tail main spar (a), main spar ready for curing (b), cured main spar (c), rear spar being prepared (d), cured and trimmed spars (e)

The vertical tail is reinforced with a single spar. Even if the horizontal tail will be connected to the fuselage through the vertical tails, the span of the vertical tails are very low to create significant bending moments. Considering the low strength requirements, the spar was designed very thin. The core of the spar was cut out of foam and affixed in position as can be seen in **Figure 36(a)**. Carbon fibre layers were placed over the core foam making a “U” shape and extending to the sides for better adhesion and pictured as in **Figure 36(b)**. The part was vacuumed and cured under

controlled temperature overnight. The final view of both vertical and horizontal tails after the internal structures are implemented and cured can be seen in **Figure 36(c)**.

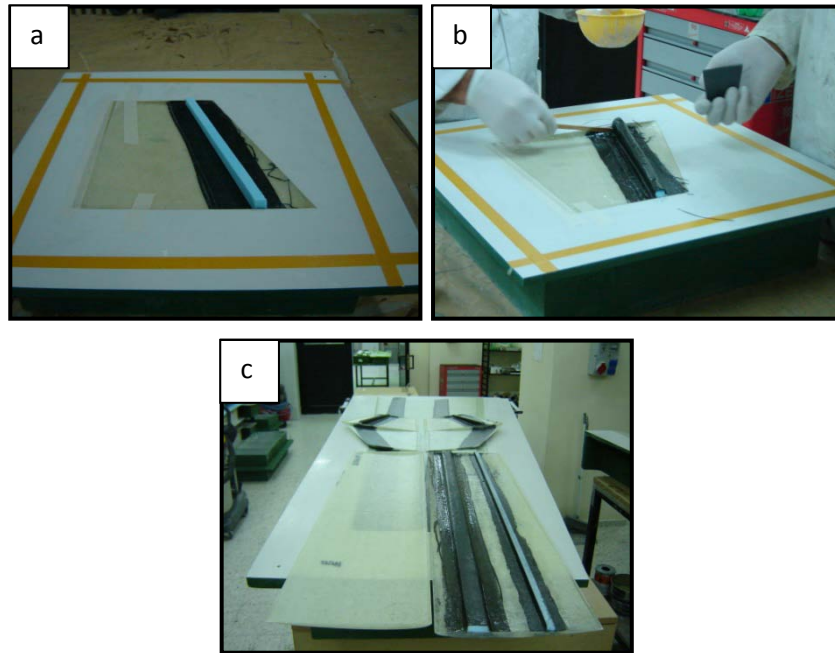


Figure 36: Vertical tail spar core (a), U shaped carbon fibre sheet placement (b), Inner structure finalized for vertical and horizontal tails (c)

Another version of the horizontal tail was manufactured as the first product could not be practically machined to cut out control surfaces as those areas were reinforced with carbon fibre fabric. The skin and front spar of the second version was manufactured identically to the first version. For the rear spar, instead of affixing the foam core first and laying “L” shaped carbon fibre strips, two opposing sides of the foam were covered with carbon fibre fabric and after curing, the foam was cut in desired width generating a foam core with its sides reinforced with carbon fibre fabric. When the core was adhered to the skin, two thin rectangular beams were obtained. Both versions of the horizontal tail can be seen in **Figure 37(a)**.

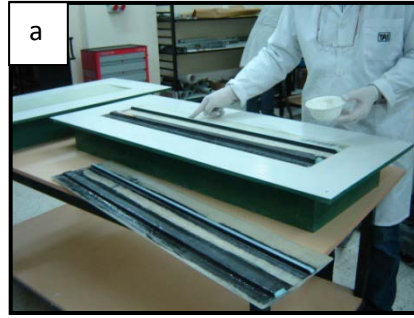


Figure 37: Two versions of the horizontal tail with different rear spars (a)

5.3.2.3 ASSEMBLY

The two halves of both the vertical and horizontal tails were assembled inside their molds for correct alignment. The skins were placed inside their molds by covering the surfaces with release agent first. The surfaces where the two half skins will confront were covered with adhesive material as in **Figure 38(a)** and the hollow areas were stuffed with spots of polyurethane foam to prevent separation as in **Figure 38(b)**. The molds were brought together, aligned with the alignment bolts and clamped tightly as in **Figure 38(c)**. After waiting for complete adhesion for a short time, the molds were separated and the assemblies were removed.

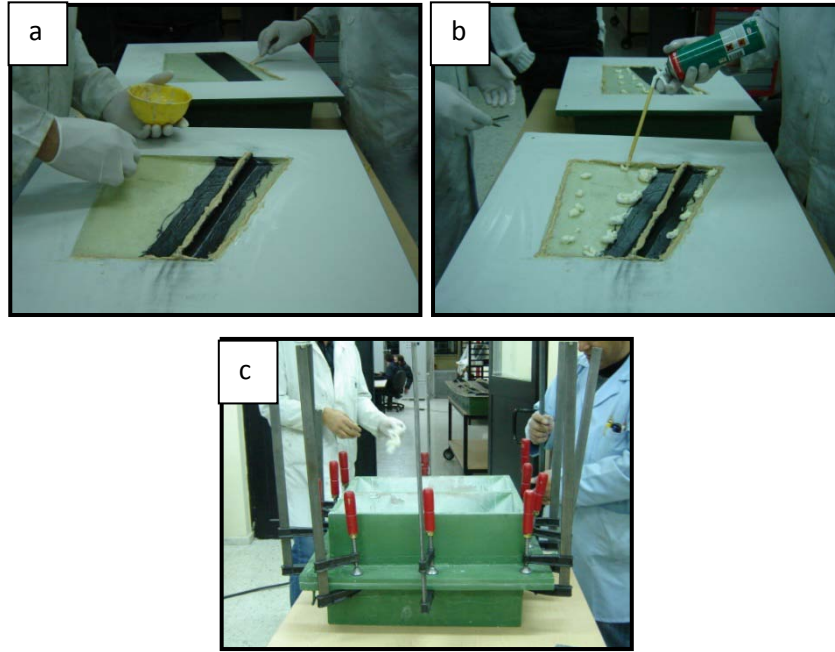


Figure 38: Adhesive is applied to surfaces of contact (a), Polyurethane foam is sprayed to hollow areas (b), Molds are clamped together (c)

5.4 LANDING GEAR

Landing gear configuration was pre-selected as tricycle type during the conceptual design phases. With the rough weight figure and performance predictions, the structural requirements of the landing gear were obtained. Considering the high-wing configuration, both the main and nose landing gears were attached to the fuselage for the sake of simplicity and practicality of the design.

The Tactical UAV is designed to take-off and land on a runway with no external services. Thus the landing gear is designed to let the Tactical UAV taxi remotely, let the wheels turn freely during take-off, withstand landing shocks during touch-down and bring the Tactical UAV to a full stop with self-contained brake system.

5.4.1 MAIN LANDING GEAR

With the tricycle landing gear configuration, the most critical loads are at the main landing gear and are during the touch-down. Considering the high loads, the material of the main landing gear is selected to be composite with carbon fibre mesh, which enables both low weight and low frontal cross section. Comparing to a similar metal landing gear, composite material has a higher elasticity and higher capability of shock absorption. Even if composite landing gear has a higher possibility of sudden failure due to fatigue, this is considered to be of less importance with the mission profile of the Tactical UAV.

5.4.1.1 MALE MOLD

Due to the simplicity of the landing gear geometry, unlike the wing, fuselage or tail, a composite mold was not produced. Instead, a wooden mold was cut from hardwood to give the landing gear the desired shape and two sheet metals were cut and bent over the wooden mold to make two rigid and impermeable surfaces for the production process. To replace vacuum in wing, fuselage and tail production, clamps were used in landing gear production, which kept the composite layers all together between the sheet metal layers and squeezed extra resin out of the material.

5.4.1.2 SKIN

Landing gear was produced with carbon fibre and composite resin, using wet lay-up technique. This time curing was performed in a non-pressurized environment in an oven at 45°C. The carbon fibre layers were cut slightly larger than the desired geometry to tolerate for shifted layers and fringed edges. Around 80 carbon fibre layers with 300 gr/m² density were used during production. The first sheet metal layer was put over the wooden mold, the carbon fibre layers were wetted with composite resin and placed above the sheet metal one over another. After the

desired thickness was achieved, the second sheet metal was placed over the layers and clamped with as many clamps as physically possible, sustaining a uniform pressure over the whole surface of the landing gear. The composite material was placed into an oven and was left inside at 45 degrees overnight. The **Figure 39(a)** displays the structure inside the oven, molded and clamped. The product was separated from the mold and the fringed edges were cut off resulting in the desired geometry as in **Figure 39(b)**.

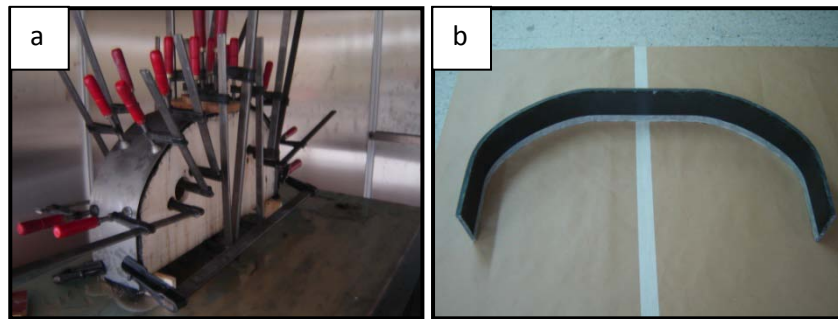


Figure 39: Main landing gear as being cured (a) and as removed from the mold (b)

5.4.1.3 WHEELS AND BRAKE SYSTEM

The main landing gear is designed to undertake the whole braking action on the ground. Considering the weight and the mission profile of the Tactical UAV, a significant braking power was essential. Furthermore, for a stable landing, an even braking in each wheel was very important. To sustain such a braking, a hydraulic brake system with individual brake discs on each wheel was selected. A central hydraulic pump controlled by a servo actuator initiates the braking and the callipers grip the brake discs evenly with the even hydraulic power to bring the Tactical UAV to a full stop. The wheels and brake system were selected from the models found on the model aircraft parts dealers, the wheel dimensions were determined in reference

to previous designs and similar aircraft on the market. The main landing gear with brake callipers and brake disks can be seen in **Figure 40(a)**. The metal shaft and connections to hold the brake calliper in position that can be seen in **Figure 40(b)** were manufactured separately from aluminium so that they can withstand high loads and can dissipate heat generated by the brake pads during braking. The brake power required was also determined by comparing with similarly weighed aircraft with similar mission profiles. As the models were limited on the market, an extended study on sizing was not performed.

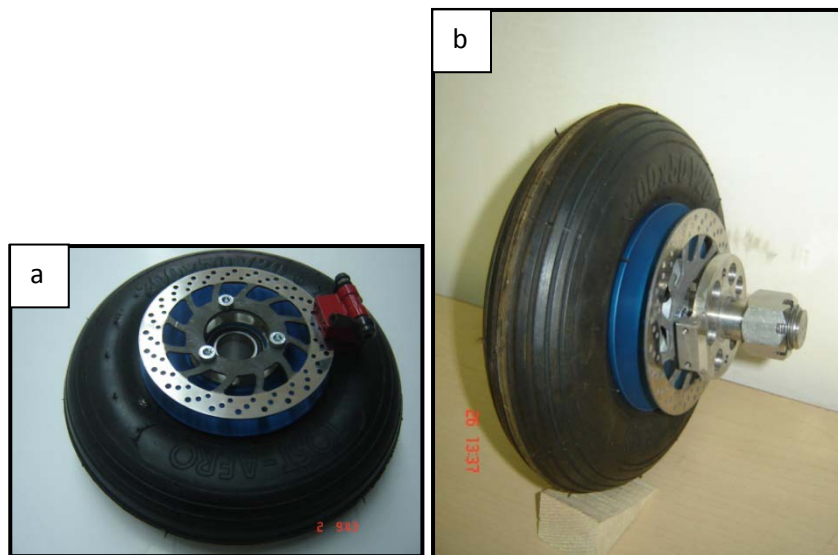


Figure 40: Main wheels with brake disks and callipers (a), with connections (b)

5.4.2 NOSE LANDING GEAR

Nose landing gear, unlike the main landing gear, faces relatively fewer loads during touch-down as it will be the second point of contact to the ground and the higher percentage of mass is located at the rear end of the aircraft. A greater purpose of the

nose landing gear is to level and steer the aircraft on the ground. Being a single, steerable wheel which needs a more precise suspension system to prevent bouncing of the nose, the nose landing gear requires a more complex design. The complexity of the nose landing gear makes it harder to produce it from composite materials and the fact that it would face lower landing forces makes metal structure a better candidate. The primary forces acting on the nose landing gear during touch-down and the lateral forces during ground handling were evaluated and with an inspiration from previous designs, detailed geometry was drawn.

5.4.2.1 METAL PRODUCTION

The nose landing gear is composed of several interconnected metal parts with spring mechanisms to enable suspension. The metal parts were manufactured separately from light aluminium alloy and connected with metal bolts and rubber mountings. Large springs constraining the movement of the landing gear work as a suspension system for which the springs were selected experimentally.

5.4.2.2 WHEELS

The wheels used on the nose landing gear are identical to those used on the main landing gear. Even if the nose landing gear requires less strength and thus a smaller wheel would be sufficient, to reduce spare part variety and increase reliability, all wheels used in Tactical UAV are identical. Differently, the nose landing gear doesn't have a brake system, thus lack brake disks and callipers.

5.4.2.3 STEERING SYSTEM

The nose landing gear is basically mounted around a central shaft whose axis passes through the point contact of the wheel with the ground. As a result, rotating the

landing gear around the central shaft requires the least torque even if the aircraft is at a full stop, which consequently reduces the required size and consumption of the corresponding servo actuator. The central shaft of the landing gear is connected to a fixed structure which, when connected to the fuselage, carries the axial forces acting on the landing gear and transfers them to the fuselage leaving radial freedom of movement. The assembled nose landing gear can be seen in **Figure 41(a)** and **Figure 41(b)** where the wheel and fuselage connection parts are all assembled.

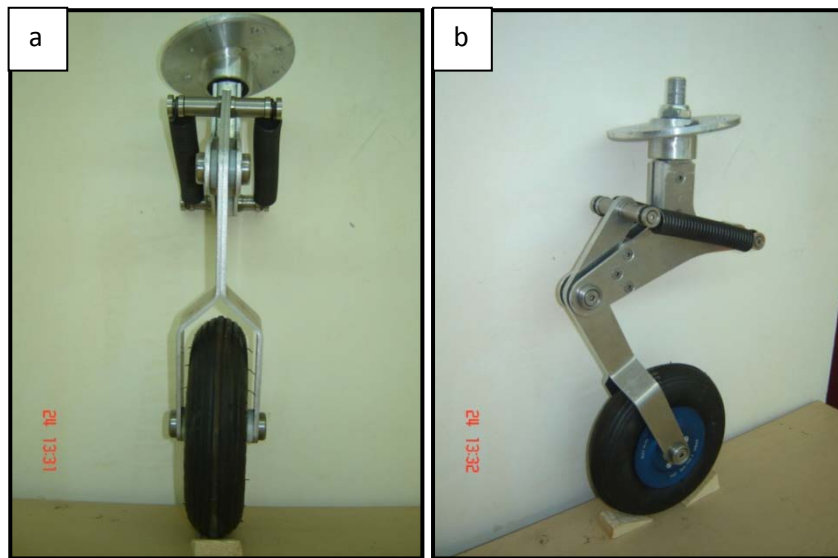


Figure 41: Nose landing gear front (a) and side (b) view

5.5 DETAIL PRODUCTION AND ASSEMBLY

5.5.1 WING

5.5.1.1 CONTROL SURFACES

The wing control surfaces that are ailerons and flaps are positioned all along the wings starting from the double ribs supporting the tail booms and ending at a safe distance from the wing tips with a small distance from each other again assuring structural safety. The control surfaces were cut from the wings using a utility knife and a fret saw without damaging either side so that the cut out parts could be used as the control surfaces themselves as in **Figure 42(a)**. The gaps between the skins were filled with wooden sticks and wedges as in **Figure 42(b)**. The wooden parts were fixed with adhesive material and the same adhesive was used to fill the gaps in skin structures due to the Rohacell 31A foam used in skin manufacturing. The overall view of the cut out parts and the adhesion process can be seen in **Figure 42(c)**. Similar procedures were applied to the control surfaces themselves and two metal hinges per each control surface were fixed at $1/3^{\text{rd}}$ and $2/3^{\text{rd}}$ of the control surface spans as in **Figure 42(d)**. The metal hinges were adhered to the control surface inserting the hinge between the skin surfaces and filling the gap with adhesive materials. When the adhesives were hardened, the outcome was the wings with moveable control surfaces. After painting the wings, the overall view as in **Figure 42(e)** gives a broader look to the control surfaces.

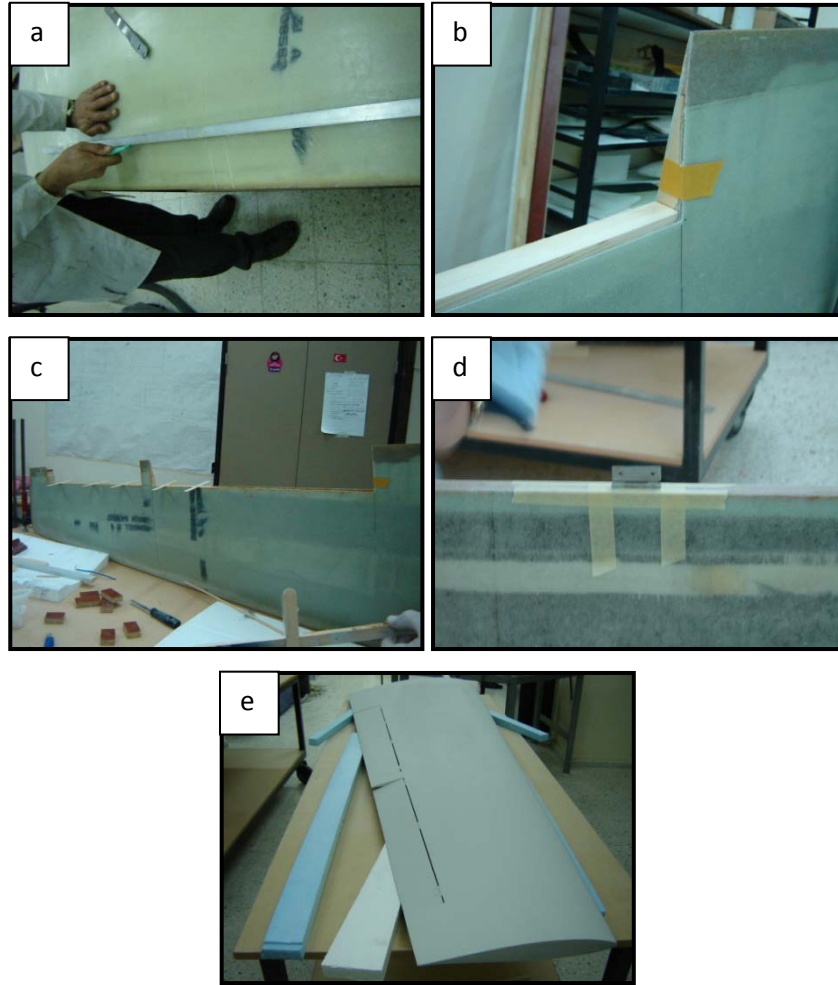


Figure 42: Control surfaces cut out of the wings (a), Gaps are filled with wooden parts (b) and adhesives (c), attached hinges (d), final view of control surfaces

5.5.1.2 SERVO DOORS AND COVERS

Wing servo doors are positioned so that the rods connected to the control surfaces do not create any unintentional torsional loads to the connections. As the servos to be used were previously decided on, the sizing of the doors were quite clear. The lower surface was not an option for servo doors as the surface was reinforced with carbon fibre fabric which is hard to cut through and cutting would weaken the structure. The doors were cut in position with a fret saw. As the upper surface of the

wings were composed of two layers of glass fibre fabric, one layer of Rohacell 31A foam and two more layers of glass fibre fabric, cutting was accomplished in two steps. The upper two glass fibre layers were cut out at first and the Rohacell 31A foam underneath appeared as seen in **Figure 43(a)**, then the remaining layers were cut out and the servo door was opened as seen in **Figure 43(b)**.

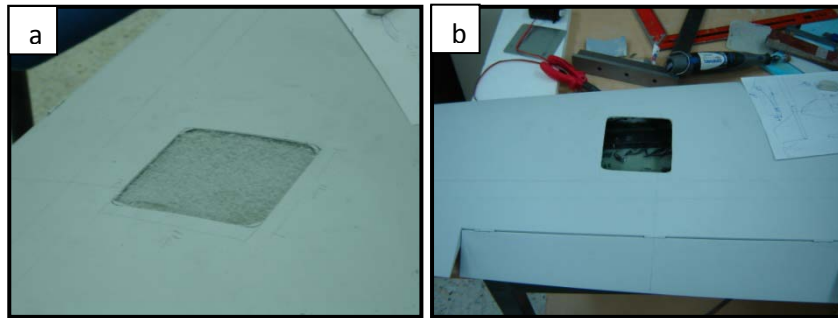


Figure 43: Servo doors cut out in two steps (a) and (b)

The frames where the servo door covers would be placed over were produced using the male mold of the wings. Two layers of glass fibre fabric wetted with epoxy resin were placed over the mold at desired position to cure with the exact form of the wing, as can be seen in **Figure 44(a)**. The sizes of the fabrics were slightly larger than the desired frame dimensions to be trimmed after curing. The frames were cured in atmospheric conditions overnight and cut to 2cm width with a fret saw as can be seen in **Figure 44 (b)**.

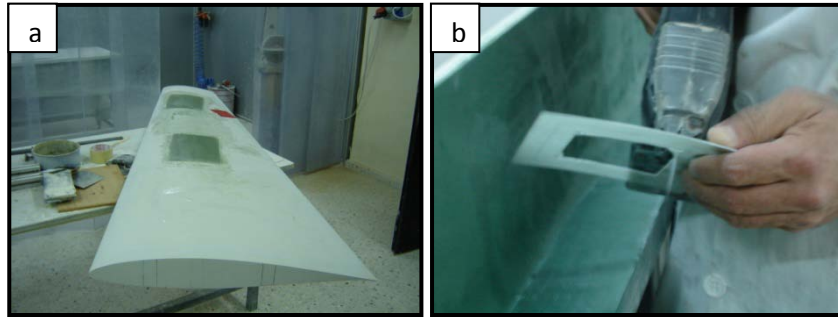


Figure 44: Servo door frames formed over the male mold (a), Frames cut in desired shape (b)

The frames were affixed around the servo doors from the inside as can be seen in **Figure 45(a)** and clamped to prevent shifting. Metal templates were manufactured in the size of the servo doors and were given the surface shape of the wing at the concerned positions as can be seen in **Figure 45(b)** being marked for their position. The surface of the frames were covered with steel putty and given form using the templates for exact match where **Figure 45(c)** displays the surface finish of the frame. The servo doors shown in **Figure 45(d)** were cleaned and painted.

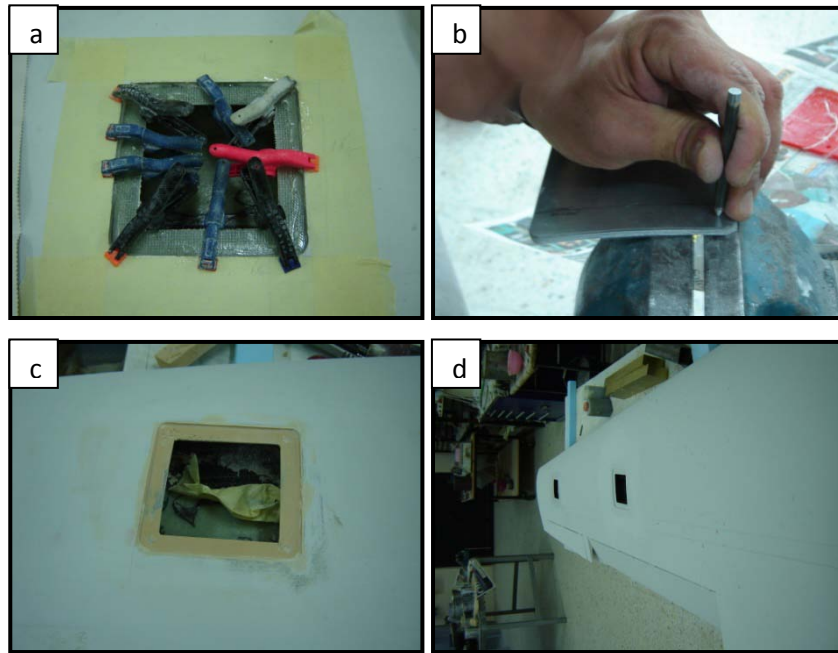


Figure 45: Servo door frame clamped in position (a), Servo door cover template (b), Servo door frame surface finish (c), Servo doors in final view (d)

The servo door covers were molded over the real wing structure for better accuracy and to prevent the extra work needed to clean and repair the surface of the male mold. A thin sheet metal was fixed to the surface of the wing with double-sided duct tape to prevent contamination of the wing surface as can be seen in **Figure 46(a)**. Glass fibre fabrics were placed over the sheet metal and wetted with epoxy resin until the desired thickness, which is the skin thickness of the wing, was obtained. Formerly, the wing structure had been thickened by the use of Rohacell 31A foam, but in a small area such as the servo door cover, usage of Rohacell 31A foam would significantly weaken the cover and possibly cause delamination, so the full thickness was obtained with glass fibre fabric. The fabrics placed over the metal sheet can be seen in **Figure 46(b)**. The fabric was cured for an hour and cut using the template produced previously. The servo door cover trimmed and placed in position can be seen in **Figure 46(c)**.

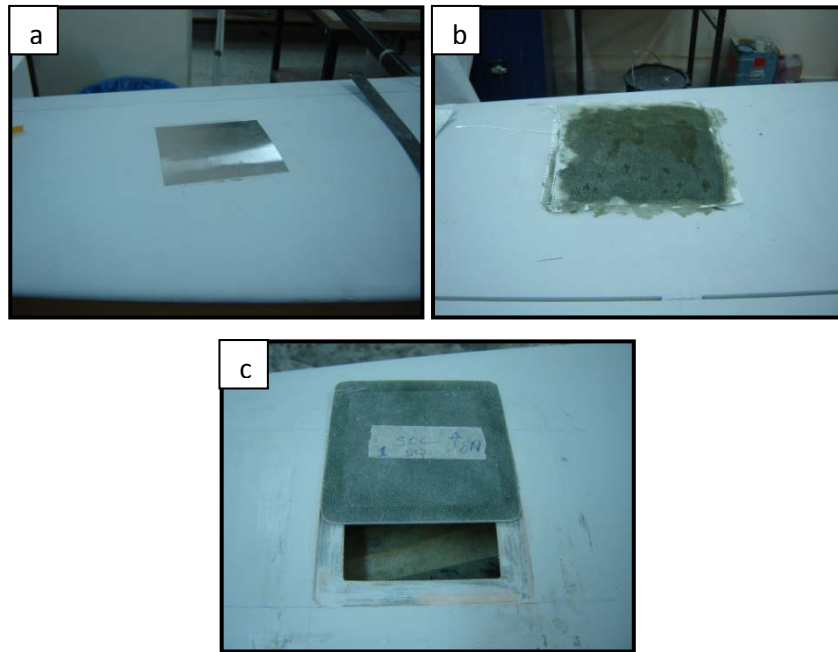


Figure 46: Sheet metal stuck over the wing to mold the servo door cover (a), Servo door cover curing over the wing (b), Servo door cover trimmed and positioned (c)

5.5.1.3 CABLE CHANNELS

One of the critical steps in production of shell structures is to take precautions to enable future access to the inner side of the structure before assembling the skins. In the wing structure, the only access doors to the inner space are the servo doors which are small, widely separated and have access to only two shells. To enable passage of cables through the wing to connect the servos to the radio receiver inside the fuselage, ribs were drilled as in **Figure 47(a)** and cable channels were placed inside the wing passing through the holes on the ribs as in **Figure 47(b)**. First channel starts from the wing root and ends at the first servo door position. The other starts at the first servo door position and ends at the second servo door position.

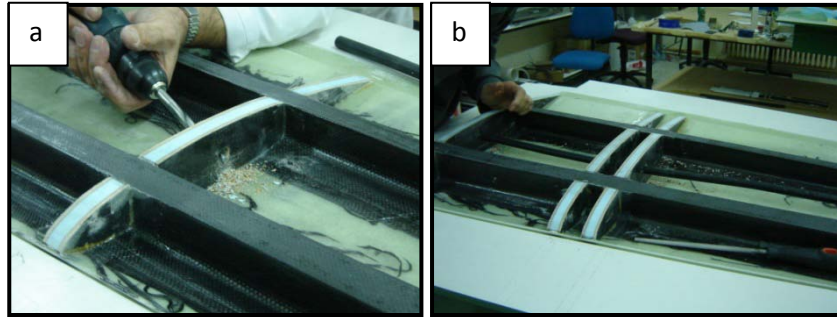


Figure 47: Holes through the ribs for cable channels (a), Cable channels laid through the wings (c)

The cable channels were fixed to the base of the wing so that they do not shift or twist due to temperature effects, exerting force on the cables passing through and harming them. **Figure 48(a)** displays the fixation of a channel at the free end with epoxy-wetted glass fibre. The cables were fixed to the ribs as well to prevent wear of the cable channels or ribs due to vibration as seen in **Figure 48(b)**. **Figure 48(c)** displays the view of the lower wing structure prior to assembly where the positions of the cable channels can be seen clearly. The signatures of the people who worked on the production, which will no longer be accessible after assembly, can also be seen in **Figure 48(c)**.

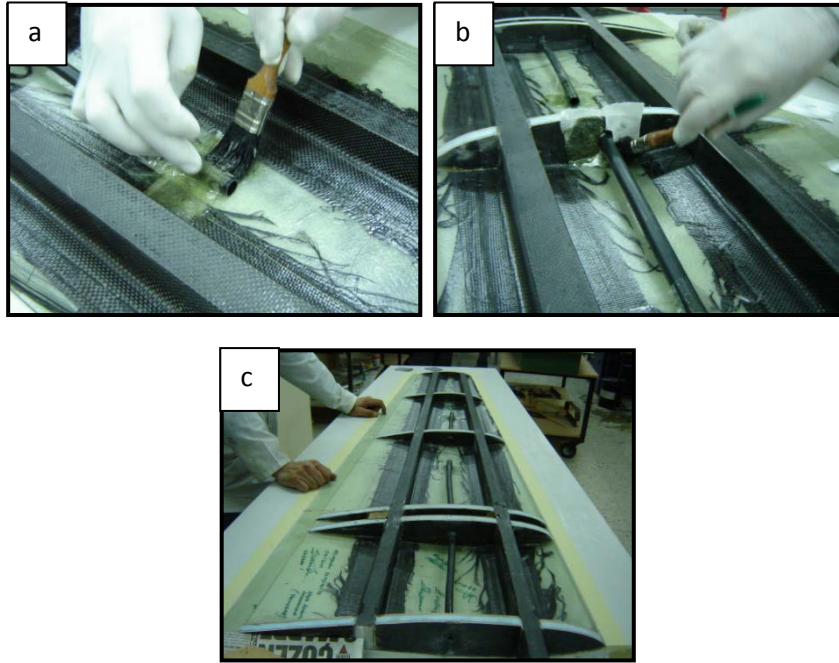


Figure 48: Cable channels fixed to the base (a) and ribs (b), final layout of the cable channels (c)

5.5.1.4 TORQUE BOX

Wing Torque box was manufactured as a standalone component and was integrated with the fuselage separately. Box manufacturing was performed by using the main spars as male molds. Firstly the wings were positioned correctly as if they were fixed to the fuselage by using specially produced templates as can be seen on **Figure 49(a)**. The templates were prepared from laminated wood and were fixed to the floor keeping the wings in position. The wings were also fixed to the templates temporarily and the main spars ended up in straight alignment. The spars were smeared with release agent material and the spars were wrapped around with carbon fibre fabric wetted with epoxy resin as can be seen in **Figure 49(b)** stretching the fabric to reduce buckling. A single long fabric was used wide enough to cover the width of two spars and long enough to wrap around the spars generating a skin thickness of 5mm.

After the skin thickness was achieved, in order to prevent the flaking of the fabric at the tips, glass fibre strips with 5cm width were wrapped around the torque box more tightly towards the tips as can be seen in **Figure 49(c)**. Flat pieces cut out of laminated wood were smeared with release agent and were positioned over the 4 outer surfaces of the torque box. These laminated woods were clamped to exert pressure on the torque box during curing process. **Figure 49(d)** represents the clamped torque box.

The final critical step in torque box manufacturing after the box was cured was to separate the torque box from the main spars. Despite the fact that the wing spars were manufactured with a slight slope to ease the wings' entry to and removal from the fuselage, and the spar surfaces were smeared with release agent, removal of the torque box from the spars was not an easy task. By applying axially outwards force to the wings, the wings were separated from each other leaving the torque box around one of the spars. As applying force on the box to hold it firmly and pull outwards also increases the friction between the box and the spar, a special set up was established. **Figure 49(e)** and **Figure 49(f)** represents the method introduced to separate the two parts. A blanket was wrapped around the torque box to prevent scratching and crack initiation. Two wooden blocks were placed in two opposite sides of the torque box and were clamped together to hold the box firmly. Another wooden block was placed inside the torque box to be able to push the spar from the inside. A separate clamp was used to push the spar from the inside and pull the torque box out. With some significant effort, the torque box was finally separated from the second wing. The final view of the torque box can be seen in **Figure 49(g)**.

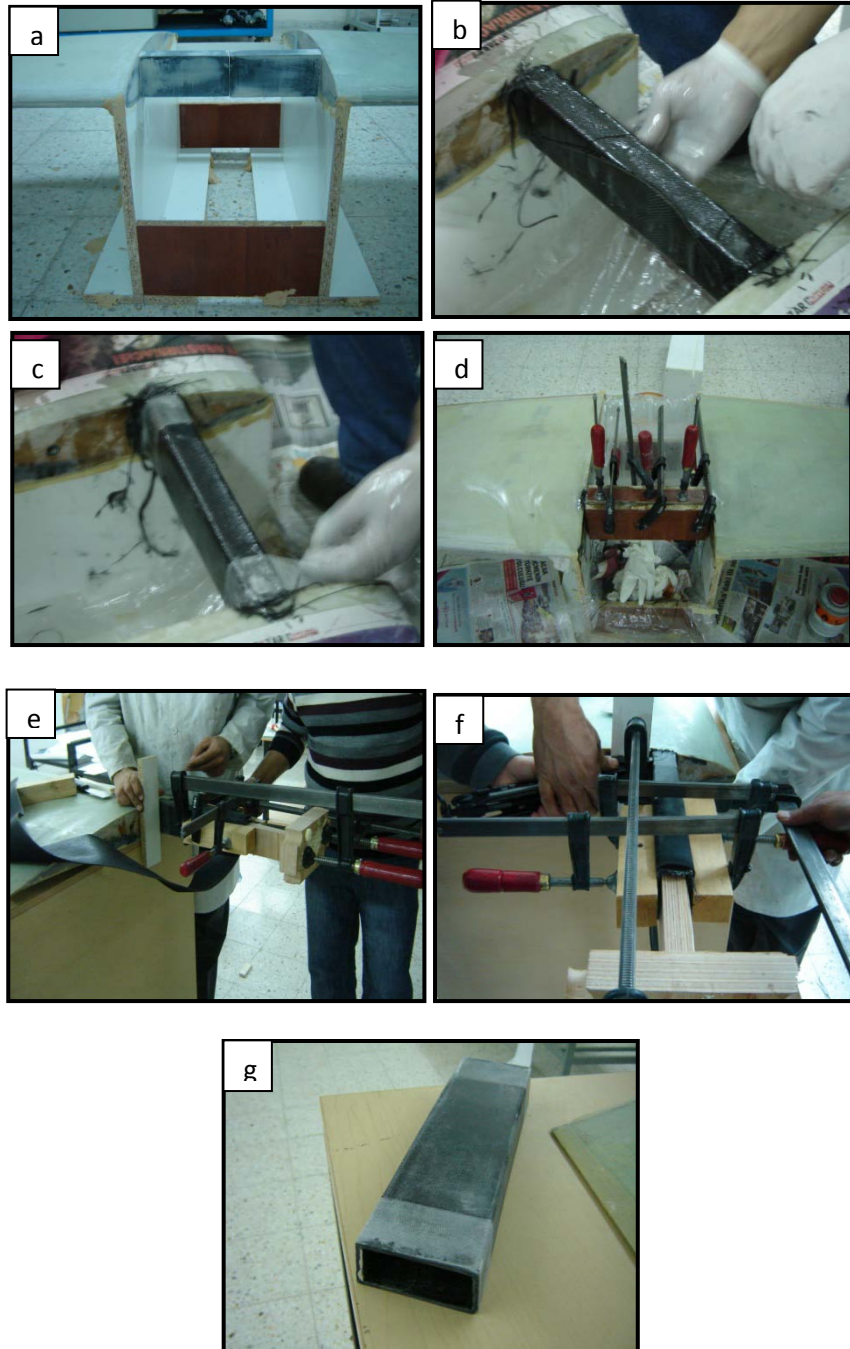


Figure 49: Wing spars correctly positioned (a), Carbon fibre fabric wrapped around the spars (b), Tips of the torque box reinforced (c), Torque box squeezed with clamps (d), Torque box separated from the spars (e,f), Torque box (g)

5.5.1.5 TAIL BOOM CONNECTIONS

Tail booms are designed to be connected to the wings as the rear end of the fuselage is occupied by the engine. The span-wise wing position where the boom is to be connected is determined by the span of the tail. At the position where the tail booms are to be connected, two ribs are positioned inside the wing structure as can be seen in **Figure 50(a)** to reinforce for the extra loads the wing assembly would create. A sandwich structure was chosen to act as a nut for the connection bolts connecting the booms to the wings. The elements of the sandwich structure can be seen in **Figure 50(b)** where the aluminium part will be acting as nuts for the bolts connecting the booms to the wing and the wooden parts will be acting as washers, holding the nuts in place and preventing it to wear the surrounding structure. Two sandwich structures were placed per wing between the two ribs and one behind each spar as can be seen in **Figure 50(c)** and adhered there with adhesive combined with chopped wood as in **Figure 50(d)**.

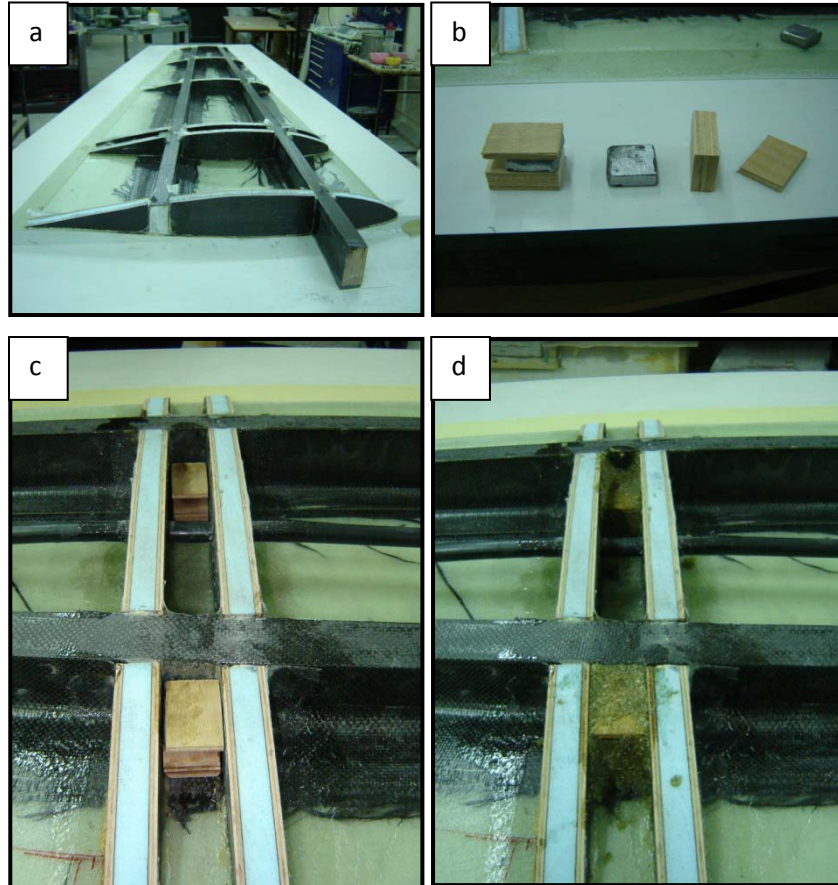


Figure 50: Two ribs in boom position (a), Sandwich structure for boom connection (b), Sandwich structures places (c) and adhered (d)

After the wing skins were assembled, the housing for tail booms was prepared. The locations where the connection bolts would pass were determined by the sandwich nuts positioned inside the wings previously. The covers of the booms were again carbon woven tubes slightly larger than the tail boom so that the boom would fit inside the tube easily. The tubes were positioned to the lower side of the wing with the same axis as the connection bolts and adhered there. The sides due to the circular profile were filled with Styrofoam wedges and the tubes were wrapped and adhered to the wing surface with epoxy-wetted glass fibre fabric. The main load carrying connection will be the bolts fixed to the inner structure of the wings so the tube was just housing the boom and acting as if the boom was thicker in the

connection areas where concentrated loads might be encountered. The tube adhered to the wing and painted can be seen in **Figure 51(a)**. As the cable connection from the fuselage to the tail can only be possible through the tail booms, and a proper connection was not prepared before finalizing the boom and tube adhesions, the leading edge area of one of the tubes was cut out and a thick rope passed from the servo door of the corresponding wing to the rear end of the boom as a guide for the cables. The leading edge cut out can be seen in **Figure 51(b)**. The inner structure of the tube-wing connection can be seen from the cut out in the same figure. The cut out was closed by manufacturing the tip section separately as can be seen in **Figure 51(c)**.

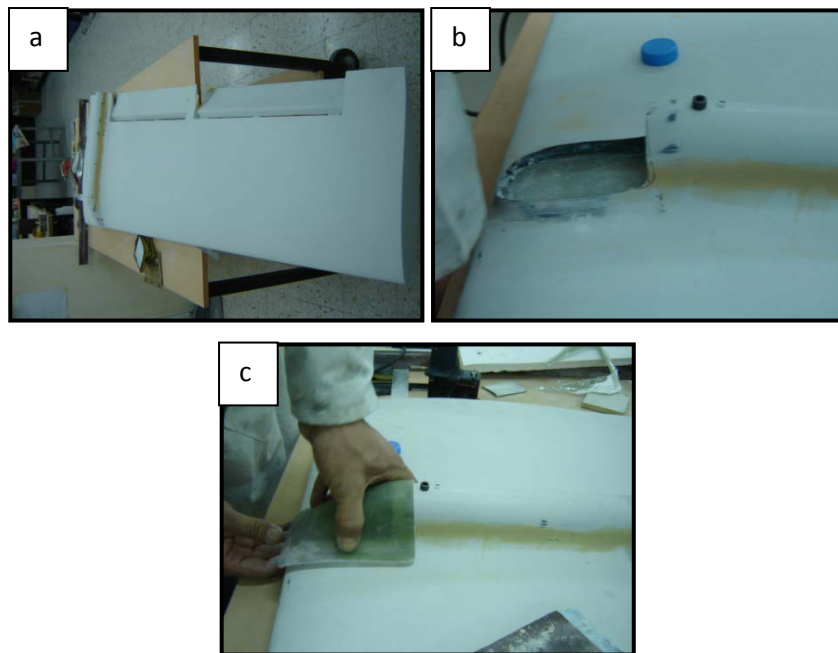


Figure 51: Tail boom tube fixed to the wing (a), Tip of the tube cut out (b), Tip part manufactured separately (c)

5.5.2 FUSELAGE

5.5.2.1 ACCESS DOOR COVERS

From a total of four access door covers, three of them excluding the parachute compartment need to be in the same elevation as the fuselage to facilitate air flow over the aircraft reducing drag. To let the covers be at surface level, thin frames composed of glass fibre composite were adhered around the access doors from the inside letting the covers sit on the frames. **Figure 52** represents the manufacturing of access door covers. In **Figure 52(a)** and **Figure 52(b)** the frame where the access door covers will sit on can be seen. In **Figure 52(b)** the frame can be seen with the access door cover which will sit on it. The cover surface and the frame were smeared with steel putty and molded together to enable exact fit. A secondary role of the frame is to support the nuts which will hold the bolts attached to the access door covers to mechanically fix the covers. **Figure 52(c)** shows the access door between the wall supporting the nose landing gear and the parachute compartment wall. The frame attachment is represented in the figure where to facilitate correct adhesion, small clamps are used. Adhesive material was smeared over the upper surface of the frame and the inner surface of the fuselage and for the duration of curing clamps exerted pressure.

For the access door covers, the pieces cut while opening the access doors were used. The access doors were cut out elegantly leaving the cut-out parts unharmed. As the pieces cut out were in exact shape and size as the access doors, the edges were sanded and they were used as the covers.

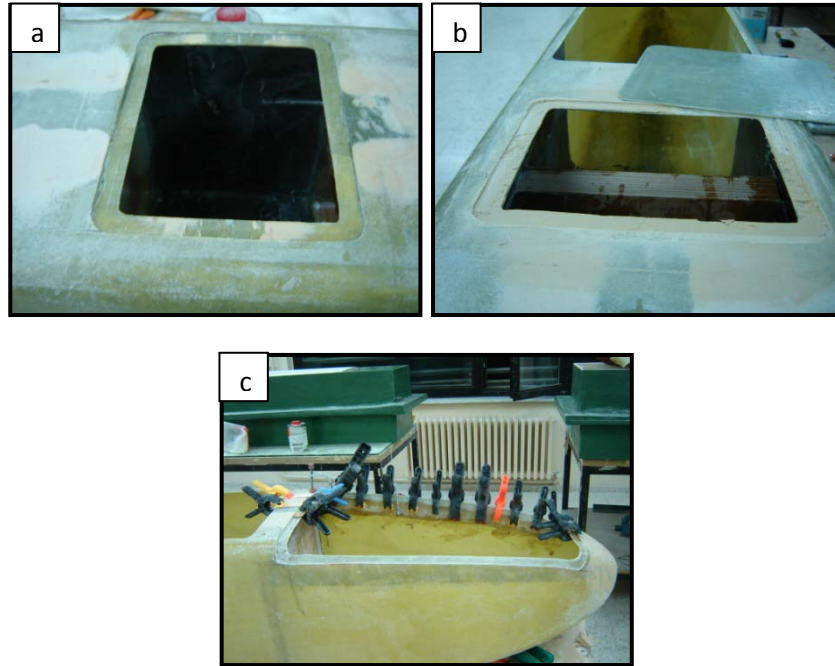


Figure 52: Access Door Covers (a,b,c)

5.5.2.2 SECTION WALLS

To strengthen the fuselage against buckling, to act as bulkheads to support the main elements such as parachute and fuel tank and to divide the space inside the fuselage to functional compartments, two additional section walls were designed. The forward section wall that can be seen in **Figure 53(a)** is positioned at the nose landing gear position. This both distributes the impact of the nose landing gear and separates the second compartment where the power source will be placed. The second section wall is placed between the front section wall and the main spar position. This section wall separates the power source compartment and the parachute compartment and distributes the impact of the parachute to the fuselage. The compartments can be seen in **Figure 53(a)**.

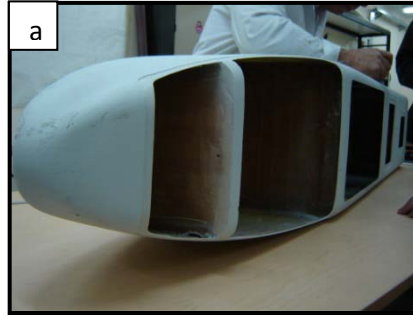


Figure 53: Section Walls (a)

5.5.2.3 PARACHUTE BOX AND COVER

The final step in inner structure of the fuselage is the parachute compartment. The compartment enables the parachute system to be completely isolated from the remaining elements and the spring mechanism deploys the parachute in an emergency without any interference as quick as possible. Parachute box was manufactured separately using a wooden mold. The mold was produced out of laminated wood plates in desired geometry. A rectangular sheet metal was pasted to the base of the mold to create a stepped up level for production of an additional access door to the lower side of the parachute compartment. Three layers of fibre-glass fabric were wetted with epoxy resin and placed over the wooden mold. In order not to wait for the large curing oven to heat up, a simple oven that was large enough to enclose the parachute box was built with Styrofoam walls and a heat gun to cure the parachute box. As the parachute box is not a load carrying structure, it was cured for a short period of time, of around an hour in the hand-made curing oven. The resulting parachute box can be seen in **Figure 54(a)**. An access door cover was produced with epoxy-wetted glass fibre composite similar to the other covers for the lower access door of the parachute box. The sides of the fuselage compartment were reinforced with thin laminated wood pieces adhered with glass fibre composite layers. The parachute box was then placed inside the parachute compartment and

affixed using epoxy-wetted fibre-glass layers. The lower side of the compartment was easily accessible through the access door. The final view of the parachute compartment can be seen in **Figure 54(b)**.

The parachute compartment cover was critical as it needs to facilitate safe operation of the parachute mechanism. A cover which should both embody the parachute tightly during flight and be easily ejected during emergencies was needed. To enable easy ejection, the cover should not be physically connected to the fuselage and should be disposable. To meet the mentioned requirements, the rear end of the cover was mounted to the fuselage through two pins which were not fixed to the fuselage but were constraining the lateral movement of the cover. Thus the connection was loosely holding the cover in position as long as the forward end of the cover was in position. The forward end of the cover was held in position with a pin controlled by a servo actuator enabling remote operation. The cover was manufactured using the male fuselage mold for correct sizing and end shaping. The basic cover was manufactured by laying epoxy-wetted fibre-glass layers over the male mold and curing in atmospheric conditions. For the ejecting of the parachute cover, a spring mechanism would be used, to hold the spring in position and to strengthen the cover against the loads generated by the spring; a reinforcing inner structure was used. As reinforcement, semi-circular Styrofoam pieces were affixed to the inner surface of the cover in a rectangular profile and to hold the spring in position, a ring shape with semi-circular cross section was cut out of Styrofoam and affixed to the cover. Both structures were covered with glass fibre fabric wetted with epoxy resin. The final form of the parachute compartment cover can be seen in **Figure 54(b)**. For the operation of the cover, the front and rear connection pins were added and when the system was triggered remotely by the servo actuator, the cover was ejected with the tension of the spring.

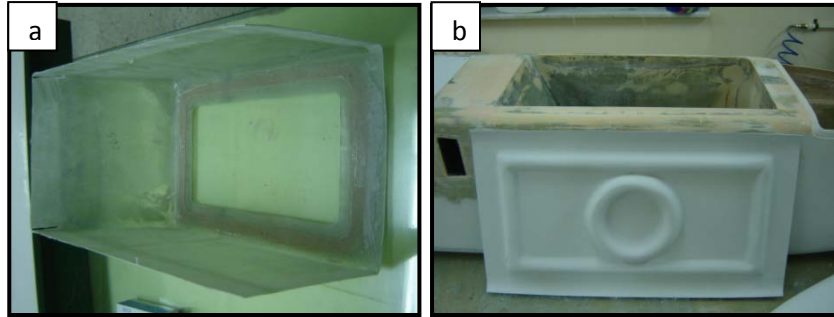


Figure 54: Parachute Box (a), Parachute compartment and cover (b)

5.5.2.4 TORQUE BOX CONNECTIONS

The torque box was manufactured separately to carry the bending loads generated by the separate lift forces generated by the two wing surfaces, before transferring the lift to the fuselage. During the fuselage manufacturing, a space was reserved over the half bulkhead for the torque box. The torque box was placed over the half bulkhead as can be seen in **Figure 55(a)** and fixed temporarily with adhesives. The torque box and the half bulkhead were wrapped together with several layers of carbon fibre fabric wetted with epoxy resin as can be seen in **Figure 55(b)**. As this connection will carry the whole weight of the aircraft during flight, instead of glass fibre, carbon fibre was used for adhesion purposes. As the final step, the space left between the torque box and the upper fuselage skin was filled with laminated wood and reinforced by covering the gap with glass fibre and carbon fibre fabrics wetted with epoxy resin ending up with an integral structure.

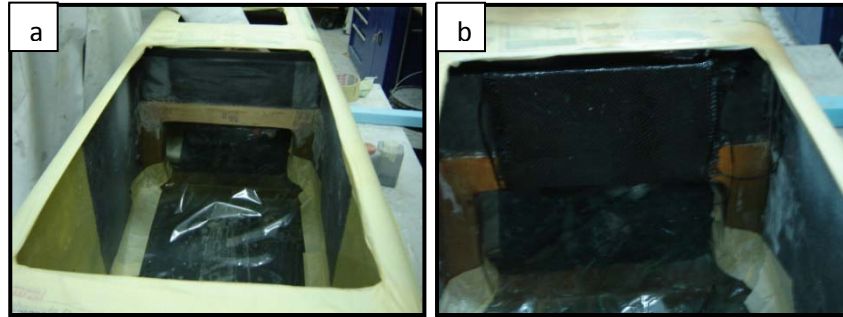


Figure 55: Torque box positioned over the bulkhead (a), Torque box fixed to the bulkhead with wetted carbon fibre fabric (b)

5.5.2.5 ENGINE MOUNT

As discussed in fuselage manufacturing, the rear end of the fuselage was strengthened with a laminated wood bulkhead from the inside. To further improve strength and to prevent movement of the bolts connecting the engine assembly to the fuselage resulting in abrasion of the composite material, a sheet metal was pasted to the back of the fuselage as can be seen in **Figure 56(a)**. The edges of the sheet metal were trimmed and the surface was covered with steel putty to create similar surface properties as the rest of the fuselage. After abrasion of the whole fuselage with sand paper, the rear view of the fuselage is displayed in **Figure 56(b)**.

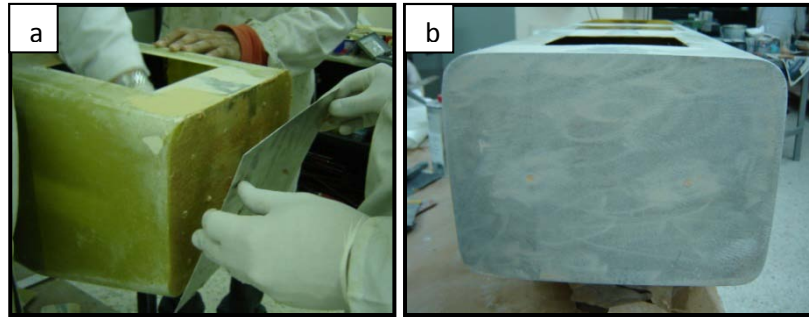


Figure 56: Sheet metal pasted to the bottom of the fuselage (a), Final view of rear end of the fuselage (b)

After the bottom of the fuselage was reinforced with laminated wood from the inside and sheet metal from the outside, the base was strong enough to support the engine loads. A specially manufactured rig was used to hold the engine in position that will both reduce the vibration transferred to the fuselage with the use of special rubber gaskets surrounding the attachment bolts, and enable easy attachment and removal of the engine. The rig was fixed to the fuselage with the use of bolts attached to rubber gaskets. The engine at this point was attached to the fuselage through the special rig by using standard bolts of the engine assembly. The aforementioned rig attached to the fuselage can be seen in **Figure 57(a)**.



Figure 57: Bulkheads and engine mount (a)

5.5.2.6 SURFACE FINISH AND FINAL LAYOUT

Figure 58(a) displays the final view of the Tactical UAV up to the extent this thesis covers. The rest of the details lying between this aircraft and airworthiness are left as future work. In **Figure 58(a)**, the fuselage is painted and the wings, the nose and main landing gear and the engine are assembled. The inner compartments can easily be seen from the figure, there are five different compartments separated by the section walls and bulkheads having their own functionalities. From the bottom to the top in **Figure 58(a)**, the first compartment includes the nose landing gear control mechanism and the pitot tube system. The second section is reserved for power source. As the power source is one of the most significant movable weights in the aircraft and the overall centre of mass is behind the desired one, the batteries are planned to be as forward as possible. The third compartment is composed of two levels among which, the lower level will be used for avionic equipment and the upper level will be for the parachute. The fourth and the fifth access doors open to the same space divided by a hollow bulkhead. This forward part of this space is reserved mainly for the fuel tank as it is close to the overall centre of gravity, so that when the fuel is depleted, the centre of gravity doesn't move much. Behind the fuel tank, the

main landing gear brake system including the hydraulic pump and the servo actuators is positioned and lastly the engine control servos are placed.



Figure 58: Final view of the Tactical UAV (a)

5.5.3 TAIL

5.5.3.1 TAIL ASSEMBLY

Tail assembly had to be done precisely as the connection regions were very thin and susceptible to external effects; they were not strong enough to carry loads due to un-

aligned assembly. Thus the vertical tails were positioned vertically at a distance equal to the width of the horizontal tail and fixed on a table using specially produced wooden jigs as can be seen in **Figure 59(a)**. The horizontal tail was positioned over the vertical tails and connection surface was filled with adhesives and filling material to make a completely matching surface as in **Figure 59 (b)**. After the tail parts are separated, the tips of the vertical tails take the profile of the horizontal tail as in **Figure 59 (c)**.

Carbon fibre tubes were attached to the base of the vertical tails to house the tail booms as in **Figure 59 (d)** with adhesives. The adhesion was strengthened and the connection surface was smoothened by covering the connection area with glass fibre fabric layers wetted with epoxy resin as in **Figure 59 (e)**. After sanding the surface, the vertical tail to tube connection gets a better surface finish as in **Figure 59 (f)**.

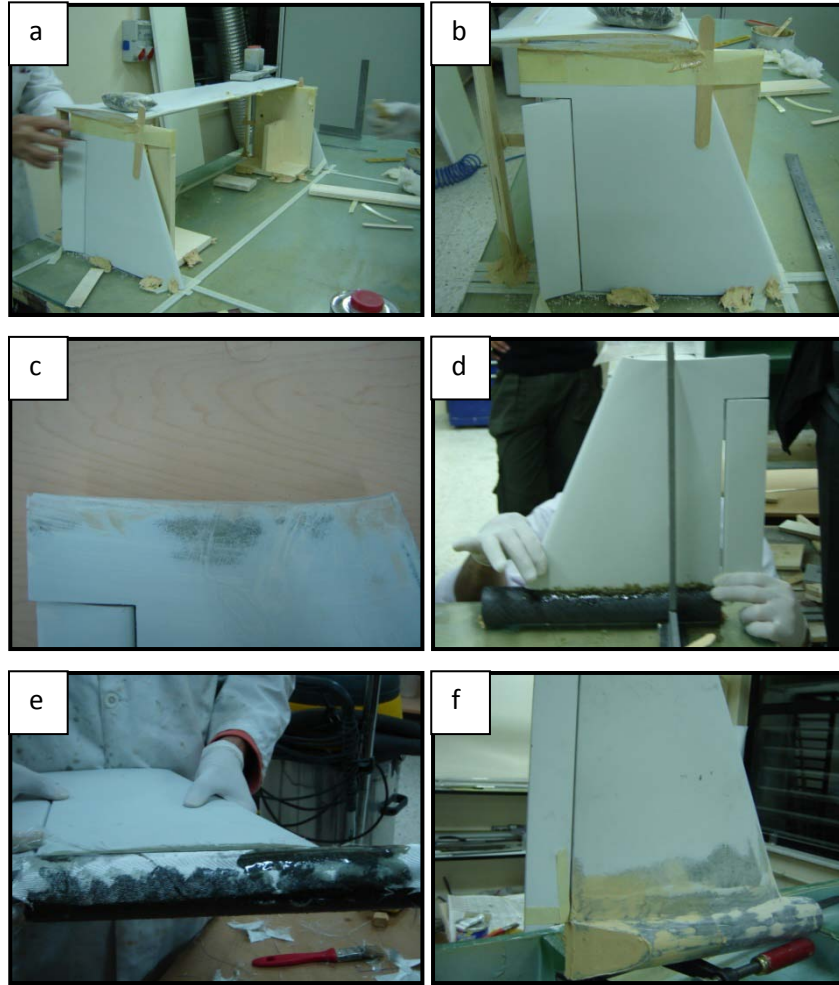


Figure 59: Tail assembly aligned with a jig (a), Connection surface is filled for complete match (b), Connection surface (c), Carbon fibre tube attached to the vertical tail (d), Tube attachment strengthened with glass fibre (e), Tube attachment surface finish (f)

The vertical tails were aligned and jigged again with the tubes at their base this time as in **Figure 60(a)**. The horizontal tail was fixed to the vertical tails with adhesive materials and covering and strengthening the area with layers of epoxy-wetted glass fibre and carbon fibre fabrics. The view of the complete tail assembly can be seen in **Figure 60(b)**. Later holes were drilled to pass boom connection bolts through the tubes at the base of the vertical tails. One of the mentioned holes can be seen in **Figure 60(c)** with a bolt screwed through.

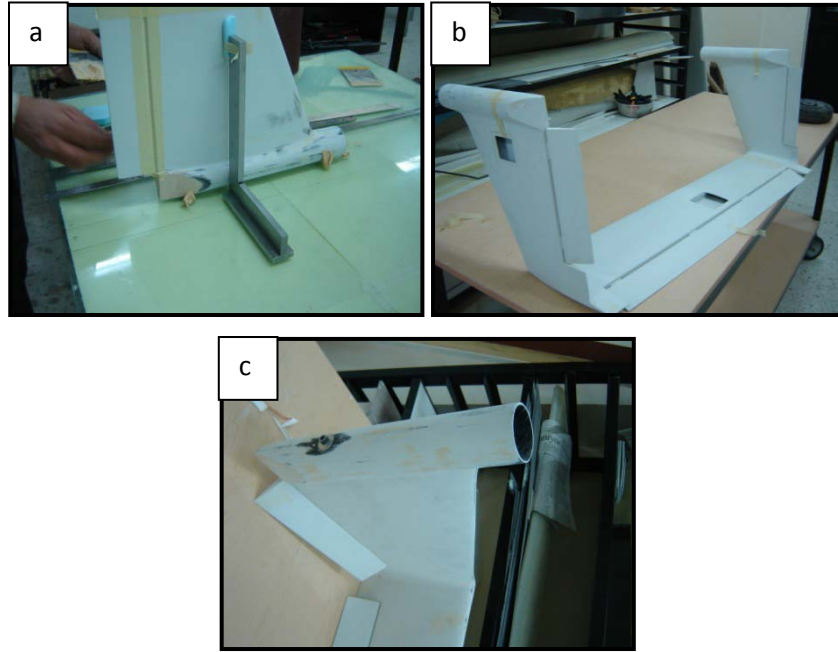


Figure 60: Tail jigged for final assembly (a), tail assembly (b), tube-to-boom connection bolt attached(c)

5.5.3.2 CONTROL SURFACES

The control surfaces of the vertical and horizontal tails are prepared very similar to the wing control surfaces. There are one control surface per each tail part adding up to two rudders and an elevator. The elevator is at its full width possible assuring a safe distance from the edges and the rudders start from a safe distance from the top and ends at the lower end of the vertical tail. As the main difference from the ailerons and flaps, the tail control surfaces are attached to the tail with plastic hinges. The horizontal and vertical tails with control surfaces completed can be seen in **Figure 61(a)** and **Figure 61(b)** respectively.

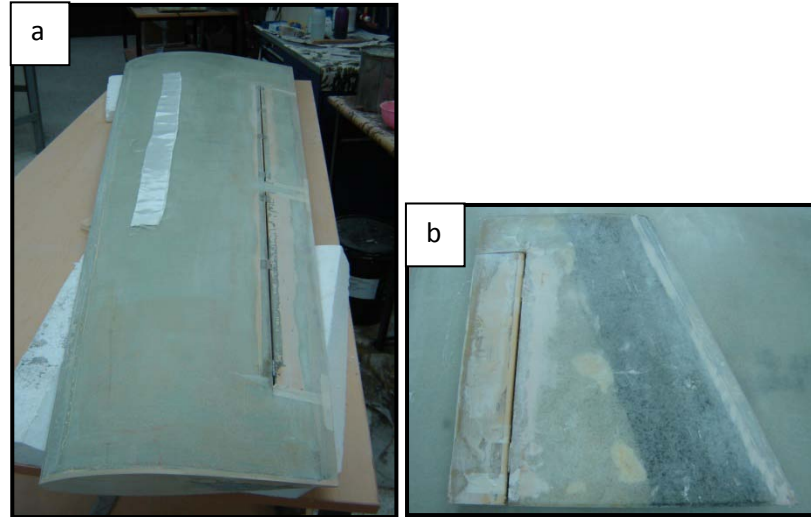


Figure 61: Control surfaces attached to horizontal (a) and vertical (b) tails

5.5.3.3 SERVO DOORS AND COVERS

Due to the limited thickness of both the vertical and horizontal tails, the servos could not be embedded into the tail structures. Instead, they were placed with an offset from the surface. Thus, a hunched servo door cover was designed. The servo doors were cut out on the bottom surface of the horizontal tail and the outer surfaces of the vertical tails. A servo was placed inside one of the doors as in **Figure 62(a)**. Using the servo in position as a mold, a cover was manufactured using glass fibre and epoxy resin, trimmed and surface finished as in **Figure 62(b)**. While the manufactured servo door cover was in position, several layers of glass fibre wetted with mold resin were placed over the cover and a mold was produced for further servo door cover manufacturing as in **Figure 62(c)**. Using the mold, the rest of the needed servo door covers were manufactured as in **Figure 62(d)**.

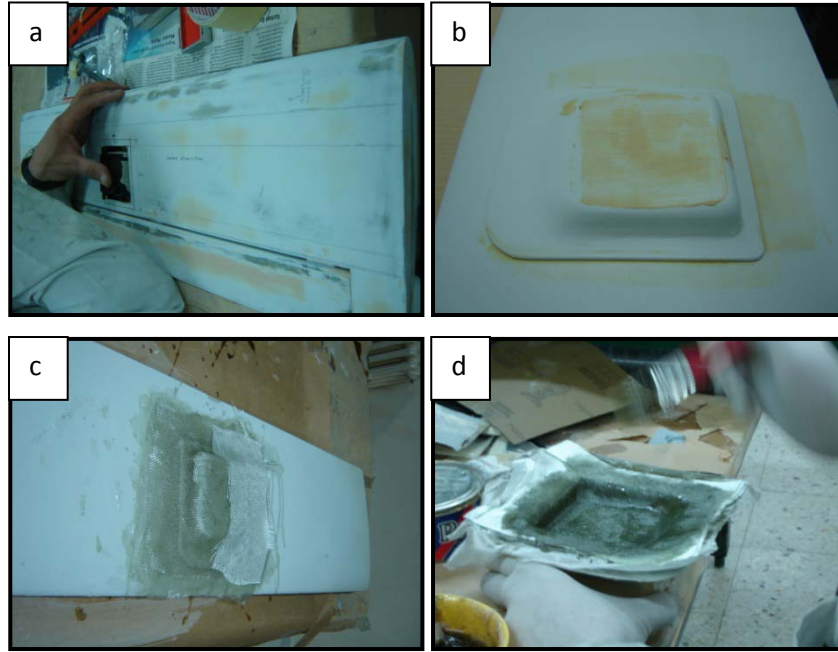


Figure 62: Servo door cut and servo placed inside (a), Prototype servo door cover (b), Servo door cover mold (c), Further production of servo door covers (d)

5.5.3.4 CABLE CHANNELS

In order to connect servo cables to the tail servos, a cable line should be passed along the tail parts. To prevent aerodynamic losses due to passage of the cables over the surface, cable channels were planned that pass through the tail parts. To pass the channels from the vertical tail to the horizontal tail and vice versa, placing the channel during assembly was not practical. Instead, after the full assembly, the edges were drilled with a cross-section enabling the insertion of cable channels as in **Figure 63(a)** and after passing the cable channels, the drilled surface was closed by covering the area with glass fibre fabric wetted with epoxy resin as in **Figure 63(b)**.

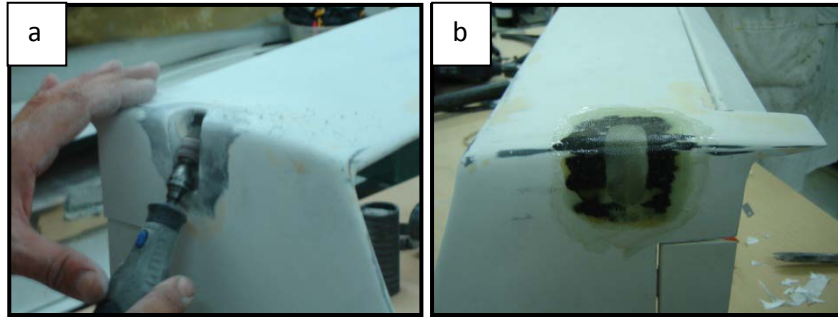


Figure 63: Holes drilled to pass cable channels (a), Holes closed and covered (b)

CHAPTER 6

DISCUSSION, CONCLUSION AND FUTURE WORK

6.1 DISCUSSION

The design offices of most of the prestigious aircraft manufacturers rely on their databases of previously designed and produced aircraft. Rather than investing extensive engineering work on preliminary and conceptual designs of the aircraft, getting the inspiration from similar aircraft and making the difference in the detailed design and manufacturing phases both reduces the costs and durations of design. Similarly, for the design of the METU TUAV, an extensive field search was performed before starting the design phase. Various competitor aircraft were investigated and a total number of six aircraft were adopted as the competitor library. Especially in the earlier stages of design, most of the initial guesses and critical parameters were determined by using these competitors. The common ground on the competitors was their mission capabilities. All were remotely piloted reconnaissance aircraft having a camera gimbal as the payload with variable sizes, mission altitudes and durations.

During the conceptual design of the aircraft, main steps of design defined in [10] were utilized and at points where the empirical methodology defined for large manned aircraft was not matching with the size and flight envelope of the METU TUAV, parameters of the competitor aircraft were duplicated instead; which were later justified by various methods and analysis such as performance analysis justifying the requirements and weighing the aircraft components justifying weight estimations. Description of design choices for a rather rare aircraft group helps the development of empirical methodologies for conceptual UAV design for future

reference. After designing each component of the aircraft individually in the light of competitor aircraft and mission requirements, a better weight estimation was performed, giving more realistic parameters for performance analysis.

When the conceptual design of the aircraft was finalized, various analysis were performed both to verify that the aircraft is capable to perform the mission it was intended for and to check if the sizing of the aircraft was performed correctly without letting any errors degrade the value of the aircraft by reduced capability in any stage of the mission. When the marketing of the aircraft is to be made, key parameters such as take-off distance and rate of climb will directly affect the mission adaptiveness and thus the value of the aircraft.

After the geometry of the aircraft was settled, material and manufacturing techniques were selected which would justify the performance requirements structurally ensuring that the targeted weight is not exceeded. When the material pool was known, detailed design of individual components were performed deciding on the exact geometry of the structure, the exact materials to be used and the thicknesses of composite structures. These steps are not in the scope of this thesis however, critical engineering decisions were summarised. For further explanation of the integral design of the wing, one can find greater detail in [7].

One of the strongest sides of the METU TUAV is that the aircraft was both designed and manufactured under the same roof, letting the mistakes made during the design phase to be eliminated during the manufacturing phase and adapting the design to the outcomes of the production reducing the need for additional prototypes.

Some weight reducing design choices were made during wing manufacturing such that as the most significant load on the wing is the bending load on the main spar, a separate torque box was designed specifically to carry the bending loads which connects the two wings enabling the wing to structurally act as a single wing without the need to manufacture them together. By this manner, the wing-fuselage connection does not need to be strong enough to overcome the high bending loads resulting in a significant weight gain. The torque box was manufactured using the main spars as the molds. Unlike a separate mold, using the real part as a mold prevents the option of adapting the mold to the manufacturing process as it is being

used in the aircraft with its exact dimensions set. After the production of the torque box, its removal from the wing spars was not an easy task. Both of the structures were manufactured at their utmost strength and precision and they were tightly fit in each other. It is advantageous that the three parts will not easily disintegrate during flight due to the tight fit but on the other hand, it will be hard to take them apart for transportation. To ease this process, a very slight taper was given to the spar which is also reflected to the torque box.

Another significant decision was on integrating different materials in the structure of the spars. The spar originally is made of a tapered foam core with carbon fibre box structure. The core acts as a mold for the carbon box and the taper reduces unnecessary weight towards the tip of the wing where relatively low loads are present. Even if the carbon box structure is strong enough to withstand high bending loads towards the root, additional material properties become significant there. The wing-fuselage connection should be temporary letting the components be separated for transportation of the aircraft. Thus, the connection should be made with bolts and nuts. At that point, flexibility of the carbon box structure that would eventually enlarge the connection holes with increasing play induced by random vibrations during flight necessitated the use of a stronger core material. Firstly use of aluminium bulkheads was planned but the significant weight of the bulkheads caused second thoughts and the material for the main spar hub section was changed to hornbeam wood. As the rear spar was not extruding outside of the hub surface, the surface transferring the loads to the fuselage was the connection bolt surface thus, the characteristics of hornbeam was not sufficient and the initial decision was followed.

Carbon fibre is extensively used as a lighter replacement of metal structures and in most of the cases is not used together with metals. The spar cores are covered with carbon fibre fabric as mentioned before and at the root area, the aluminium bulkhead replaces the foam core and the carbon fibre structure gets in contact with aluminium bulkhead. This unusual condition in the presence of an electrolyte, which is in our case the unavoidable humidity in the air, causes the two metallic structures having different levels of activity exchange electrons. This exchange causes galvanic corrosion of aluminium which in time destroys the structural integrity of the

bulkhead failing the load carrying structure. These undesired effects were eliminated simply by electroplating the aluminium bulkhead with non-anodic protective coating and placing few layers of glass fibre fabric between the aluminium core and the carbon fibre box where these layers cured with epoxy filling act as a perfect insulator preventing electron exchange. Thus an uncommon source of failure which can catastrophically cause collapsing of the aircraft during flight was removed with a simple procedure even before the aircraft makes its first flight.

Some reinforcements similar to the spar root modification were made to the component attachment areas such as the tail boom attachment area on the wings and the engine attachment surface on the rear end of the fuselage. These reinforcements were made both to increase the strength of the connection and to improve the resistivity of the area to failure due to looseness and free play caused by in-flight vibrations. The engine being the major source of vibration was connected to the fuselage by the use of bolts with rubber sleeves reducing the vibrations transferred to the fuselage, but still, the bolts vibrating in a composite housing enlarge the holes in a very short duration causing the failure of the connection. Similarly the tail structure fluctuating all through the flight with a less frequency but higher amplitude can cause the connection bolts to tear down the wing in a short flight. Thus for both connections, metal parts were placed as reinforcements.

The tail structure, on the other hand, is very thin and lightweight that it is not practical to place metal inserts into both vertical and the horizontal tail to strengthen the connection areas. Rather than strengthening the surfaces against abrasion, the source of abrasion was removed in the tail. The tail was assembled permanently creating an integrated tail structure so that the whole structure vibrates as a whole that is not harming the connections. The horizontal and the vertical tail parts were assembled first by cutting the facing surfaces in an exact match and then using an adhesive and covering the area with glass fibre fabric wetted with epoxy resin. Even if composite adhesion does not result in an assembly as strong as a single structure cured at once, still composite adhesion prevents free movement of the sub-parts resulting in bonding failures. For the connection of the tail booms to the tail structure, two short tubes into which the tail booms can tightly fit were again permanently assembled to the tail structure. Similarly another two enclosing tubes

were integrated to the wing structure to house the tail booms. The assembly of the tail to the fuselage was performed by inserting the tail booms into the housing tubes on both ends and fixing the booms to the tubes using bolts. The connection areas of the booms were reinforced using small wooden pieces adhered to the inner side of the boom against vibration sourced problems. Even if an integral tail structure reduces transportability by requiring a large compartment to carry the tail and reduces serviceability by eliminating the possibility of replacing the horizontal and vertical tails independently in case of a local damage; the safe operation of the tail is sustained in return of much lower weight compared to bolted individual tail parts. As an extra weight on the tail structure both affects the centre of gravity adversely and causes a large bending moment on the tail booms requiring even stronger and heavier boom structure, an integral tail structure was found more feasible. For the same weight concern, the vertical and horizontal tails don't have ribs. Considering the significantly lower loads on the tail compared to the wings, the spars are sufficient to carry the loads.

A major drawback on the completeness of the METU TUAV project right now is the incomplete validation of the design and manufacturing phases. There had been some computer aided structural and aerodynamic analysis on the specific parts which proved that the aircraft is airworthy. One of the previous studies on the wing structures of METU TUAV proved that: "Based on the structural analyses results, it is concluded that the wing is safe based on static limit load analyses performed at minimum manoeuvring and dive speeds. Deflection and dynamic analysis showed that the wing was relatively stiff, and this effect was also reflected in the approximate divergence speed which turned out to be quite high. Thus, before the first flight, sufficient level of confidence has been built up in the structural integrity of the wing structure." [7] Further structural studies are being performed on the carrying structures of the METU TUAV by performing destructive tests on specimens representing the spars and the ribs. Yet no significant progression has been reached by this time.

Additionally, various tests have been performed on the test bench designed and manufactured specifically for the Limbach L275 engine and the sea level power expectations were fulfilled during these tests. On the test bench, the start up

methods were also developed which is not an easy task on the field for an aircraft that is neither equipped with a starter nor possesses an automatic mixture adjuster. The test setup was not used for fuel consumption analysis that would validate the manufacturer specifications of the engine but with an addition of a sensitive flow meter to the test setup, a detailed fuel consumption map can be obtained.

6.2 CONCLUSION AND FUTURE WORK

This thesis gives an overview of the design and manufacturing of METU Tactical Unmanned Air Vehicle (METU TUAV). In this thesis, the conceptual design phase and performance analysis to support the design have been summarized. Without introducing the detailed design, material selection and production techniques are conferred and the manufacturing of METU Tactical UAV is presented in great detail.

In this era, unlike the past century, weight and size are no more advantages in aviation. Light-weight and cheap UAV's have taken over the crown of last century's noisy and big reconnaissance aircraft that fly in the upper atmosphere. Composite technology is exactly what is needed to provide light and strong materials for this era's UAV requirements. In METU TUAV project, a TUAV was manufactured with composite materials, which has military and civil applications in reconnaissance missions.

The manufacturing of the Tactical UAV utilizes composite material technology where the focus of the thesis is on the usage of composite materials starting at mold manufacturing and resuming even in small touch ups and adhesions, mentioning the critical decisions and production tips.

A major cost element in composite manufacturing, which is the mold, was also produced with composite materials, integrating composite technology in every step of production. For prototype manufacturing, the mold does not need to be durable for large numbers of production cycles, thus the use of composite molds, which is both easy to manufacture and practical to modify, has decreased the cost and increased the effectiveness of mold manufacturing.

Especially the composite production of the fuselage where carbon, aramid and glass fibre fabrics are used generating a hybrid web, utilizes advanced composite technologies. With the web structure, the fuselage becomes durable to different kinds of loads making the fuselage both resistive to unidirectional flight loads and tough to keep its integrity after crashes and hits during flight tests.

The separately manufactured and reinforced composite structures are assembled and brought into correct alignment finalizing the METU TUAV structure. After the integration of components such as landing gears, engine and servos; the METU TUAV structure will be finalized.

Within the scope of the ongoing METU TUAV project, the fuel depot and its connections to the engine will be laid. The electronic equipments and control systems will be integrated and a cable web will be furnished inside the TUAV. Then the METU TUAV will be ready for flight tests and further improvement of the design.

The most critical future works for the METU TUAV to prove itself and the methods used in its production will be the flight tests. When the METU TUAV succeeds in its flight tests and validates the initial requirements, the METU TUAV project will pass into a stage of development, where, in the light of flight test outcomes, minor modifications to the design will be made and additional prototypes will be manufactured to improve the performance characteristics.

In the future manufacturing processes, more integrated techniques such as co-curing of skin and reinforcements might be used to increase strength and decrease weight.

REFERENCES

- [1] Zingg, Simon, et al. MAV Navigation through Indoor Corridors Using Optical Flow. Zurich : Autonomous Systems Lab, 2007.
- [2] Prospects of Advanced Tactical RVP's. Seidel, F. Bristol : Royal Aeronautical Society and the Department of Aeronautical Engineering of the University of Bristol, 1979. Remotely Piloted Vehicles International Conference. p. 2.1.
- [3] GlobalSecurity.org. Unmanned Air Vehicles. Global Security. [Online] 15 December 2008. [Cited: 30 August 2010.]
<http://www.globalsecurity.org/intell/systems/uav-intro.htm>.
- [4] Wikimedia Foundation Inc. Unmanned Aerial Vehicle. Wikipedia. [Online] 29 August 2010. [Cited: 30 August 2010.]
http://en.wikipedia.org/wiki/Unmanned_aerial_vehicle.
- [5] Arjomandi, Dr. Maziar. Classification of Unmanned Aerial Vehicles. Adelaide : University of Adelaide, 2006.
- [6] Shephard's. Unmanned Vehicles Handbook. Bucks, England : The Shephard Press, 1995.
- [7] Soysal, Serkan. Structural Design, Analysis and Composite Manufacturing Applications for a Tactical Unmanned Air Vehicle. Ankara : Department of Aerospace Engineering, Middle East Technical University, 2008.
- [8] Soysal, Serkan, Kayran, Altan and Alemdaroğlu, Nafiz. Dubai : American University of Sharjah, 2009. 7th International Conference on Composites.

- [9] Kargin, Volkan. Design of an Autonomous Landing Control Algorithm for a Fixed Wing UAV. Ankara : Department of Aerospace Engineering, Middle East Technical University, 2007.
- [10] Raymer, Daniel P. Aircraft Design: A Conceptual Approach. Sylmar, California : AIAA Education Series, 1992.
- [11] Hoerner, S. F. Fluid Dynamic Drag. Brick Town, N. J., USA : Hoerner Fluid Dynamics, 1965.
- [12] Andersen, John D. Aircraft Performance and Design. s.l. : McGraw Hill, 1999.
- [13] AIPMA. Plastic Process. The All India Plastics Manufacturers' Association. [Online] 2009. [Cited: 30 August 2010.]
<http://www.aipma.net/info/plasticprocess.htm>.
- [14] Vakum Torbalama Yöntemi ile Kompozit Malzemeden Yapı Üretimi, Örnek Bir Havacılık Uygulaması. Turgut, Tahir, et al. 2007, Mühendis ve Makina, TMMOB Makina Mühendisleri Odası Aylık Yayın Organı 566.
- [15] Materials Engineering Institute. Composites II: Material Selection and Applications Course 31 Lectures 1, 5, 6, 10. Ohio : ASM International, 1989.
- [16] Composite Manufacturing of the Wing of a Tactical. Soysal, Sercan, et al. Dubai : American University of Sharjah, 2009. 7th International Conference on Composites.
- [17] Bir Taktik İnsansız Hava Aracının Kompozit Gövde Kalıbı ve Kompozit Gövde Üretimi. Şenelt, Engin, Kayran, Doç. Dr. Altan and Alemdaroğlu, Prof. Dr. Nafiz. Eskişehir : 2010. II. Ulusal Havacılık ve Uzay Konferansı.